Degago, S. A. *et al.* (2011). *Géotechnique* **61**, No. 10, 897–908 [http://dx.doi.org/10.1680/geot.9.P.112]

Use and misuse of the isotache concept with respect to creep hypotheses A and B

S. A. DEGAGO*, G. GRIMSTAD†, H. P. JOSTAD*†, S. NORDAL* and M. OLSSON‡

Time-dependent settlements of thick in situ clay layers are normally analysed based on results of thin laboratory specimens. However, the time used to complete primary consolidation is significantly different for laboratory specimens and in situ soil layers. Two totally different cases, referred to as creep hypotheses A and B, have been used as a basis of discussion to assess the effect of creep during the primary consolidation phase. Several laboratory and field experiments have been conducted to study the effect of soil layer thickness on the time-dependent compressibility of a soil layer. Some of these tests seemed to support hypothesis A, others hypothesis B, and in some cases showed a behaviour between the two. As a result this question has continued to be a controversial topic among researchers, and remains to be an issue that needs to be resolved. In this study, some relevant experimental investigations from the literature are thoroughly studied and critically reviewed, and also explained consistently using the isotache concept. This work indicates that the isotache approach can capture the main characteristics of the time-dependent compressibility of clays during both the primary and secondary consolidation phases. It is also shown that the misuse of the isotache concept, as reported in the literature, may give a confusing picture of reality. Based on the considered data, it is demonstrated that the measured time-dependent compressibility of clays agrees well with hypothesis B.

KEYWORDS: clays; compressibility; consolidation; creep; deformation; settlement

Les tassements en fonction du temps d'épaisses couches d'argile in situ sont normalement analysés sur la base de spécimens de laboratoire de faible épaisseur. Toutefois, les délais nécessaires pour la réalisation de la consolidation primaire sont sensiblement différents pour les spécimens de laboratoire et les couches de sol in situ. On a utilisé deux cas totalement différents, désignés hypothèses de glissement A et B, comme éléments de base pour des discussions, dont le but était d'établir l'effet du glissement au cours de la phase de consolidation primaire. On a effectué plusieurs expériences en laboratoire et sur le terrain afin d'étudier l'effet de l'épaisseur des couches de sol sur la compressibilité en fonction du temps de la couche de sol. Certains de ces tests semblent favoriser l'hypothèse A, d'autres l'hypothèse B, et, dans certains cas, un comportement situé entre les deux. En conséquence, ce problème reste une question controversée entre les chercheurs, ainsi qu'un problème à résoudre. Dans la présente étude, on procède à une étude approfondie ainsi qu'à l'examen critique de certaines recherches expérimentales pertinentes dans des ouvrages sur cette question, que l'on explique logiquement en appliquant le concept des isotaches. La présente communication indique que le principe des isotaches permet de saisir les principales caractéristiques de la compressibilité des argiles en phase de consolidation primaire et secondaire. Elle indique également que l'application erronée du concept de l'isotache, décrit dans des ouvrages, risque de fausser la réalité des choses. Sur la base des données examinées, on démontre que la compressibilité des argiles mesurée en fonction du temps est en parfait accord avec l'hypothèse B.

INTRODUCTION

The settlement behaviour of in situ soft soil layers is normally studied based on test results deduced from laboratory specimens. In geotechnical practice, standard oedometer and triaxial tests are usually conducted to study soil deformation as a response to an applied action of stress and time. Laboratory specimens are subjected to loading that reproduces the action of stress in the field; however, reproducing the action of time is not easy, since significantly different timescales are involved. Still, time-dependent settlements of thick in situ soft soil layers are usually analysed based on experimental results derived from thin laboratory specimens. The time duration to complete primary consolidation is considered to be an important difference between laboratory specimens and in situ soil layers. In the laboratory, consolidation may last for the order of minutes, whereas in thick in situ clay layers the consolidation period could be of the order of several decades (Larsson & Mattsson, 2003; Leroueil, 2006). Therefore, in order to achieve acceptable field predictions, it is very important to understand the time-scaling effect between a thin laboratory specimen and a thick in situ soil layer. How to extrapolate the time-dependent behaviour of clays from fast laboratory tests towards slow field condition has been a topic of active debate among researchers (Mesri, 2003; Leroueil, 2006). This paper aims to clarify the controversies related to scale effects, based on a critical review of laboratory tests from the literature, supported by illustrative numerical analyses.

Manuscript received 12 September 2009; revised manuscript accepted 15 October 2010. Published online ahead of print 22 February 2011. Discussion on this paper closes on 1 March 2012, for further details see p. ii.

* Norwegian University of Science and Technology, Trondheim, Norway.
† Norwegian Geotechnical Institute, Oslo, Norway.
‡ Chalmers University of Technology, Gothenburg, and Swedish Geotechnical Institute, Gothenburg, Sweden.

BACKGROUND

In their state-of-the art report, Ladd *et al.* (1977) raised an important question related to creep during primary consolidation. The fundamental question was: 'Does creep act as a separate phenomenon while excess pore pressures dissipate during primary consolidation?' If it does, then for a given effective vertical stress increment the end-of-primary (EOP) vertical strain depends upon the duration of primary

consolidation, and hence on the thickness of the consolidating soil layer. Such a consideration led to the realisation of two possible extreme effects of sample thickness, which are summarised in Fig. 1 in terms of hypotheses A and B. In hypothesis A, the strain at EOP is assumed to be independent of the consolidation period, whereas hypothesis B predicts an increasing EOP strain with increasing consolidation period or increasing sample thickness.

A possible implication of the two creep hypotheses in terms of effective stress–void ratio (strain) is stated as follows. Hypothesis A predicts that the relationship between EOP void ratio (strain) and effective stress is the same for both laboratory and field conditions. This means that the EOP preconsolidation stress is identical for laboratory specimens and in the in situ condition. Hypothesis B yields a relationship between an in situ EOP strain and effective stress that is different from the corresponding laboratory curve, such that the in situ EOP preconsolidation stress is lower than that determined from an EOP laboratory test. Admitting that Ladd *et al.* (1977) were themselves biased towards hypothesis A, they conclude that 'Little definitive data exists to show which of the two hypotheses is more nearly correct for the majority of cohesive soils.' Since 1977, this concern has continued to be a topic of active discussion among researchers, and remains an issue that needs to be resolved. A summary of some of the discussions can be found in Mesri (2003) and Leroueil (2006).

Early work by researchers studying creep (Šuklje, 1957; Bjerrum, 1967; Janbu, 1969; Šuklje, 1969) assumed that the creep rate was given by the current effective stress and the current void ratio (strain). In other words, any combination of void ratio (strain), effective stress and rate of change of void ratio (strain rate) is considered to be unique throughout the primary and secondary consolidation phases. These formulations can be classified as isotache models, and imply hypothesis B. Such approaches have been advocated and used as a basis for further research developments that consider creep during primary consolidation (e.g. Svanø *et al.*, 1991; Kutter & Sathialingam, 1992; Den Haan, 1996; Stolle *et al.*, 1999; Vermeer & Neher, 1999; Kim & Leroueil, 2001; Nash & Ryde, 2001; Yin *et al.*, 2002; Imai *et al.*, 2003; Leroueil, 2006; Laloui *et al.*, 2008; Leoni *et al.*, 2008; Watabe *et al.*, 2008b; Grimstad & Degago, 2010; Grimstad *et al.*, 2010; Karim *et al.*, 2010; Nash, 2010). Other researchers, supporting hypothesis A, found experimentally that the EOP void ratio seemed to be independent of the consolidation period (Mesri & Godlewski, 1979; Choi, 1982; Mesri & Choi, 1985; Feng, 1991; Mesri, 2003; Mesri & Vardhanabhuti, 2006; Mesri, 2009). This group of researchers also advocate the existence of creep during primary consolidation, but they believed that the role of creep is controlled by total strain rate as a function of stress state and effective stress rate, indicating that there is no unique relationship among effective stress, strain and strain rate during primary consolidation (Mesri, 1990; Feng, 1991; Mesri *et al.*, 1995; Mesri, 2009). Their argument can be elaborated by the subsequent statements: soil compression is caused by two interrelated contributions, which are due to change in effective stress (stress compressibility) and change in time (time compressibility). It is assumed that the combination of these two interrelated components varies according to the effective stress rate and the duration of primary consolidation. Hence the difference in effective stress rate and consolidation duration that exists between thin and thick soil layers is claimed to govern the contribution of the stress and time compressibility components to yield an EOP void ratio (strain) that is independent of the consolidation period.

Several laboratory and field experiments have been conducted to investigate the effects of layer thickness on the compressibility of clayey soils (Berre & Iversen, 1972; Aboshi, 1973; Felix, 1979; Aboshi *et al.*, 1981; Choi, 1982; Mesri & Choi, 1985; Kabbaj *et al.*, 1988; Feng, 1991; Imai & Tang, 1992; Tsukada & Yasuhara, 1995; Chih-Hao, 2002; Li *et al.*, 2004; Tanaka, 2005; Konovalov & Bezvolev, 2005; Watabe *et al.*, 2008a, 2009; Degago *et al.*, 2010). Most of these tests have been conducted to examine the two creep hypotheses and, as a consequence, have played a significant role in advocating them. In this paper, laboratory investigations that focused on assessing the creep contribution during primary consolidation are thoroughly studied and critically reviewed, along with the support of illustrative numerical analyses. The numerical model used in the analyses is based on the isotache concept, which is described in the next section.

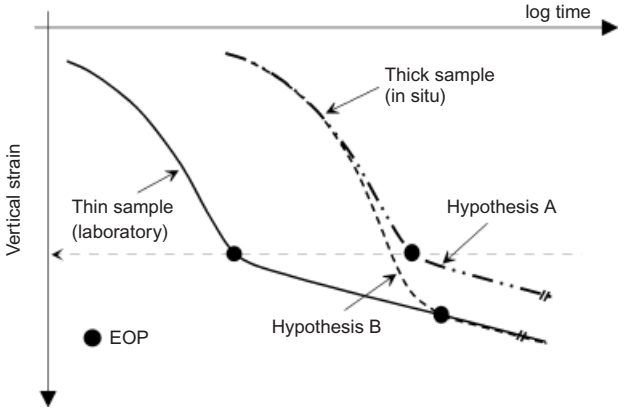

Fig. 1. Effect of sample thickness according to creep hypotheses A and B (after Ladd *et al.*, 1977). Note: same $\Delta\sigma'/\sigma'_{v0}$ for both samples

THE ISOTACHE CONCEPT

The isotache concept was originally proposed by Šuklje (1957) in order to describe rate effects on the compressibility of clayey soils. This approach states that the rate of change of void ratio is given by the prevailing void ratio and effective stress.

The concept of isotaches can be illustrated using the sketch shown in Fig. 2. The series of parallel broken lines in the figure are creep isotaches. Each creep isotache corresponds to a constant void ratio rate, $\dot{e}_{j+n}$. This means that any combination of void ratio, vertical effective stress and rate of change of void ratio is unique, and this remains valid during the entire soil compression process (primary and secondary consolidation phases). For instance, consider a soil element close to a draining boundary. The initial state of this soil element is assumed to be given by point A. A vertical total stress increment, $\Delta\sigma'_v$, is then applied and left to creep for some time. The path followed is represented by the solid line ABCDE. This path is dependent on the distance of the soil element from the drainage boundary, as the effective stress rate and strain rate are governed by the consolidation process. Depending on the duration of the applied effective stress, the final state of the soil element can be B, C, D or E.

In this paper, the isotache concept is used to provide numerical illustrations. These simulation results are used to demonstrate the implications of the isotache approach. Two types of idealised case are considered. The first case demonstrates the compressibility characteristics of two different specimen thicknesses. The second case shows the local compressibility of soil elements within a thick specimen, but

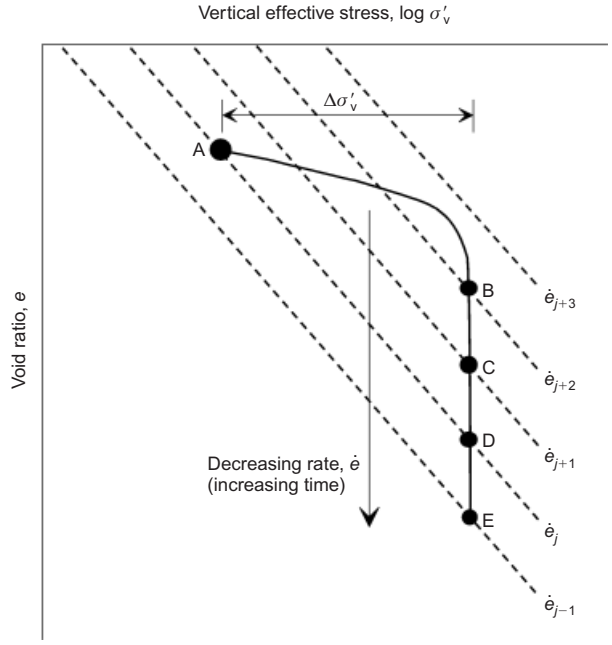

Fig. 2. Illustration of the isotache concept

located at different distances from the drainage boundary. The finite-element code PLAXIS (2D version 9) with the soft soil creep (SSC) model (Stolle *et al.*, 1999; Vermeer & Neher, 1999) was utilised in the numerical simulations. Even though SSC is used in this study, it must be acknowledged that there are several models based on the isotache concept that produce essentially similar results.

CASE I: COMPRESSIBILITY OF SPECIMENS WITH DIFFERENT THICKNESSES

Description of simulation

Two idealised specimens with thicknesses of 1 cm and 10 cm were simulated in a uniaxial strain condition with drainage at the top. The loading and drainage conditions were defined to resemble oedometer conditions. Both specimens were initially prestressed to $\sigma'_v = 10$ kPa, $\sigma'_h = 5{\cdot}2$ kPa. The initial preconsolidation stress, p'_c, was specified to be 100 kPa. This p'_c value corresponds to a preconsolidation stress obtained in a test of one day's duration, between each load increment, in an incremental oedometer test. A standard incremental oedometer loading scheme was adopted with applied vertical stresses of 25 kPa (a vertical stress increment of 15 kPa), 50 kPa, 100 kPa, 200 kPa, 400 kPa, 700 kPa, 1200 kPa and 2000 kPa. For the EOP oedometer test simulations, the incremental load duration lasted until 99% of the initial excess pore pressure increment had dissipated. The soil parameters adopted for the simulations are listed in Table 1. The definitions of the SSC compressibility parameters, in isotropic compression, are illustrated in Fig. 3 in terms of volumetric strain ε_v, mean effective stress p' and time t. The SSC model uses a shape parameter M that controls the steepness of the cap. In this paper, the parameter M was chosen such that it is determined based on the coefficient of earth pressure under virgin loading (K_0^{NC}) considerations (for further details see the PLAXIS user's manual).

Table 1. Soil properties adopted for the oedometer simulations

Soil parameter	Value
Permeability, k: m/s	5×10^{-9}
Earth pressure coefficient under virgin loading, K_0^{NC}	0·52
Modified swelling index, κ^*	0·021
Modified compression index, λ^*	0·091
Modified creep index, μ^*	0·0033
Friction angle, ϕ: degrees	30
Poisson's ratio for unloading–reloading: ν_{ur}	0·15

Simulation results of idealised case I

Standard EOP simulations. Standard incremental oedometer test schemes were simulated under EOP conditions for the thin (1 cm) and thick (10 cm) specimens. The axial deformation at the top of the specimens, δ_v, was normalised by the respective initial height, h_i. This gives a strain measure that will be referred to in this paper as a nominal strain.

The curved lines in Fig. 4 show vertical strain, ε_v, against the effective stress history path followed by a soil element close to the top of each specimen. The end points at each of the stress increments mark the final EOP state of the specimens. When these EOP points are connected for a stress state above the initial p'_c, they define an isotache corresponding to the rate at EOP consolidation. Hence, when the EOP points are connected, they define a reference isotache that corresponds to an EOP strain rate (in Fig. 4, the symbols with a dot on top are used to identify the creep isotaches corresponding to the 1 cm and 10 cm thick specimen). For a load increment that takes place in a stress regime well before reaching p'_c, the behaviour of both the thin and thick specimens is strongly influenced by elasticity, and the contribution from creep is insignificant. Hence both specimens follow the same path until they approach the initial preconsolidation stress, p'_c. However, while approaching the initial p'_c, differences start to arise as strain rate effects come into play. It is also seen that the thick specimen yields at a lower effective stress than the thin specimen. The difference in the EOP nominal strain remains constant during the normally consolidated regime. This also means that the incremental EOP nominal strains of the two speci-

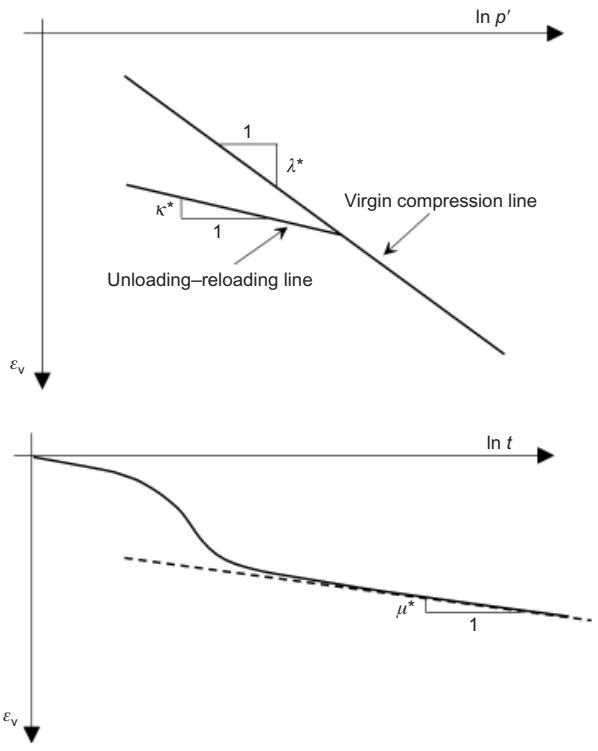

Fig. 3. Definition of SSC parameters (PLAXIS user's manual)

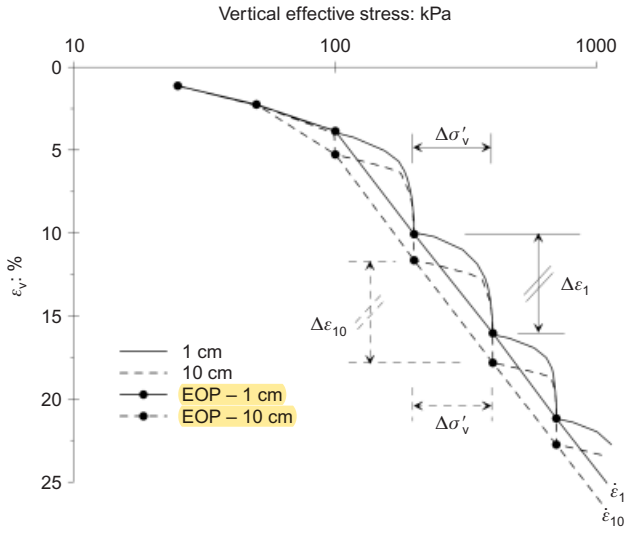

Fig. 4. EOP paths followed by soil element close to top of specimens (curved lines) and isotache lines corresponding to EOP state of specimens (straight lines)

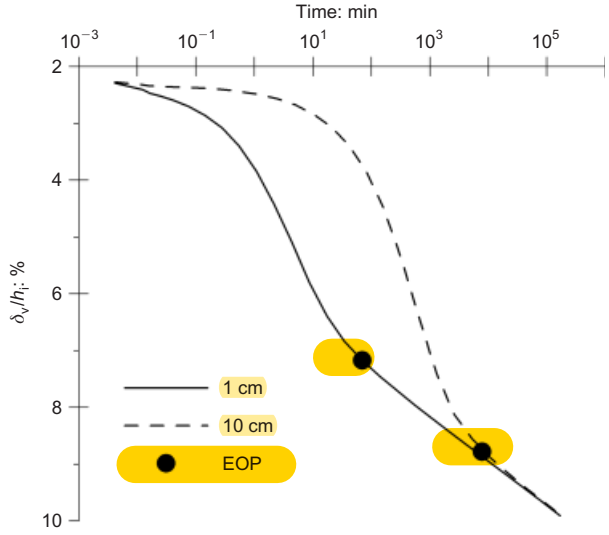

Fig. 5. Load increment from 50 to 150 kPa exceeding initial $p'_c = 100$ kPa

mens become practically equal for effective stress increments in the normally consolidated regime. What actually happens, in Fig. 4, can be further elaborated by considering the interplay between the creep rate and the corresponding consolidation period. Before the initial p'_c, both specimens have a similar creep rate. During an effective stress increment that exceeds the initial p'_c, the consolidation periods will be significantly different for the two specimens, and this leads to different EOP strains. However, for stress increments in the normally consolidated regime, the thin specimen deforms with a higher creep rate for a shorter consolidation period, whereas the thick specimen deforms with a lower creep rate for a longer consolidation period. Consequently, the incremental EOP strains, in the normally consolidated regime, will be almost the same for both specimens.

The overall picture of the EOP consolidation process of the thin and thick specimens is presented in Fig. 4. The next step is to take a closer look at the effect of creep at different effective stresses in reference to the initial preconsolidation stress, p'_c. Consolidation behaviour that takes place well before approaching the initial p'_c is not interesting, as no distinction can be made between the thin and thick specimens. However, the consolidation behaviours close to p'_c and after exceeding the initial p'_c are investigated in separate simulations.

Load increment that exceeds the initial preconsolidation stress, p'_c. To study the creep phenomenon while exceeding the initial p'_c, both specimens were incrementally loaded following a standard loading procedure, with an EOP condition, up to 50 kPa. This ensured that both specimens were in an overconsolidated state regime, and that the test simulations therefore started at the same effective stress–nominal strain or effective stress–void ratio state. Subsequently an additional load increment of 100 kPa was applied such that the initial $p'_c = 100$ kPa was exceeded. Afterwards, both specimens were left to creep at 150 kPa for 100 days. Fig. 5 shows that both specimens essentially start at the same point but end up having different EOP nominal strains. The EOP nominal strain is larger for the thick specimen. However, after a long time, the nominal strain–time curves of the thin and thick specimens converge to the same line.

Load increment immediately after exceeding initial preconsolidation stress, p'_c. To study the settlement characteristics at the beginning of the virgin stress regime, both specimens were incrementally loaded following a standard loading procedure, with an EOP condition, up to 200 kPa. This ensured that the initial $p'_c = 100$ kPa was exceeded. Afterwards, both specimens were allowed to creep for 100 days under 200 kPa. The results are presented in two ways as shown in Figs 6(a) and 6(b). When the specimens reach the initial p'_c at 100 kPa the void ratios (nominal strains) become different, and this defines the starting state for the next stress increment. When an additional 100 kPa increment is applied, giving a total stress of 200 kPa, both specimens yield a different EOP void ratio, that increases with specimen thickness. After creeping for a longer duration at 200 kPa, the deformation–time curves of the two specimens converge to the same line, as shown in Fig. 6(a). However, the calculated results can also be presented in a different way, as shown in Fig. 6(b). In this case only the changes in the nominal strain within the actual load increment are presented. It is observed that the EOP nominal strain increments are closer to each other, and show only a slight tendency to increase with the greater thickness. This is because the effect of exceeding the initial p'_c is pronounced to some extent. The final parts of these curves are parallel, and will never converge to the same line.

Load increment long after exceeding initial preconsolidation stress, p'_c. The aim of this simulation is to study the deformations at a stress level that is sufficiently greater than the initial p'_c. Hence both specimens were incrementally loaded following a standard EOP loading procedure up to 400 kPa, and left to creep for 100 days at this stress level. The results of this simulation are presented in Figs 7(a) and 7(b). The shapes of the curves are very similar to the shapes obtained when the samples were loaded from 100 kPa to 200 kPa. However, the slight tendency of the EOP incremental nominal strain to increase with sample thickness observed at 200 kPa (see Fig. 6(b)) is not observed when the specimens are loaded from 200 kPa to 400 kPa (Fig. 7(b)). The main reason is that the effect of exceeding the initial p'_c of 100 kPa does not affect the incremental nominal strains for the load increment between 200 and 400 kPa. This means that the EOP incremental nominal strains are almost identical

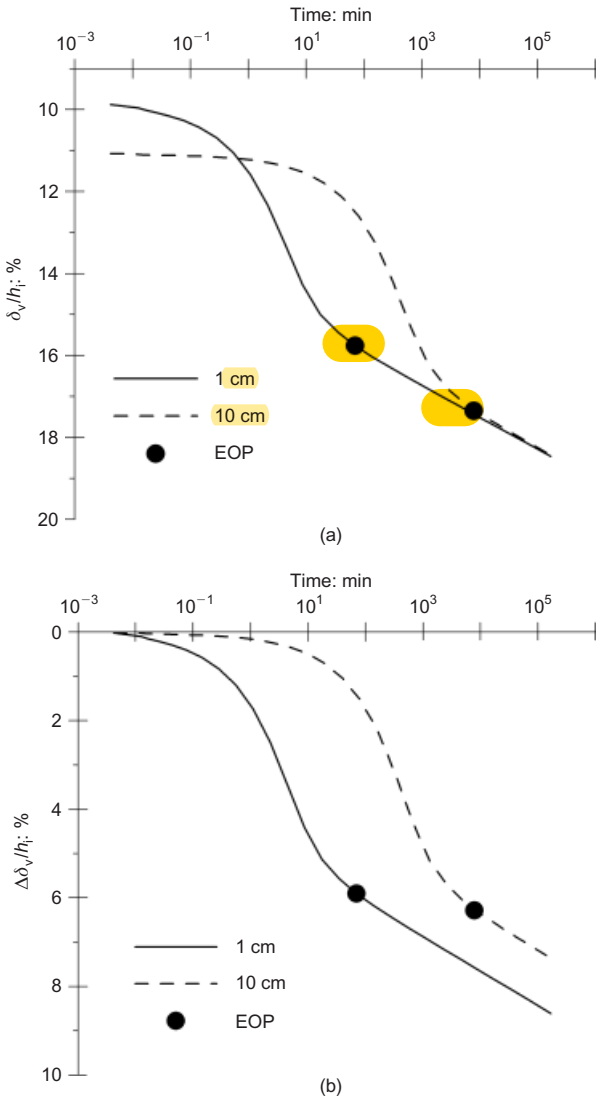

Fig. 6. Load increment from 100 to 200 kPa in terms of: (a) absolute nominal strains; (b) incremental nominal strains. Allowed to creep after EOP at 200 kPa

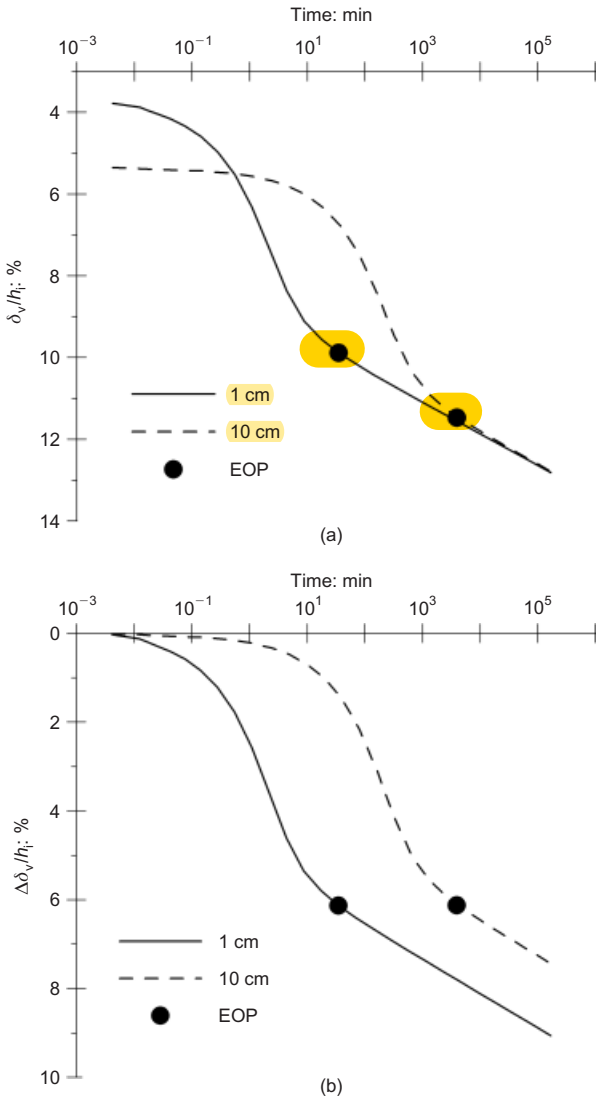

Fig. 7. Load increment from 200 to 400 kPa in terms of: (a) absolute nominal strains; (b) incremental nominal strains. Allowed to creep after EOP at 400 kPa

for the thin and thick specimen when the load increment is sufficiently above the initial p'_c.

Literature review of EOP experiments on specimens of different thicknesses

The results from the idealised cases presented in the previous section will be used critically to discuss previously conducted EOP experiments on specimens of varying thickness. The tests reviewed are discussed in chronological order. The experiment conducted by Feng (1991) and Choi (1982) on specimens 127 and 508 mm thick, which were used to advocate hypothesis A, are addressed in a separate paper (Degago *et al.*, 2009) and will not be discussed here. However, it is worthwhile mentioning that Degago *et al.* (2009) have shown that re-interpretation of these tests, for consistent EOP criteria, yields results that support hypothesis B. In addition, these test observations were compared with numerical simulations using an isotache model that gave results that fit very well with the measurements.

當初 Feng (1991) 和Choi (1982) 的試驗數據都是用來支持假設A是成立的。但 Degago et al (2009) 重新解　釋這些試驗數據後，　發現這些試驗都支持假設B是成立的。

Experiment by Aboshi (1973). Aboshi (1973) conducted a series of carefully designed laboratory and field tests with varying specimen sizes. The investigated soil was reconstituted sedimentary marine clay from Hiroshima Bay. In order to avoid the effects of friction and stress distribution on the side walls, all the tests had similar diameter (d) to height (h) ratios given by $d/h = 3$. In addition, silicone oil was used to avoid possible side friction. Three different heights, 2, 4·8 and 20 cm, were tested in the laboratory, whereas another two heights, 40 and 100 cm, were tested in the field.

A preliminary consolidation stage up to 20 kPa, which is necessary to perform the test in a normally consolidated regime, was limited in time by the end of primary consolidation. Afterwards settlements of long duration were conducted by one loading step from 20 to 80 kPa. The incremental EOP nominal strains for specimen heights of 2, 4·8, 20, 40 and 100 cm were respectively approximated as 7·3%, 7·4%, 8·2%, 7·8% and 8·4% using Taylor's graphical construction, and 8·25%, 8·2%, 8·3%, 8·35% and 8·9% using Casagrande's graphical construction (Choi, 1982; Oka, 2005).

The experiments conducted by Aboshi (1973) have been widely discussed by various researchers (see below), and were perceived differently. Aboshi (1973) concluded that the observed soil behaviour deviates from the isotache theory, proposed by Šuklje (1957), because the measured settlement curves tend to be parallel instead of converging to one line. Choi (1982) and Mesri (2009) re-interpreted the EOP nominal strains to show that they are more or less similar to

each other. Mesri & Choi (1985) and Mesri (2009) argued that the observed range of EOP strains for different thicknesses is in agreement with hypothesis A, and the observed small variations could be due to issues related to possible problems linked to single lead increment tests. These test results (see Fig. 8) have also been claimed to show that the real soil behaviour lies in between hypotheses A and B (Yasuhara, 1982; Leroueil *et al.*, 1985; Imai & Tang, 1992; Hawlader *et al.*, 2003; Li *et al.*, 2004; Watabe *et al.*, 2009). Oka (Oka *et al.*, 1986; Oka, 2005) described Aboshi's observation as hypothesis C (a hypothesis between A and B), and proposed a numerical procedure that simulates the possible creep hypotheses A, B and C.

The authors' view on these experiments is presented as follows. Soil specimens of Hiroshima Bay with different thicknesses were reconstituted for different durations with an increasing time for an increasing specimen thickness. The results of the actual stress increment (20 to 80 kPa) were presented in terms of incremental nominal strains against time. These tests were conducted after exceeding the initial p'_c. Hence they correspond to the idealised case shown in Fig. 6(b). The slight increase in the incremental EOP nominal strain with increasing specimen thickness can also be seen both in the experiment and in the simulated idealised case.

When the isotache concept was first presented (Šuklje, 1957), it was meant to describe the compressibility of soils subjected to long-term creep, such that the primary consolidation phase plays a minor role in the whole compression process. The consequence of this is that the time–settlement curves of thick and thin specimens converge to the same line or void ratio. Hence the next stress increment will start at the same void ratio, irrespective of the thickness or stress history, and the time–settlement curves again converge to the same line and so on, analogous to Fig. 5. Aboshi (1973) originally presented the experimental results in Fig. 6(b) format, and compared them with a set of isotaches plotted in Fig. 6(a) format. In other words, the experiments were plotted in terms of change in nominal strain, but they were compared against a set of isotaches valid for total nominal strains. As a consequence, Aboshi wrongly concluded that

> the creep settlement curves of every tests become almost parallel in their final stages. However these creep settlement curves do not coincide in one line on the creep curve of standard oedometer test, as shown in Šuklje's isotaches theory.

Aboshi 錯誤的得出結論...

The main observation can be summarised as follows. There is a slight tendency for the EOP nominal strain increment to increase with increasing thickness. This agrees with simulation results of the idealised case where the load step exceeds the initial p'_c, as shown in Fig. 6(b). The effect of increasing EOP nominal strain with thickness, as implied by hypothesis B, would have been significantly larger if the experimental results were presented for the whole stress history in terms of the absolute nominal strain or void ratio.

Experiment by Imai & Tang (1992). Imai & Tang (1992) developed a system of interconnected consolidometers, and carefully conducted a series of experiments on a marine clay from Yokohama Bay. The tested material was carefully reconstituted such that the desired uniformity of the soil was maintained. Each sub-specimen had a thickness of 0·5 cm and a diameter of 6 cm. Special measures were also taken to minimise possible errors that could arise from such thin specimens.

Prior to the main experiment, each thin specimen was preconsolidated to an effective vertical stress of 39·2 kPa. A set of EOP tests were conducted using the interconnected system, such that incremental loads were applied until 99% of the initial excess pore pressure was dissipated. The initial total specimen thicknesses studied under EOP conditions were 1, 2 and 4 cm.

The results of the last load increment, from 156·8 kPa to 313·6 kPa, are shown in Fig. 9, and were used by Imai & Tang to verify hypothesis A. These results correspond to the idealised case illustrated in Fig. 7(b). The reason why the experiments seem to agree with hypothesis A is that they are presented in terms of change in void ratio, and the stress range is far above the initial p'_c. It is worth mentioning that Imai & Tang have conducted another set of experiments to illustrate the possibility of obtaining results in accordance with hypothesis B. To achieve this, they let their thin and thick specimens creep for the same duration of 24 h, and then studied the EOP void ratio that resulted from the next load increment. This test procedure is not a true EOP test, as neither of the specimens started from its respective EOP states. Verification of hypothesis B using these results was considered to be incorrect and misleading according to Mesri (2003), as the comparison lacks consistency in EOP procedure. However, had Imai & Tang (1992) presented their

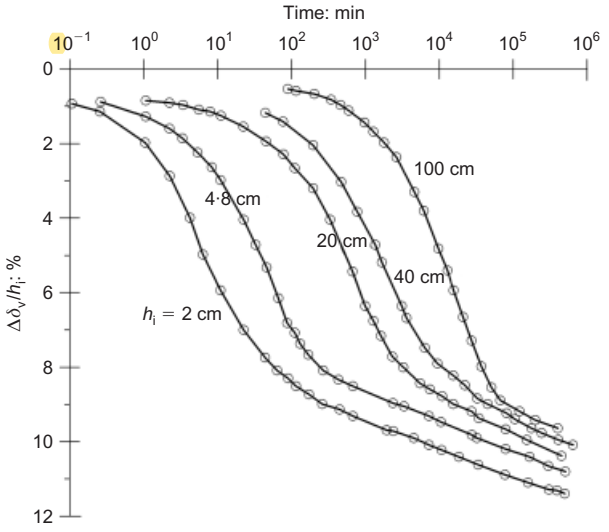

Fig. 8. Results of consolidation test on samples of different thickness (after Aboshi, 1973)

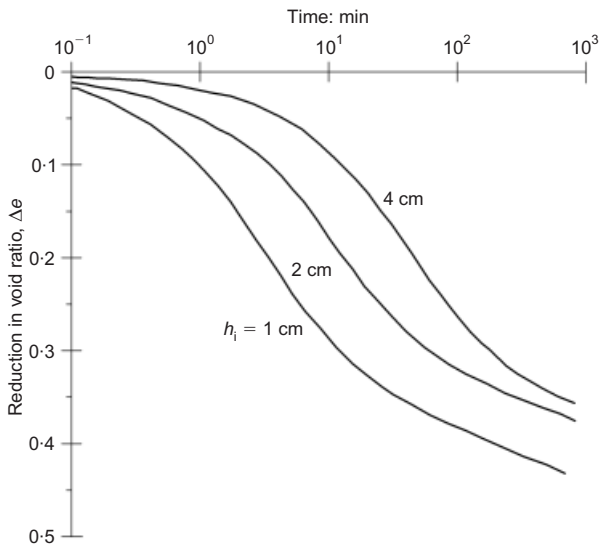

Fig. 9. Experimental results for specimens of different thickness during last loading increment (after Imai & Tang, 1992)

EOP test results (Fig. 9) in terms of absolute void ratio, rather than change in void ratio, they would have verified hypothesis B without even the need to do another experiment with an inconsistent EOP procedure.

Experiment by Konovalov & Bezvolev (2005). Konovalov & Bezvolev (2005) conducted EOP consolidation tests on natural clayey soil originating from a post-glacial marine lithorine deposit. A specially designed consolidometer was used to test specimens with a diameter of 5·5 cm, and with the possibility of varying the specimen thickness within the range 1–10 cm. The consolidometer used an impenetrable rubber jacket and incompressible confined liquid to avoid the possibility of friction along the lateral surface of the samples. This was considered to be important to control the uniformity of the test specimens.

The test specimens were reconsolidated back to their in situ state, depicted by an effective stress of 30 kPa. Subsequent to reconsolidation, the test specimens were subjected to a stepped loading for a duration defined by 95% dissipation of the initial excess pore pressure. After reaching an effective stress level of 230 kPa using this EOP loading procedure, the specimens were subjected to an additional stress increment of 200 kPa and left to creep for more than 70 days.

Figure 10 shows the results of the last load increment (230 to 430 kPa) in two ways, as originally presented by Konovalov & Bezvolev (2005). These results support the isotache concept as shown in Figs 7(a) and 7(b). The experiments demonstrated that disregarding the effect of the void ratio–stress history of a soil has the consequence of giving a confusing picture of reality.

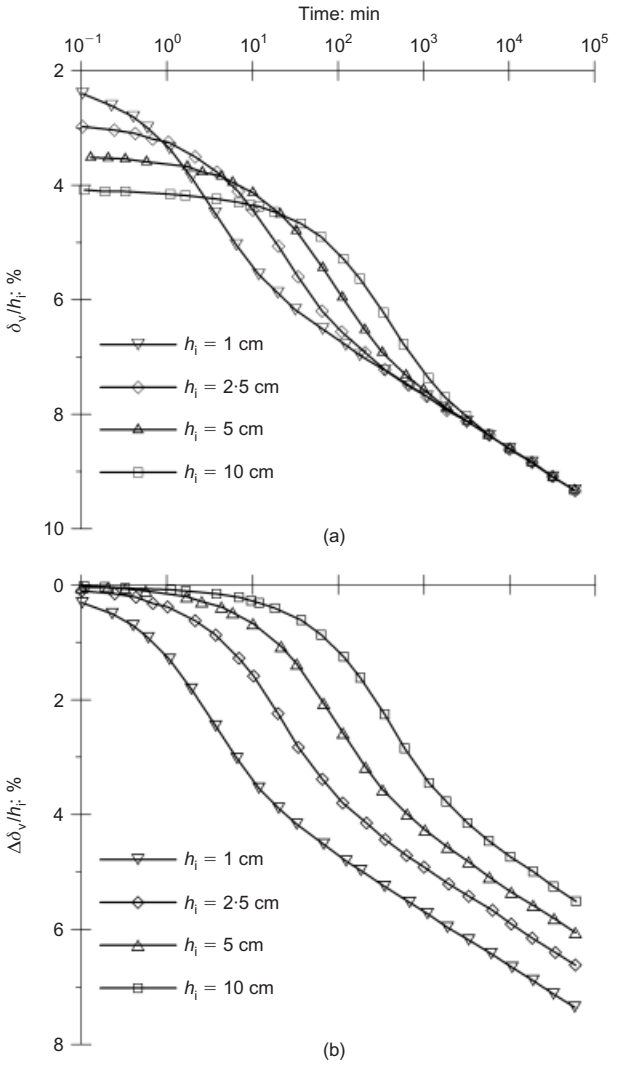

Fig. 10. Consolidation curves for load increment from 230 to 430 kPa in terms of (a) overall nominal strain; (b) incremental nominal strains (after Konovalov & Bezvolev, 2005)

CASE II: LOCAL COMPRESSIBILITY OF SOIL ELEMENTS WITHIN A SPECIMEN

Description of the simulation

In this idealised case, the isotache principles are illustrated by considering the local compressibility of soil elements within a specimen. The behaviours of soil elements located at different distances from a drainage boundary are studied for three different stress regimes in reference to the initial p'_c.

A 50 cm thick soil specimen with a diameter of 6·35 cm was studied under isotropic triaxial loading and one-way drainage conditions. A very fine mesh of 15 node elements was adopted under axisymmetric condition. The soil was considered to have an initial preconsolidation stress, p'_c, of 74 kPa, corresponding to a test of one day's duration, between each load increment, in an incremental oedometer test. An incremental loading scheme was adopted with applied isotropic stresses, σ_c, of 14 kPa, 28 kPa, 41 kPa, 62 kPa, 83 kPa and 125 kPa. The loading stages were adopted from a similitude experiment conducted by Feng (1991). All stress increments were applied instantaneously and kept constant until 95% dissipation of the initial excess pore pressure was achieved. The soil parameters adopted for the SCC model are listed in Table 2. These soil parameters represent the Batiscan clay, as reported by Feng (1991). The geometry of the finite-element model is shown in Fig. 11.

Table 2. Soil parameters adopted for isotropic triaxial simulations based on Feng (1991)

Soil parameter	Value
Permeability, k_v: m/day	$6 \times 10-5$
Earth pressure coefficient under virgin loading, K_0^{NC}	0·60
Change of permeability, c_k	1·10
Initial void ratio, e_0	2·25
Modified swelling index, κ^*	0·0084
Modified compression index, λ^*	0·189
Modified creep index, μ^*	0·0059
Friction angle, ϕ: degrees	30
Poisson's ratio for unloading–reloading, ν_{ur}	0·15

Simulation results

Deformation responses were studied at points 1, 2, 3 and 4 (shown in Fig. 11), which divide the thick specimen into equal sections of four 12·5 cm high sub-specimens. The incremental axial compressions of each sub-specimen, $\Delta\delta_v$, are normalised by the initial sub-specimen height, h_i, of 12·5 cm and they are presented for the three different stress regimes with reference to the initial p'_c. Before and after exceeding the initial p'_c, simulation results (Fig. 12(a) and (c)) showed that the incremental deformation–time curves of the four sub-specimens came to the same point at the EOP state. Nevertheless, the same set of curves will never come to the same point at the EOP state for a stress increment that exceeds the initial p'_c (Fig. 12(b)). However, if the whole specimen is left to creep for a very long time after the EOP state, such that the consolidation period becomes

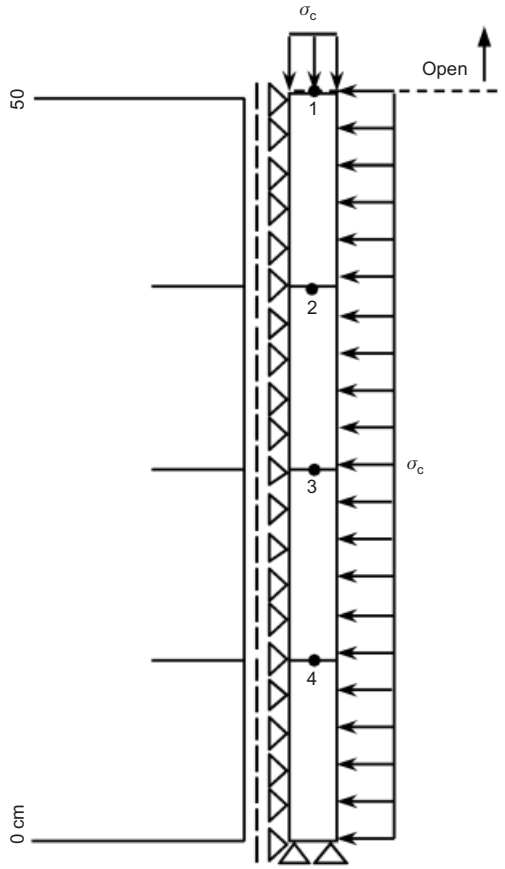

Fig. 11. Axisymmetric FE model of triaxial specimen

an insignificant part of the total time, then all deformation–time curves of the sub-specimens converge to the same point.

The deformation characteristics of different soil elements within one thick specimen are analogous to the deformation behaviour observed in specimens of different thickness, except that in the first case there is one EOP time defined for the whole sample, whereas in the latter case there are different EOP times for the respective thicknesses. The implication of isotaches, for soil elements located at different distances from the drainage boundary (Fig. 11), can be elaborated by considering the interplay between creep rate and the time for which the applied effective stress is sustained (the 'effective creep time'). Even though there is only one EOP time considered for the entire specimen, the sub-specimen that is closest to the drainage boundary (the top sub-specimen) sustains the applied effective stress for a longer time than the sub-specimen located farthest from the drainage boundary (the bottom sub-specimen). This is because consolidation is completed instantaneously at the open drainage boundary and the top sub-specimen immediately continues to the secondary consolidation phase whereas the bottom sub-specimen experiences only the primary consolidation phase. Hence the top sub-specimen has a longer effective creep time than the bottom sub-specimen.

Before exceeding the initial p'_c, all the sub-specimens start at a similar creep rate; however, during an effective stress increment that exceeds the initial p'_c, the effective creep time is different for each sub-specimen, and this leads to different sub-specimen EOP strains. As a result, the sub-specimens closer to the drainage boundary experiences higher EOP strain than the sub-specimens located farther from the drainage boundary. After exceeding the initial p'_c, the top and bottom sub-specimens no longer start at similar

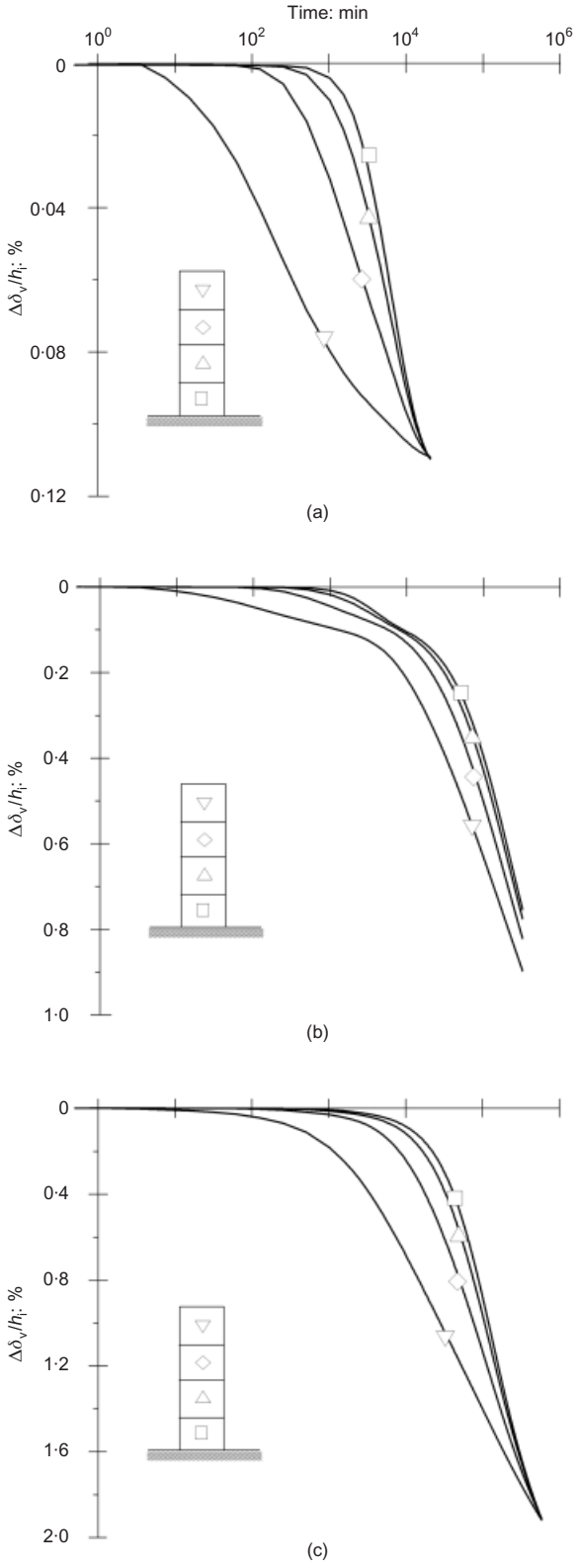

Fig. 12. Incremental nominal strains at different points within one thick specimen with reference to initial p'_c (after Feng, 1991): (a) before exceeding initial p'_c; (b) exceeding initial p'_c; (c) after exceeding initial p'_c

creep rates, as the top sub-specimen has a lower creep rate than the bottom sub-specimen. Hence, for stress increments in the normally consolidated regime, the top sub-specimen deforms with a lower creep rate for a longer effective creep time, whereas the bottom sub-specimen deforms with a higher creep rate for a shorter effective creep time. As a

result, the incremental sub-specimen EOP strains, in the normally consolidated regime, will be practically the same for all sub-specimens.

Experiment by Feng (1991)

Feng (1991) conducted experimental investigations of natural soft clays that included EOP tests of high-quality block samples on Batiscan and St-Hilaire clays. Specimens with an initial thickness of 508 mm and a diameter of 63·5 mm were tested from each of the two clay samples. The 508 mm thick specimen was obtained by interconnecting four 127 mm thick sub-specimens in series. The tests were conducted in triaxial cells with an isotropic incremental loading scheme and one-way drainage condition. The triaxial apparatus was preferred to avoid problems related to side friction that exist in an oedometer cell. Each isotropic load increment was maintained until the final excess pore pressure was approximately 1 kPa. The data acquisition method was primarily based on the total volume change reading of a burette and an axial compression device mounted on the top of each specimen. Similar tests have also been conducted by Choi (1982) on San Francisco Bay Mud and Saint-Alban clay. However, the tests conducted by Feng (1991) are preferred for this illustration, by the virtue of the fact that there exists additional information on the axial compression of each sub-specimen during the test.

The incremental loading sequence for Batiscan clay was 14, 28, 41, 62, 83 and 138 kPa, and for St-Hilaire clay it was 34, 62, 97 and 138 kPa. From the 508 mm thick specimen tests, Feng (1991) estimated the value of the initial preconsolidation stress to be 52 kPa for Batiscan and 76 kPa for St-Hilaire clay.

The compressibility of the clay specimen in the triaxial stress state is preferably studied using the volumetric strains. However, since the volume of water expelled from the individual sub-specimens was not measured during the test, the axial compressions of the individual sub-specimen were studied instead. Such information will equally provide the general trend of the deformation characteristics of the soil elements. The incremental axial nominal strains within each sub-specimen are presented, in Fig. 13, for the three different stress regimes with reference to the initial p'_c.

Feng (1991) was interested in studying the local (sub-specimen) void ratio change within the 508 mm thick specimen in order to investigate the time and stress compressibility of the clays. To do this, the local void ratios had to be interpreted based on the total volume change and four local axial compression measurements. Hence the measured total volume change was distributed among the four sub-specimens using two different approaches, which are described in detail by Feng (1991: 549–554). Feng referred to the two procedures as approach A and approach B. Approach A was used for the stress increments before and after the stress exceeded the initial p'_c, and approach B was used for the stress increment that exceeded the initial p'_c. In approach A, the volumetric deformations were scaled proportionally based on the axial deformations. This resulted in volume–time relationships of the sub-specimens that essentially became analogous to the axial compression–time plot, where the local change in nominal strain at the EOP is identical for all sub-specimens. Hence approach A yielded local volume (void ratio) changes that were unique for all sub-specimens, and Feng considered these interpreted results to be in line with creep hypothesis A. However, Feng opted to use approach B for stress increments that exceeded the initial p'_c. Based on the time–axial compression measurements of the stress increments that spanned the initial p'_c (Fig. 13), Feng argued that 'approach A cannot be used for this increment, since these axial compression curves do not merge with each other at the end of primary consolidation. Therefore a different approach is required.' In other words, if approach A had been used for the stress increment that exceeded the initial p'_c, then the interpreted local void ratio changes would not have been unique for the sub-specimens. In approach B the local volumetric changes are directly calculated assuming the validity of creep hypothesis A. In this way, the local volume change–time plots of the four sub-specimens were 'adjusted' to come to the same point at the EOP state. It should, however, be acknowledged that the measured volumetric changes were considerably larger than the axial compression during this step (i.e. significantly larger horizontal strain than axial strain). The reason for this special behaviour is assumed to be that the soil first started to yield in the horizontal direction before yielding in the axial direction, which means that the horizontal preconsolidation stress was lower than the vertical preconsolidation stress (typical anisotropic behaviour can be found in normally consolidated clay; e.g. Leroueil, 2006). It is, though, still difficult to understand why Feng opted to use a significantly different ratio of horizontal to axial strain, in the different sub-specimens, for the load step that exceeded the initial p'_c. The 'adjusted' results were later presented as 'experimental evidence' showing a unique EOP void ratio for soil elements located within the thick specimen (Feng 1991; Mesri *et al.*, 1994; Mesri, 2003). It is important to note that this 'adjustment' affected all interpreted results that come after exceeding the initial p'_c. Other researchers (Leroueil *et al.*, 1986; Leroueil, 1996, 2006; Leroueil & Marques, 1996) have previously suggested that the reason why the interpreted local void ratio of the sub-specimens of the St-Hilaire clay, for the stress increment of 97–138 kPa (after exceeding the initial p'_c), seemed unique could be due to 'uniformisation' of the strain rate at the EOP state. However, this study has shown that for all the stress increments, starting from the step that exceeds the initial p'_c, there is no 'uniformisation' of strain rate at EOP. It only seemed uniform because the results were reset, and the information on the sub-specimen isotaches was hidden. It is clear that it is only the incremental axial compression–time curves that converge to the same point for the stress increment after the initial p'_c; otherwise, the absolute axial compression curves will maintain their differences, which arose while exceeding the initial p'_c.

The trends of the experimental results of both Batiscan and St-Hilaire clays (Fig. 13) are in complete agreement with the isotache concept as illustrated in the idealised case II (Fig. 12). In all cases the axial deformations are presented in terms of the change in nominal strain. These curves start and end at the same point for stress increments before and after the initial p'_c, but will never come to the same point for the stress increment that exceeds the initial p'_c. In fact, the results of idealised case II, which were simulated using representative parameters of Batiscan clay, show very good agreement with the experimental observations shown in Fig. 13(a), (c) and (e).

CONCLUSIONS

With regard to the effect of creep during primary consolidation, two extreme cases, named creep hypotheses A and B, have been used as a basis of discussion. Various laboratory data as well as field observations have been presented in the literature that seem to support either of the two hypotheses. Therefore the main motivation of this work was to explain, in a consistent manner, laboratory test results relevant to the two creep hypotheses. As a result, selected test results are thoroughly studied and critically assessed.

In response to the important question raised by Ladd *et*

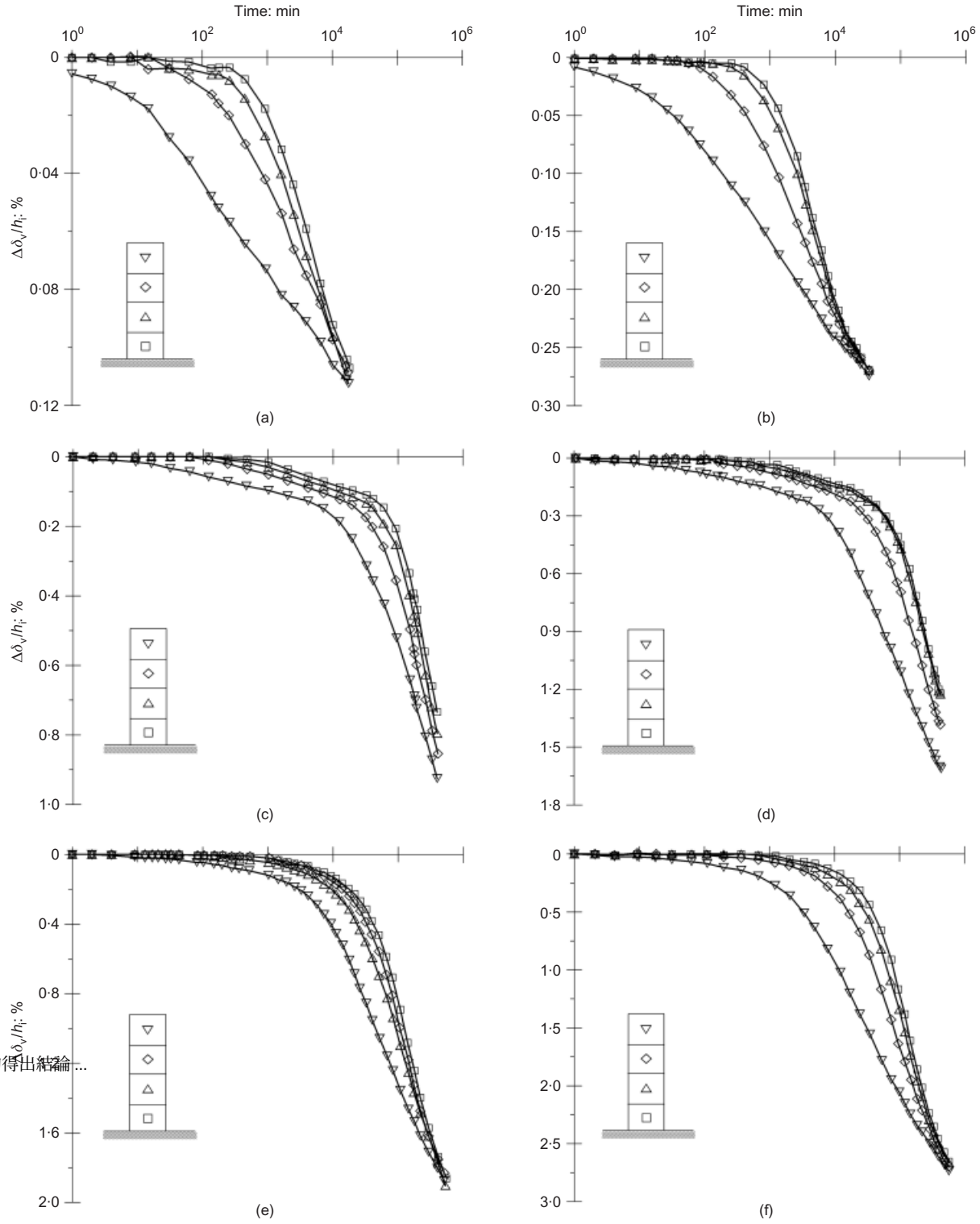

Fig. 13. Incremental sub-specimen nominal strains against time: before exceeding initial p'_c for (a) Batiscan clay, 28–41 kPa, (b) St-Hilaire clay, 34–62 kPa; exceeding initial p'_c for (c) Batiscan clay, 41–62 kPa, (d) St-Hilaire clay, 62–97 kPa; after exceeding initial p'_c for (e) Batiscan clay, 62–83 kPa, (f) St-Hilaire clay, 97–138 kPa (after Feng, 1991)

本研究已表明已有足夠確定數據驗明假說B與粘性土的測得的行為一致。

Aboshi 錯誤的得出結論...

... 但是， 這對一般的應力歷史不適用。從這角度而言， 被研究已證明了假說A是錯的...

al. (1977), this study has shown that there exist definitive data to demonstrate that hypothesis B agrees very well with the measured behaviour of cohesive soils. Experimental observations that were previously used to claim hypothesis A have herein been explained consistently using a model based on the isotache concept.

It is only when considering the incremental strain (change in void ratio), during stress increment in the normally consolidated regime, that there seems to be a unique EOP strain (void ratio) for both the thin and the thick specimens. However, this is not valid for a general stress history. With this aspect, this work has demonstrated that hypothesis A is wrong for stress increments that exceed the initial preconsolidation stress, as well as for stress increments even in the normally consolidated regime when the whole effective stress–strain (void ratio) history is considered. This study has also shown that results that have been used to validate hypothesis A have been presented misleadingly, and in one case also adjusted inconsistently.

An important observation from this study is that the compressibility of clay must be studied taking into account the effect of previous stress history. For single load increment tests it is important to keep track of the starting void ratio, along with the corresponding preconsolidation stress.

Future developments related to the compressibility of natural clays should be focused on enhancing models that are based on the isotache framework. Parts of the important extensions include modelling anisotropy and structure/destructuration effects.

ACKNOWLEDGEMENTS

The work described in this paper is supported by the Research Council of Norway through the International Centre for Geohazards (ICG). Their support is gratefully acknowledged. This is ICG contribution No. 302.

Researchers whose works have been discussed in this paper are greatly acknowledged and appreciated for providing high-quality test results that made this study possible.

REFERENCES

Aboshi, H. (1973). An experimental investigation on the similitude in the consolidation of a soft clay, including the secondary creep settlement. *Proc. 8th Int. Conf. Soil Mech. Found. Engng, Moscow* **4**, No. 3, 88.

Aboshi, H., Matsuda, H. & Okuda, M. (1981). Preconsolidation by separate-type consolidometer. *Proc. 10th Int. Conf. Soil Mech. Found. Engng, Stockholm* **3**, 577–580.

Berre, T. & Iversen, K. (1972). Oedometer tests with different specimen heights on a clay exhibiting large secondary compression. *Géotechnique* **22**, No. 1, 53–70, **doi**: 10.1680/geot.1972.22.1.53.

Bjerrum, L. (1967). Engineering geology of Norwegian normally consolidated marine clays as related to settlements of buildings. *Géotechnique* **17**, No. 2, 81–118, **doi**: 10.1680/geot.1967.17.2.81.

Chih-Hao, T. (2002). *The behavior of compression and consolidation for clays* (in Chinese). PhD thesis, National Central University, Taiwan.

Choi, Y. K. (1982). *Consolidation behavior of natural clays*. PhD thesis, University of Illinois at Urbana-Champaign, Urbana-Illinois.

Degago, S. A., Grimstad, G., Jostad, H. P. & Nordal, S. (2009). The non-uniqueness of the end-of-primary (EOP) void ratio-effective stress relationship. *Proc. 17th Int. Conf. Soil Mech. Geotech. Engng, Alexandria* **1**, 324–327.

Degago, S. A., Jostad, H. P., Olsson, M., Grimstad, G. & Nordal, S. (2010). Time- and stress-compressibility of clays during primary consolidation. *Proc. 7th Eur. Conf. Numer. Methods Geotech. Engng, Trondheim*, 125–130.

Den Haan, E. J. (1996). A compression model for non-brittle soft clays and peat. *Géotechnique* **46**, No. 1, 1–16, **doi**: 10.1680/geot.1996.46.1.1.

Feng, T. W. (1991). *Compressibility and permeability of natural soft clays and surcharging to reduce settlements*. PhD thesis, University of Illinois at Urbana-Champaign, Urbana-Illinois.

Felix, B. (1979). *Fluage et consolidation undimensionnels des sols argileux*. PhD thesis, DI Paris VI (in French).

Grimstad, G. & Degago, S.A. (2010). A non-associated creep model for structured anisotropic clay (n-SAC). *Proc. 7th Eur. Conf. Numer. Methods Geotech. Engng, Trondheim*, 3–8.

Grimstad, G., Degago, S. A., Nordal, S. & Karstunen, M. (2010). Modeling creep and rate effects in structured anisotropic soft clays. *Acta Geotech*. **5**, No. 1, 69–81.

Hawlader, B. C., Muhunthan, B. & Imai, G. (2003). Viscosity effects on one-dimensional consolidation of clay. *ASCE Int. J. Geomech*. **3**, No. 1, 99–110.

Imai, G. & Tang, Y. X. (1992). Constitutive equation of one-dimensional consolidation derived from inter-connected tests. *Soils Found*. **32**, No. 2, 83–96.

Imai, G., Tanaka, Y. & Saegusa, H. (2003). One-dimensional consolidation modeling based on the isotache law for normally consolidated clays. *Soils Found*. **43**, No. 4, 173–188.

Janbu, N. (1969). The resistance concept applied to deformations of soils. *Proc. 7th Int. Conf. Soil Mech. Found. Engng, Mexico City* **1**, 191–196.

Kabbaj, M., Tavenas, F. & Leroueil, S. (1988). In situ and laboratory stress–strain relations. *Géotechnique* **38**, No. 1, 83–100, **doi**: 10.1680/geot.1988.38.1.83.

Karim, M. R., Gnanendran, C. T., Lo, S.-C. R. & Mak, J. (2010). Predicting the long term performance of a wide embankment on soft soil using an elastic-viscoplastic model. *Can. Geotech. J.* **47**, No. 2, 244–257.

Kim, Y. T. & Leroueil, S. (2001). Modeling the viscoplastic behavior of clays during consolidation: application to Berthierville clay in both laboratory and field conditions. *Can. Geotech. J.* **38**, No. 3, 484–497.

Konovalov, P. A. & Bezvolev, S. G. (2005). Analysis of results of consolidation tests of saturated clayey soils. *Soil Mech. Found. Engng* **42**, No. 3, 81–85.

Kutter, B. L. & Sathialingam, N. (1992). Elastic-viscoplastic modelling of the rate-dependent behaviour of clays. *Géotechnique* **42**, No. 3, 427–442, **doi**: 10.1680/geot.1992.42.3.427.

Ladd, C. C., Foott, R., Ishihara, K., Schlosser, F. & Poulos, H. G. (1977). Stress-deformation and strength characteristics. state-of-the-art report. *Proc. 9th Int. Conf. Soil Mech. Found. Engng, Tokyo* **2**, 421–494.

Laloui, L., Leroueil, S. & Chalindar, S. (2008). Modeling the combined effect of strain rate and temperature on one-dimensional compression of soils. *Can. Geotech. J.* **45**, No. 12, 1765–1777.

Larsson, R. & Mattsson, H. (2003). *Settlements and shear strength increase below embankments*, Report 63. Linköping: Swedish Geotechnical Institute.

Leoni, M., Karstunen, M. & Vermeer, P. A. (2008). Anisotropic creep model for soft soils. *Géotechnique* **58**, No. 3, 215–226, **doi**: 10.1680/geot.2008.58.3.215.

Leroueil, S. (1996). Compressibility of clays: fundamental and practical aspects. *ASCE J. Geotech. Engng Div.* **122**, No. 7, 534–543.

Leroueil, S. (2006). Šuklje Memorial Lecture: The isotache approach. Where are we 50 years after its development by Professor Šuklje? *Proc. 13th Danube Eur. Conf. Geotech. Engng, Ljubljana* **2**, 55–88.

Leroueil, S. & Marques, M. E. S. (1996). Importance of strain rate and temperature effects in geotechnical engineering. In *Measuring and modeling time dependent soil behaviour* (eds T. C. Sheahan and V. N. Kaliakin), Geotechnical Special Publication 61, pp. 1–60. New York: ASCE

Leroueil, S., Kabbaj, M., Tavenas, F. & Bouchard, R. (1985). Stress–strain–strain rate relation for the compressibility of sensitive natural clays. *Géotechnique* **35**, No. 2, 159–180, **doi**: 10.1680/geot.1985.35.2.159.

Leroueil, S., Kabbaj, M., Tavenas, F. & Bouchard, R. (1986). Closure of 'Stress–strain–strain rate relation for the compressibility of sensitive natural clays' by Leroueil, Kabbaj, Tavenas & Bouchard (1985). *Géotechnique* **36**, No. 2, 288–290, **doi**: 10.1680/geot.1986.36.2.288.

Li, S., Shirako, H., Sugiyama, M. & Akaishi, M. (2004). Time effects on one-dimensional consolidation analysis. *Proc. Schl. Eng. Tokai Univ. Ser. E* **29**, 1–8.

Mesri, G. (1990). Discussion of 'Viscous-elastic-plastic modeling of one-dimensional time-dependent behavior of clays' by Yin & Graham (1989). *Can. Geotech. J.* **27**, No. 2, 259–261.

Mesri, G. (2003). Primary and secondary compression. In *Soil behavior and soft ground construction* (eds J. T. Germaine, T. C. Sheahan and R. V. Whitman), Geotechnical Special Publication 119, pp. 122–166. Reston, VA: ASCE.

Mesri, G. (2009). Discussion of 'Effects of friction and thickness on long-term consolidation behavior of Osaka Bay clays' by Watabe, Udaka, Kobayashi, Tabata & Emura (2008). *Soils Found*. **49**, No. 5, 823–824.

Mesri, G. & Choi, Y. K. (1985). The uniqueness of the end-of-primary (EOP) void ratio-effective stress relationship. *Proc. 11th Int. Conf. Soil Mech. Found. Engng, San Francisco* **2**, 587–590.

Mesri, G. & Godlewski, P. M. (1979). Closure of 'Time and stress-

compressibility interrelationship' by G. Mesri & P. M. Godlewski (1977). *ASCE J. Soil Mech. Found. Div.* **105**, No. GT1, 106–113.

Mesri, G. & Vardhanabhuti, B. (2006). Closure of 'Secondary compression' by Mesri & Vardhanabhuti (2005). *J. Geotech. Geoenviron. Engng* **132**, No. 6, 817–818.

Mesri, G., Lo, D. O. K. & Feng, T. W. (1994). Settlements of embankments on soft clays. *Proceedings of Settlement '94: Vertical and Horizontal Deformations of Foundations and Embankments, College Station, TX* **1**, 8–56.

Mesri, G., Feng, T. W. & Shahien, M. (1995). Compressibility parameters during primary consolidation. *Proceedings of the international symposium on compression and consolidation of clayey soils*, Hiroshima, Vol. 2, pp. 1021–1037.

Nash, D. F. T. (2010). Influence of destructuration of soft clay on time-dependent settlements. *Proc. 7th Eur. Conf. Numer. Methods Geotech. Engng, Trondheim*, 75–80.

Nash, D. F. T. & Ryde, S.J. (2001). Modelling the consolidation of compressible soils subject to creep around vertical drains. *Géotechnique* **51**, No. 4, 257–273, **doi**: 10.1680/geot.2001.51.4.257.

Oka, F. (2005). Computational modelling of large deformations and the failure of geomaterials. Theme lecture. *Proc. 16th Int. Conf. Soil Mech. Geotech. Engng, Osaka* **1**, 47–95.

Oka, F., Adachi, T. & Okano, Y. (1986). Two-dimensional consolidation analysis using an elasto-viscoplastic constitutive equation. *Int. J. Numer. Anal. Methods Geomech*. **10**, No. 1, 1–16.

Stolle, D. F. E., Vermeer, P. A. & Bonnier, P. G. (1999). Consolidation model for a creeping clay. *Can. Geotech. J.* **36**, No. 4, 754–759.

Šuklje, L. (1957). The analysis of the consolidation process by the isotaches method. *Proc. 4th Int. Conf. Soil Mech. Found. Engng, London* **1**, 200–206.

Šuklje, L. (1969). *Rheological aspects of soil mechanics*. London: John Wiley & Sons.

Svanø, G., Christensen, S. & Nordal, S. (1991). A soil model for consolidation and creep. *Proc. 10th Int. Conf. Soil Mech. Found. Engng, Florence* **1**, 269–272.

Tanaka, H. (2005). Consolidation behaviour of natural soils around p_c value-inter-connected oedometer test. *Soils Found*. **45**, No. 3, 97–105.

Tsukada, Y. & Yasuhara, K. (1995). Scale effects in one-dimensional consolidation of clay. *Proceedings of the international symposium on compression and consolidation of clayey soils*, Hiroshima, pp. 211–216.

Vermeer, P. A. & Neher, H. P. (1999). A soft soil model that accounts for creep. In *Beyond 2000 in computational geotechnics: 10 Years of Plaxis* International (ed. R. B. J. Brinkgreve), pp. 249–261. Rotterdam: Balkema

Watabe, Y., Udaka, K., Kobayashi, M., Tabata, T. & Emura, T. (2008a). Effects of friction and thickness on long-term consolidation behavior of Osaka Bay clays. *Soils Found*. **48**, No. 4, 547–561.

Watabe, Y., Udaka, K. & Morikawa, Y. (2008b). Strain rate effect on long-term consolidation of Osaka Bay clay. *Soils Found*. **48**, No. 4, 495–509.

Watabe, Y., Tanaka, M., Sassa, S., Kobayashi, M. & Udaka, K. (2009). Effects of specimen thickness and skeletal structure on consolidation behavior around yield stress. *Proc. 17th Int. Conf. Soil Mech. Geotech. Engng, Alexandria* **1**, 696–699.

Yasuhara, K. (1982). A practical model for secondary compression. *Soils Found*. **22**, No. 4, 45–56.

Yin, J. -H., Zhu, J. G. & Graham, J. (2002). A new elastic-viscoplastic model for time-dependent behavior of normally and over consolidated clays: Theory and verification. *Can. Geotech. J.* **39**, No. 1, 157–173.

Primary Consolidation and Creep of Clays

Samson Abate Degago

CREBS IV, Delft

Norwegian Public Roads Administrations (SVV)
Formerly, Norwegian University of Science and Technology (NTNU)

January 08, 2014

Statens vegvesen
Norwegian Public Roads Administration

To begin with…..

- This study was motivated by the core theme of 1st CREBS workshop held in Oslo in 2006.
- In CREBS II (Pisa, 2007) a need for in-depth study, e.g. in form of a PhD study, was stressed by Adjunct Professor Hans Petter Jostad.
- This study was then initiated and conducted at Norwegian University of Science and Technology (NTNU) (2007–2011) in collaboration with Norwegian Geotechnical Institute (NGI) and Chalmers University of Technology.
- Researchers who are directly involved in this work are acknowledged as
  - ✓ Hans Petter Jostad (NGI)
  - ✓ Gustav Grimstad (NTNU)
  - ✓ Steinar Nordal (NTNU)
  - ✓ Mats Olsson (Chalmers and NCC)
  - ✓ Peter Hedborg (Chalmers)
- The work has also benefited from valuable feedbacks, discussions and review critics by several other researchers.

General

Measurements

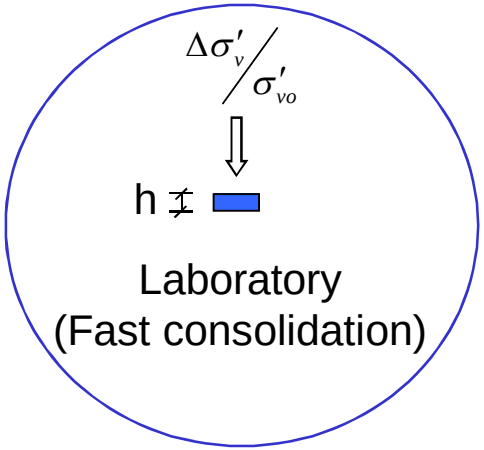

Significantly different consolidation times

Prediction

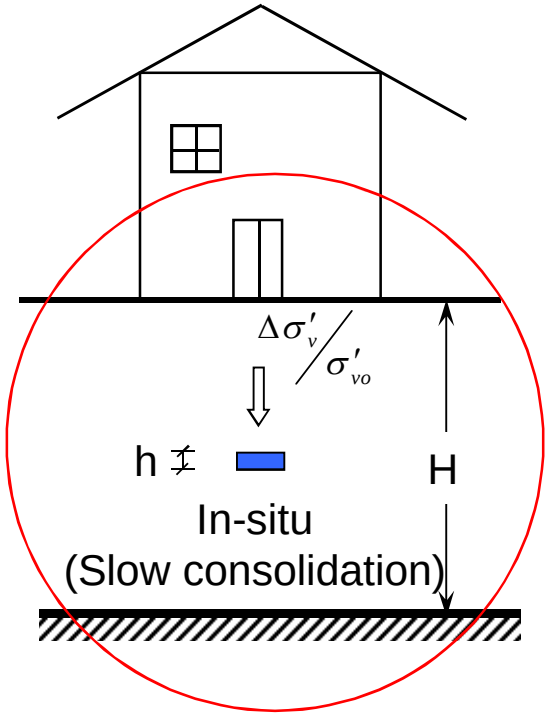

Two hypotheses on role of creep during primary consolidation

- Proposed by Ladd et al. (1977). "*Does creep act as a separate phenomenon while excess pore pressures dissipate during primary consolidation?*"

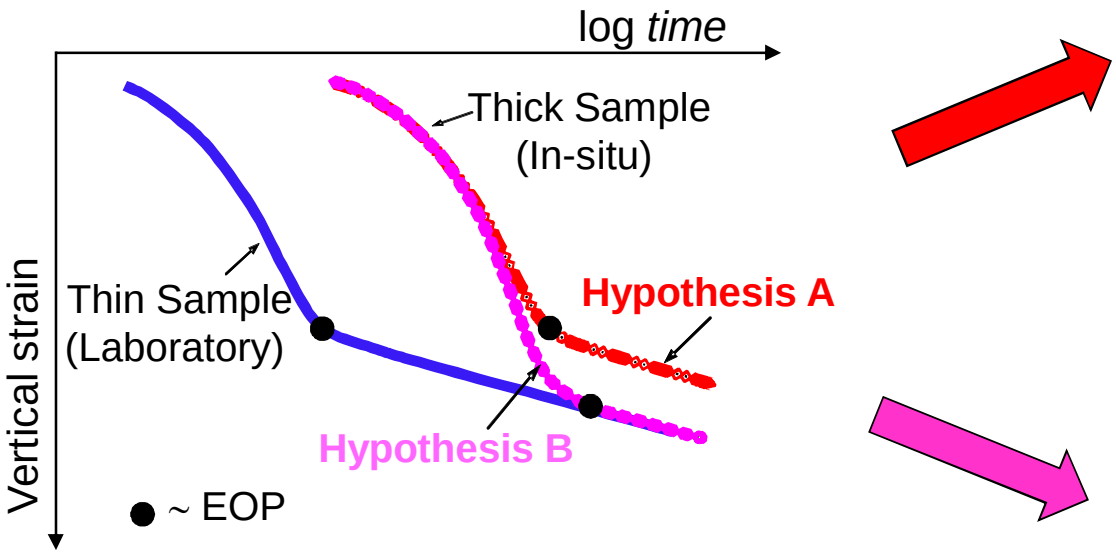

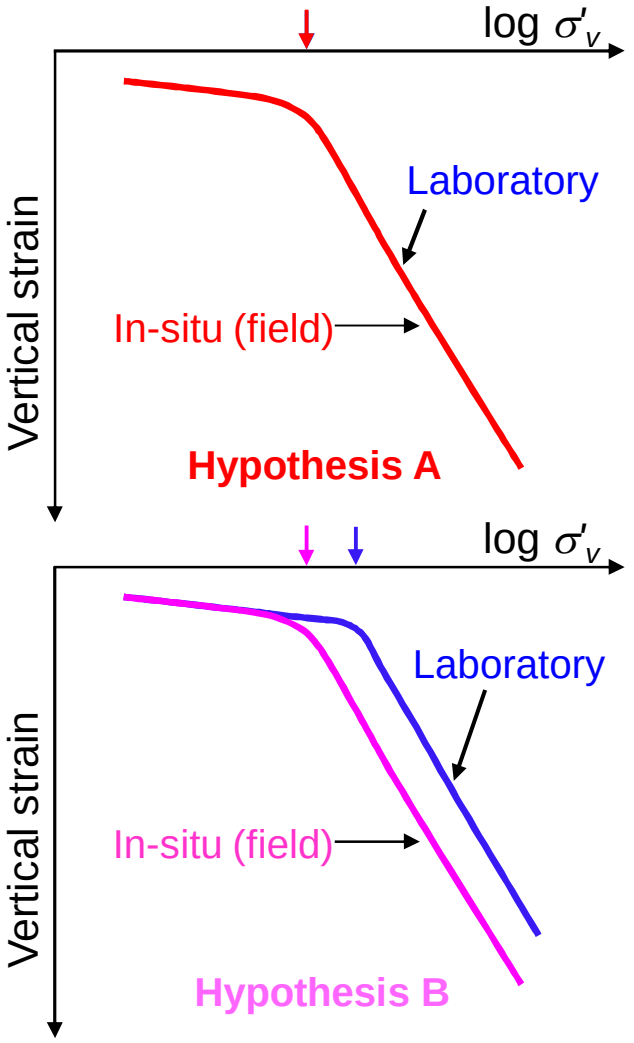

Fig. Hypothesis **A** and **B** (after Ladd *et al.*, 1977)

- Advocates of the two different creep hypotheses have *independently* presented voluminous laboratory and field data to substantiate their opinions.

Experimental substantiation of the two hypotheses, e.g.

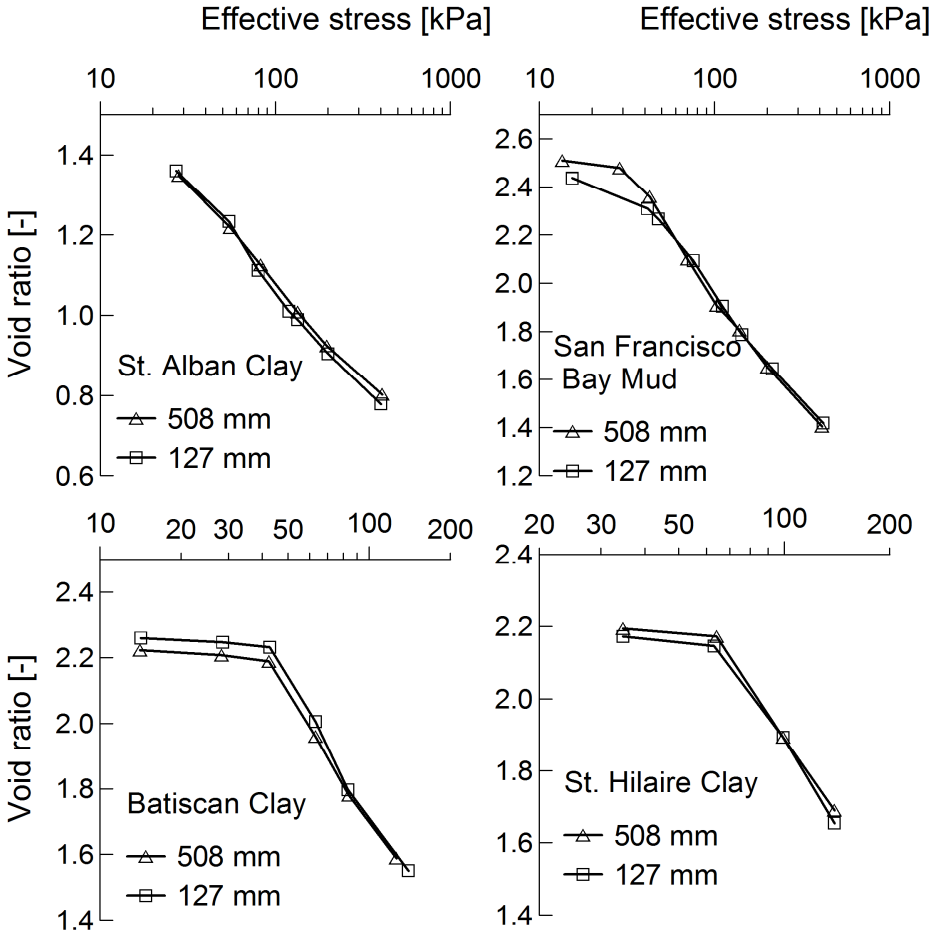

Fig.: EOP laboratory tests supporting **hypothesis A** (after Choi, 1982; Feng, 1991)

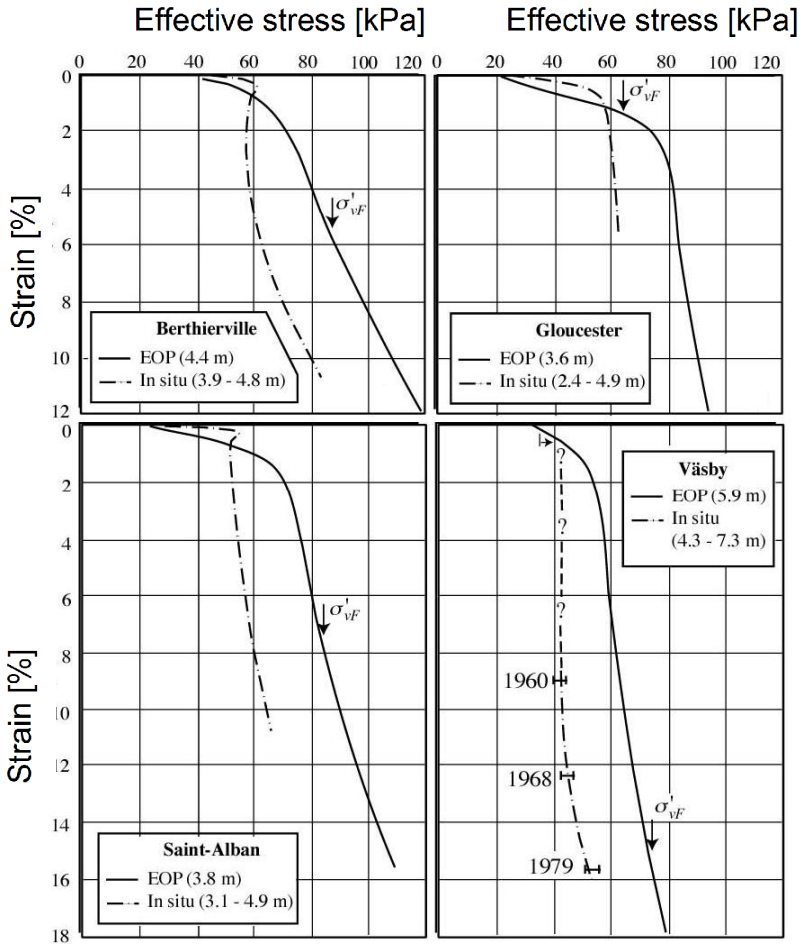

Fig.: In-situ and EOP laboratory tests that support **hypothesis B** (after Kabbaj *et al.*, 1988)

Numerical substantiation of the two hypotheses, e.g.

- Analysis of field cases using constitutive models based on the two hypotheses

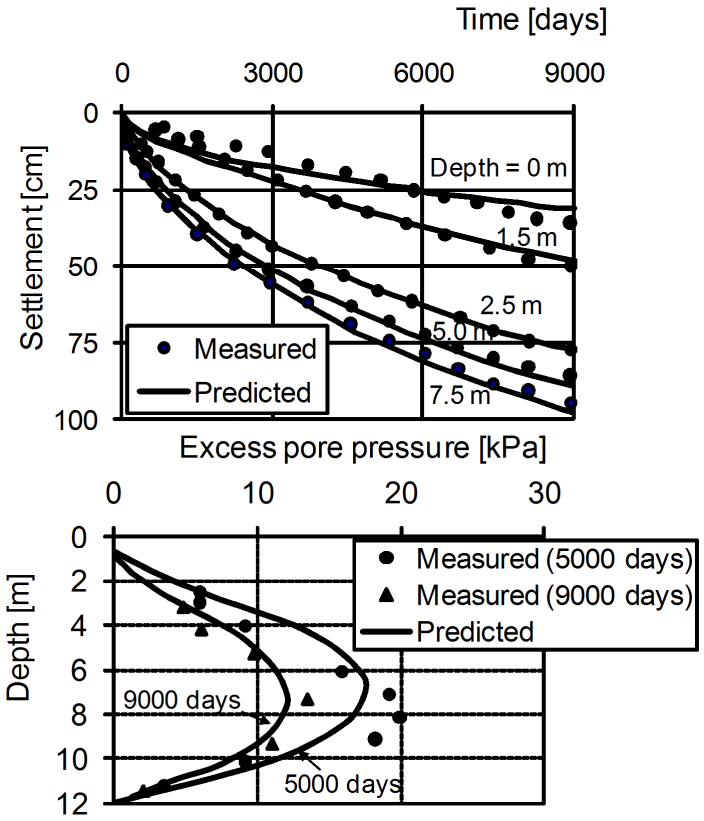

Fig. : Measurement Vs. predictions at Skå-Edeby test fill using **hypothesis A** model (after Mesri and Lo, 1989)

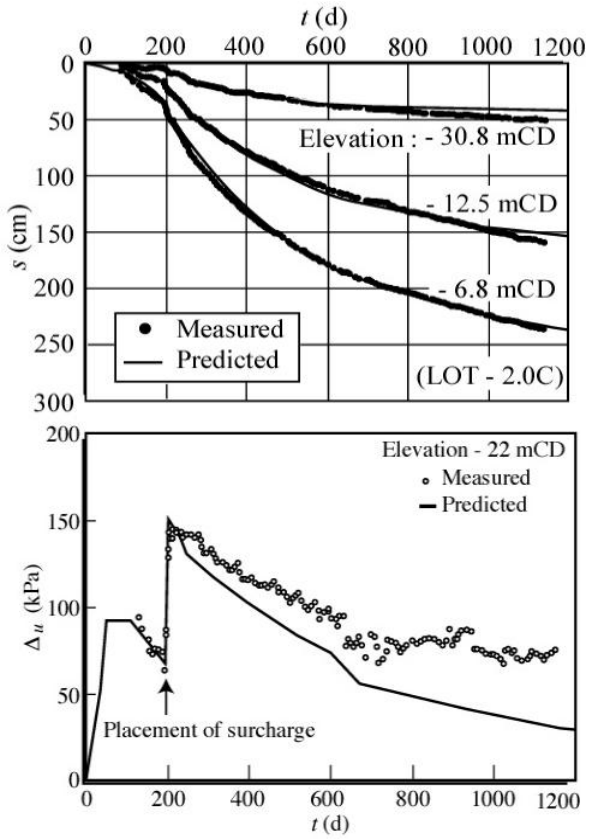

Fig. : Measurements Vs. predictions at Changi Airport using **hypothesis B** model (Cao *et al.*, 2001)

More on the two creep hypotheses

- With an inclination to hypothesis A, Ladd *et al.* in 1977 concluded that "*little definitive data exists to show which of the two hypotheses is more nearly correct for the majority of cohesive soils*".
- Ever since, the topic became a topic of active debate and discussion and remained to be an issue that needed to be resolved.
- This discussion was re-started by NGI in 2006 at 1st CREBS workshop, where advocates from both sides as well as others have attended.
- In 2007, this study was initiated and carried out at NTNU, NGI and Chalmers with additional funding from ICG (International Center for Geohazards).

Main motivation and objectives – CREBS I

- How to extrapolate creep from short time observation to long term predictions ?
- The two conflicting hypotheses are well substantiated with laboratory and field data. Why ?
- Constitutive models based on the two hypotheses are seen to produce acceptable field predictions. Study and evaluate the models based on field cases.
- To increase understanding on time- and stress-compressibility of clays during primary consolidation.
- To produce the most convincing creep hypothesis and a numerical tool that can consistently explain laboratory and field observations.

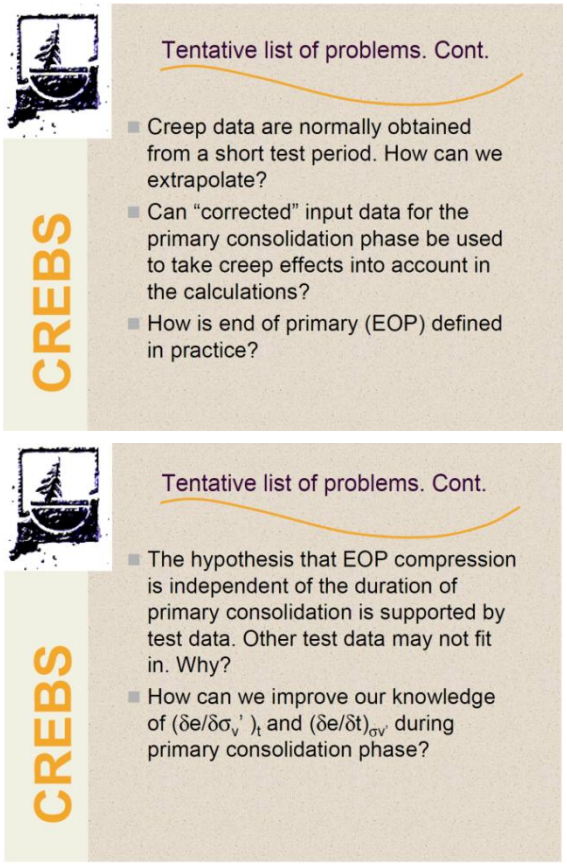

Fig. : Tentative list of problems as presented in the 1st CREBS workshop (Jostad, 2006)

Outline of the presentation

- Laboratory studies
  - Part I: Specimens of varying thicknesses
  - Part II: Soil element compressibility (varying consolidation duration)
- Field studies
- Present the hypotheses for a specific case
  - A look at the relevant laboratory tests
  - Numerical studies

Laboratory studies I: Creep hypotheses for varying soil layer thicknesses

- EOP strain-effective stress relationships: the creep hypotheses

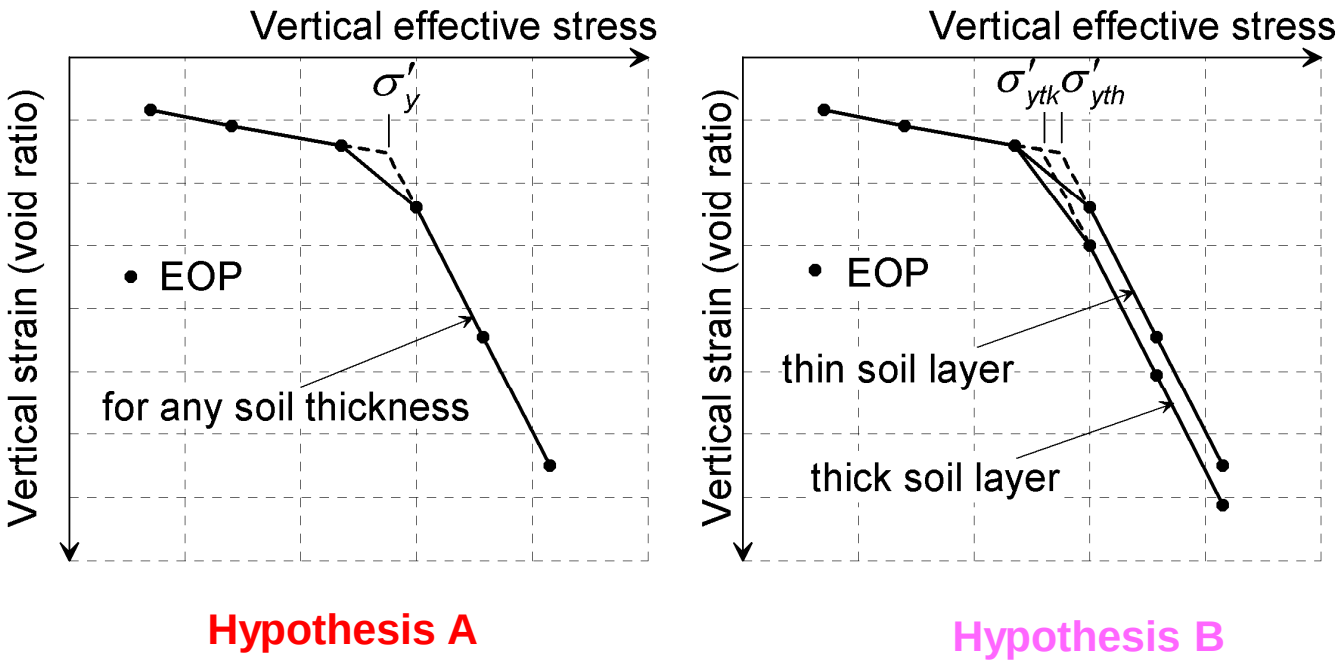

Fig.: Principle sketch of the two creep hypotheses for varying soil layer thicknesses

- EOP strain-effective stress relationships: laboratory tests

- End effects (testing problem) ?

- Strain rate effects ?

✓ Evaluate the 508 mm thick specimen (the action and the reaction)

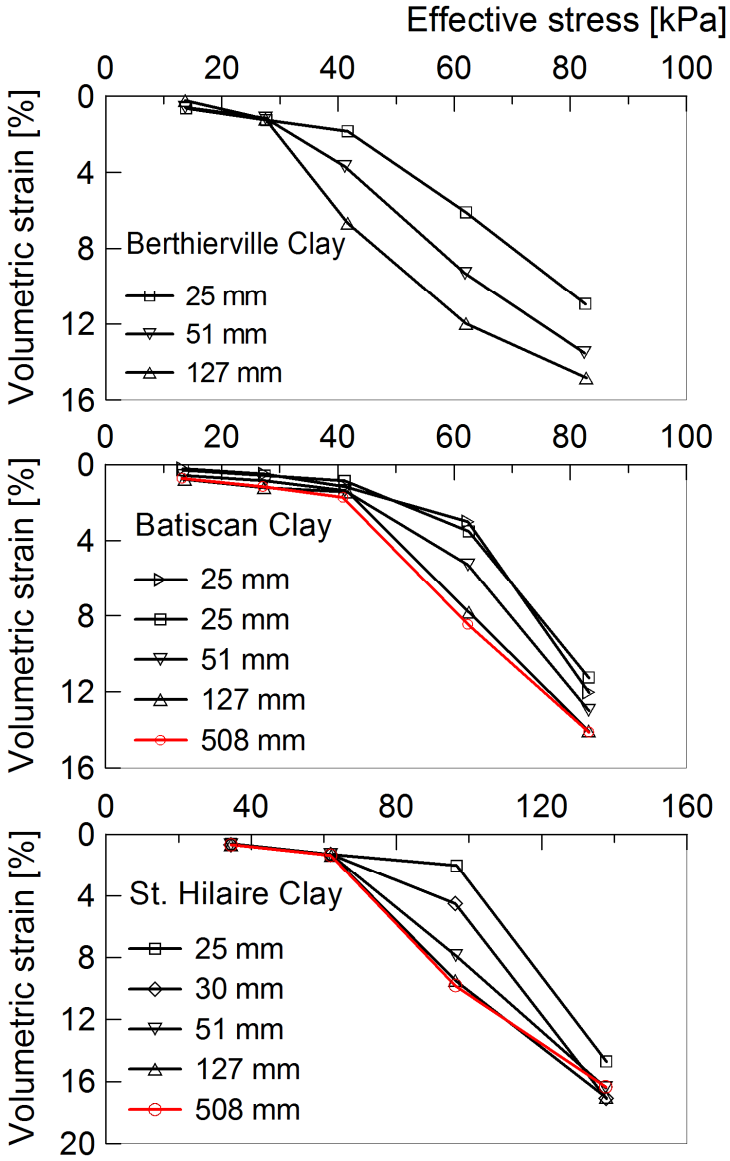

Fig. : EOP $\Delta V/Vo-\sigma'$ relationships for various thicknesses (after Feng, 1991)

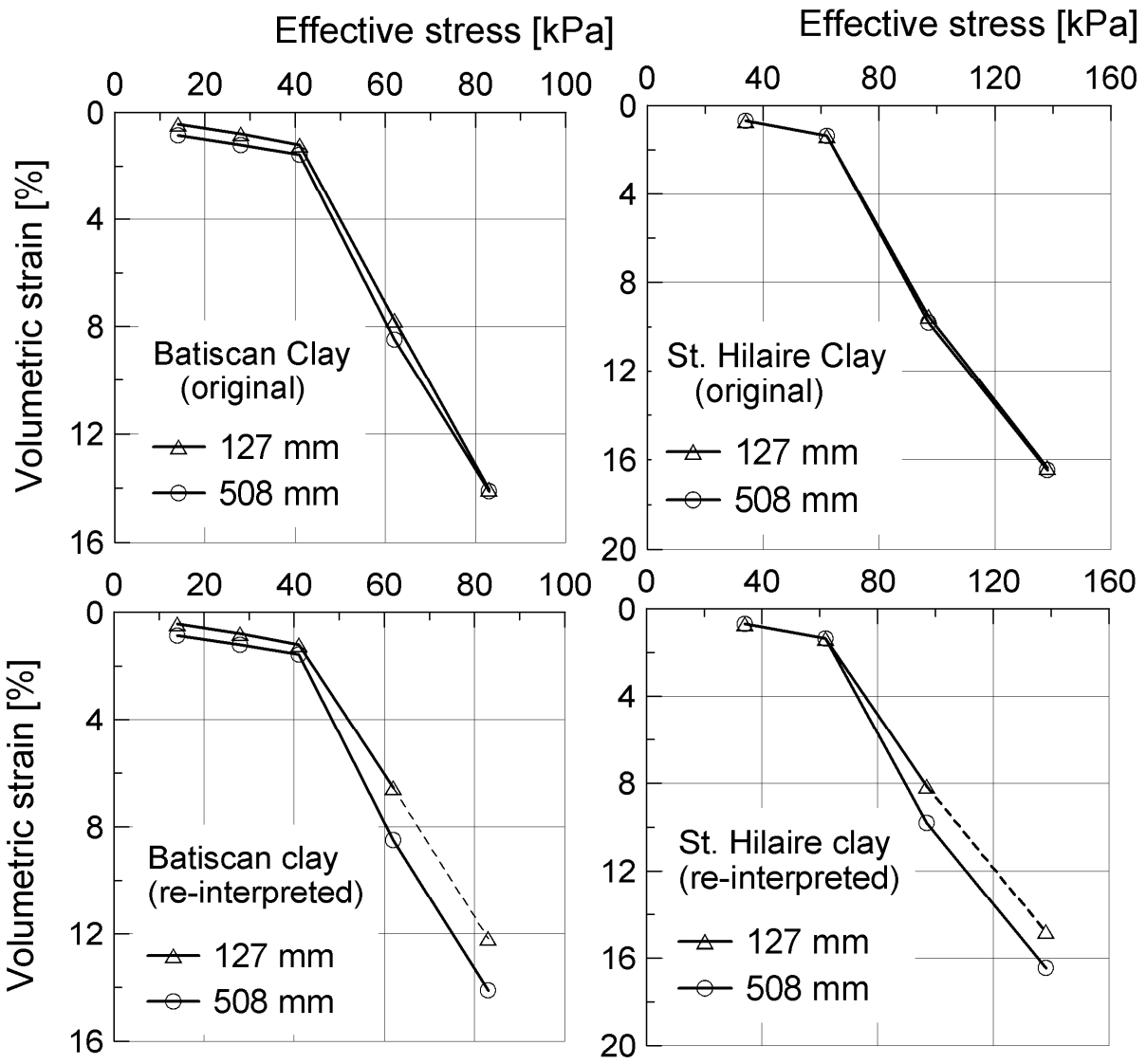

Hyphothesis A

Inconsistent EOP criterion

不一致的主固结完成时间 > 导致错误得支持假设A

Re-interpretation

Hyphothesis B

Consistent EOP criterion

Fig.: Original and re-interpreted volumetric strain–effective stress relationships

Numerical study of raw experimental data with hypothesis B model

- Similar load sequence and duration adopted from the actual test.
- Identical set of soil parameters for the thin and thick specimen
- Three load increments with respect to p'_c

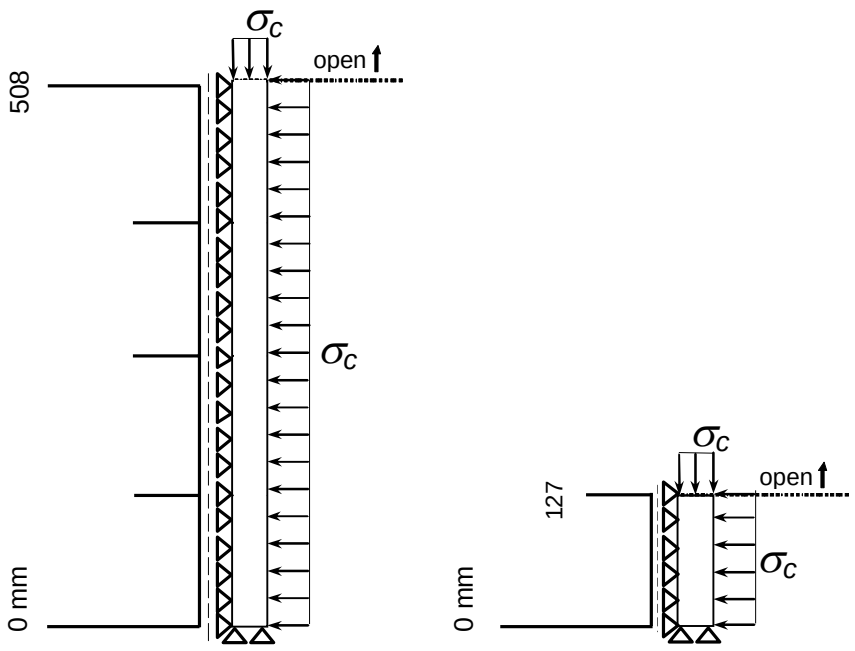

Fig.: Axisymmetric FE-model of the triaxial specimens

- Numerical study of raw experimental data with hypothesis B model

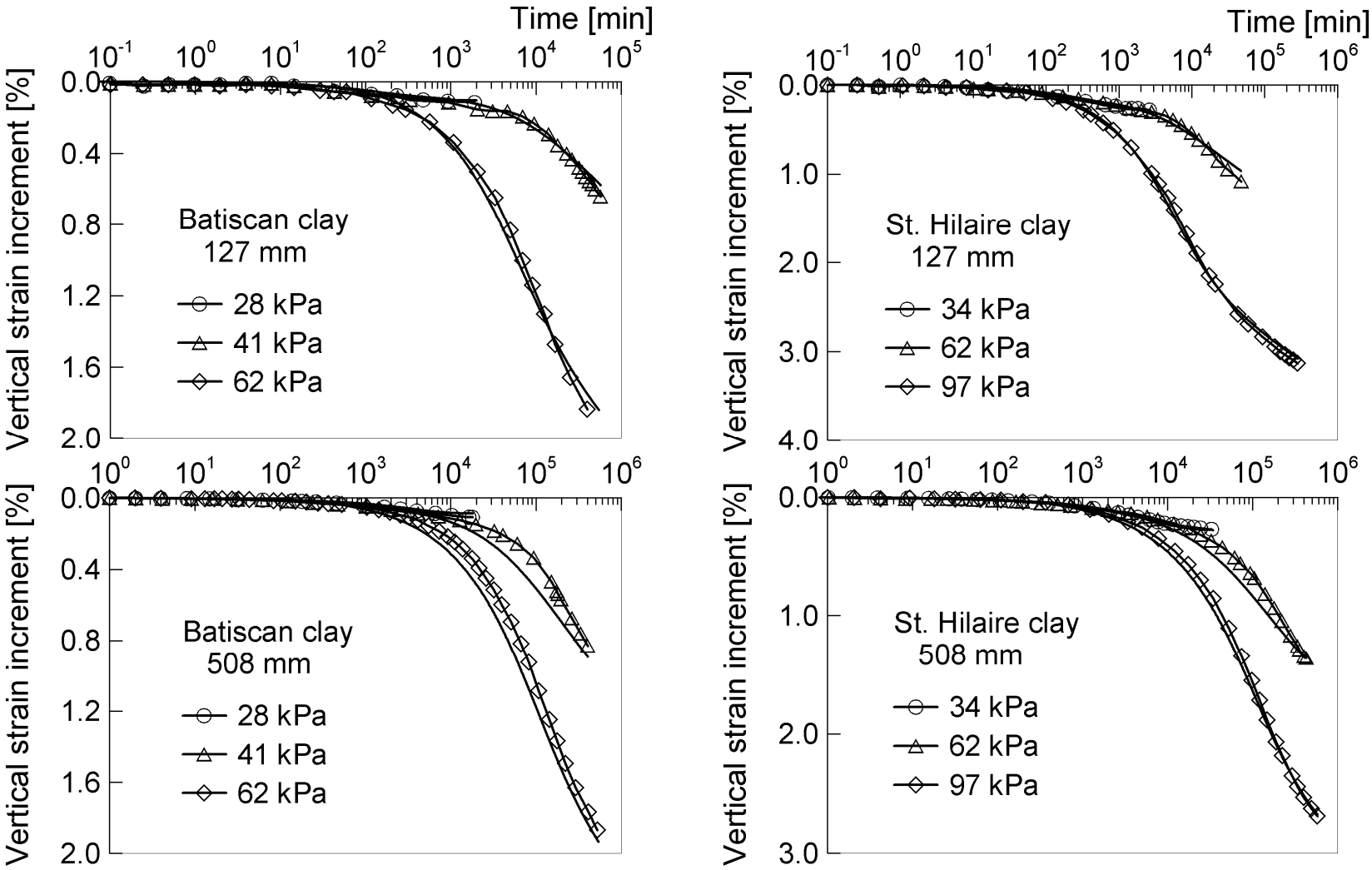

Fig.: Numerical simulation (smooth lines) vs. measurements (lines with symbols)

Strain-time relationships: the creep hypotheses

- Hypothesis A

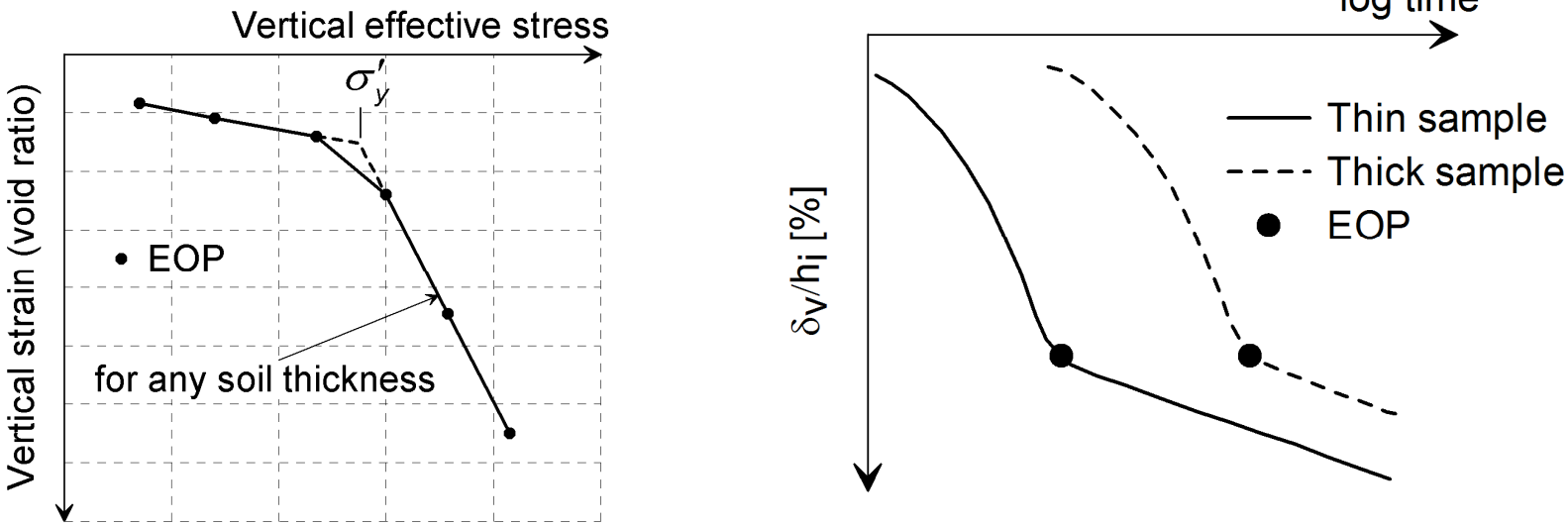

Fig. : Principle sketches of action–response relationships according to hypothesis A

- Hypothesis B

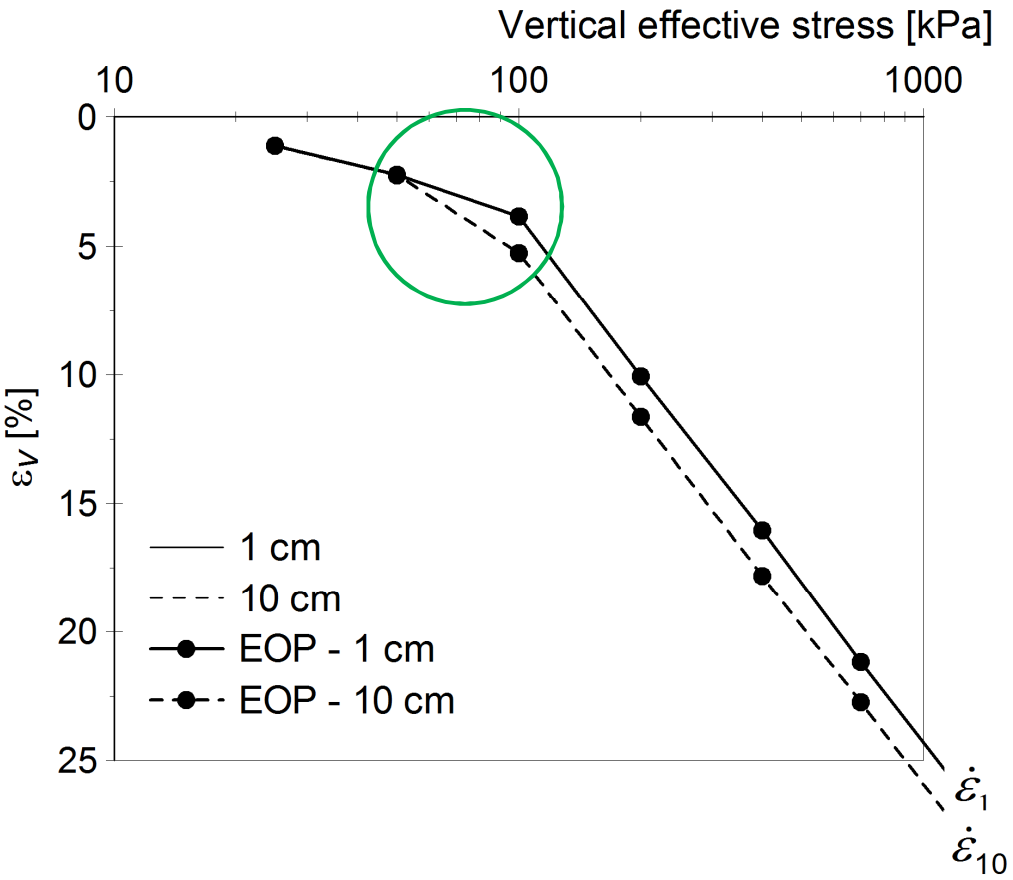

Fig.: Effective stress–Strain and Strain-Time relationships according to hypothesis B

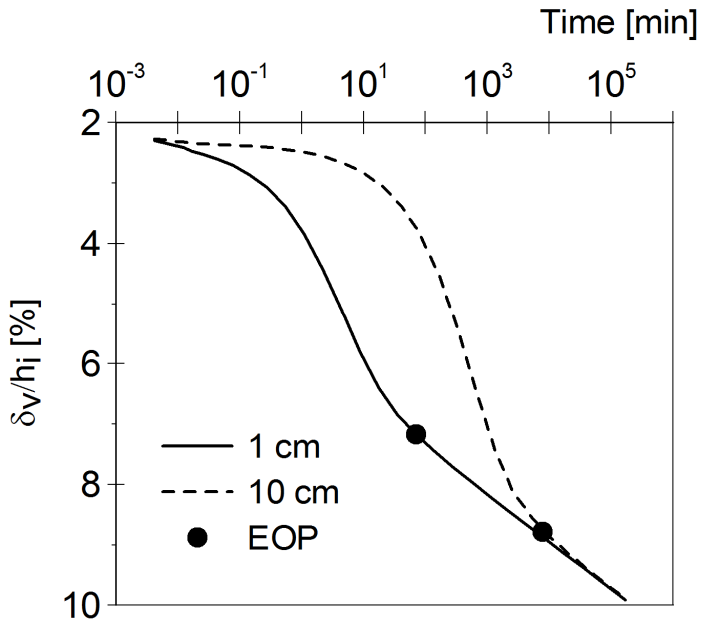

Fig. : $\Delta\sigma'$ = 50–150 kPa, p'_c = 100 kPa (allowed to creep at 150 kPa for 100 days)

- Hypothesis B

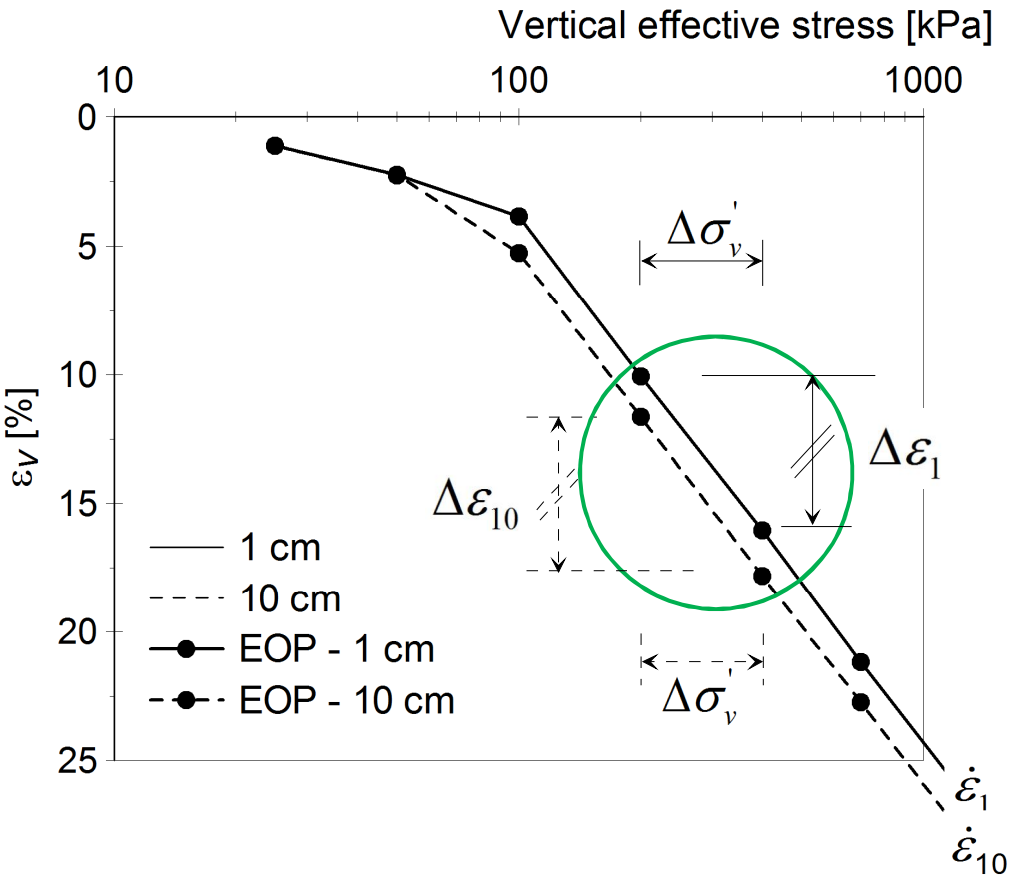

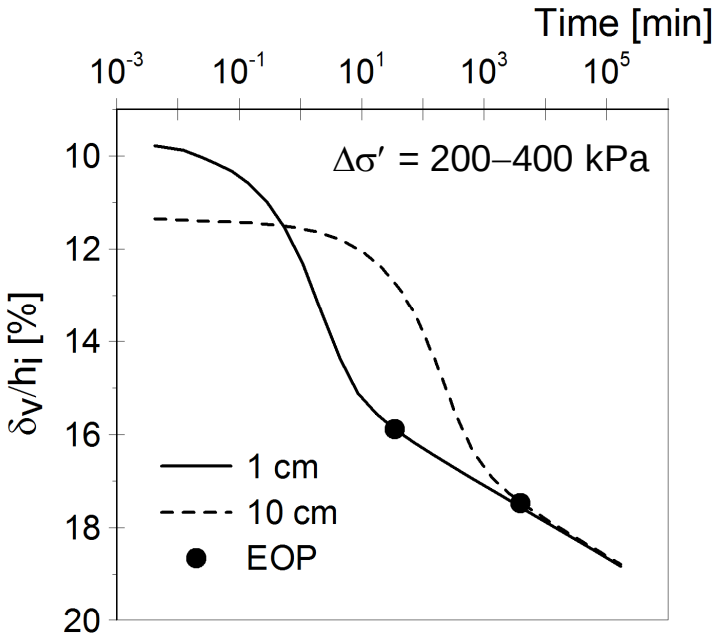

Fig.: Effective stress–Strain and Strain-Time relationships according to hypothesis B

Some typical experimental observations

- Single load increment tests after exceeding initial p'_c

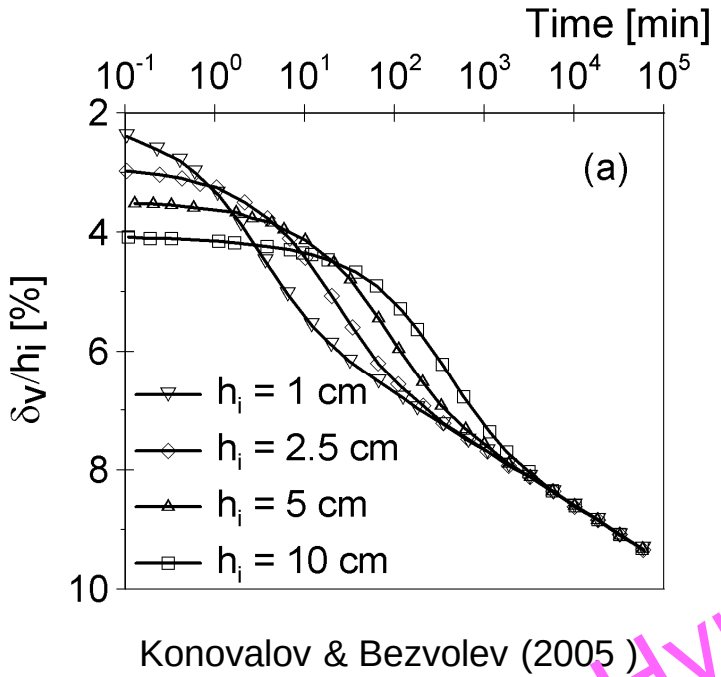

Konovalov & Bezvolev (2005)

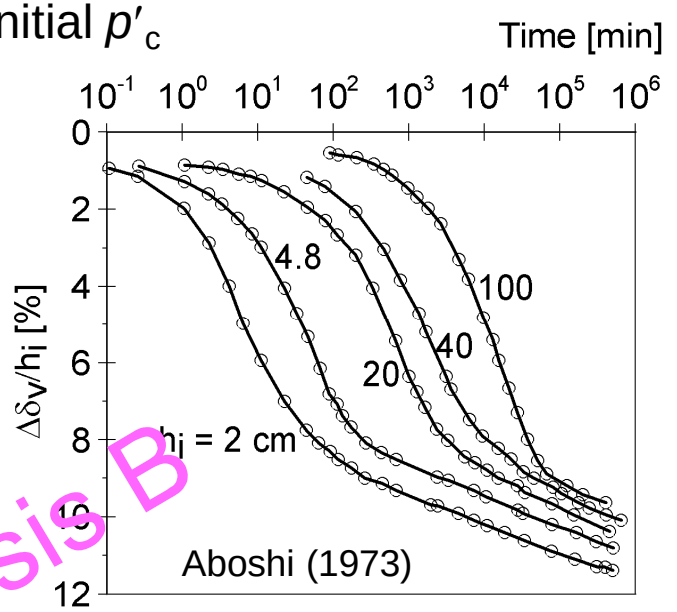

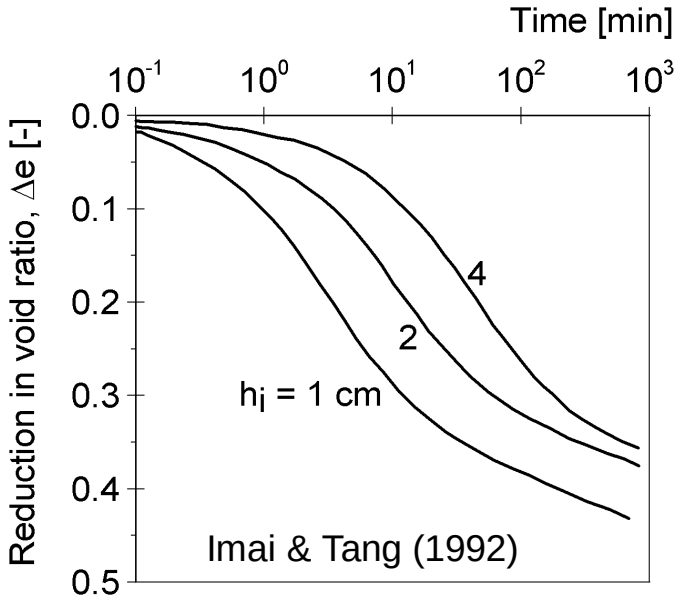

Hypothesis B

(Degago et al. (2011), *Géotechnique* 61(10))

Laboratory studies I: Creep hypotheses for varying soil layer thicknesses

Final remarks

- ✓ Laboratory tests on specimens of varying thicknesses imply hypothesis B.
  - EOP strain-effective stress relationship is not unique.
  - EOP strain increases with increasing consolidation duration
- ✓ Numerical simulation results using hypothesis B model can explain experimental measurements.

Laboratory studies II: Creep hypotheses for soil element compressibility

- The two hypotheses are best differentiated by consolidation duration of soil layers than soil layer thickness

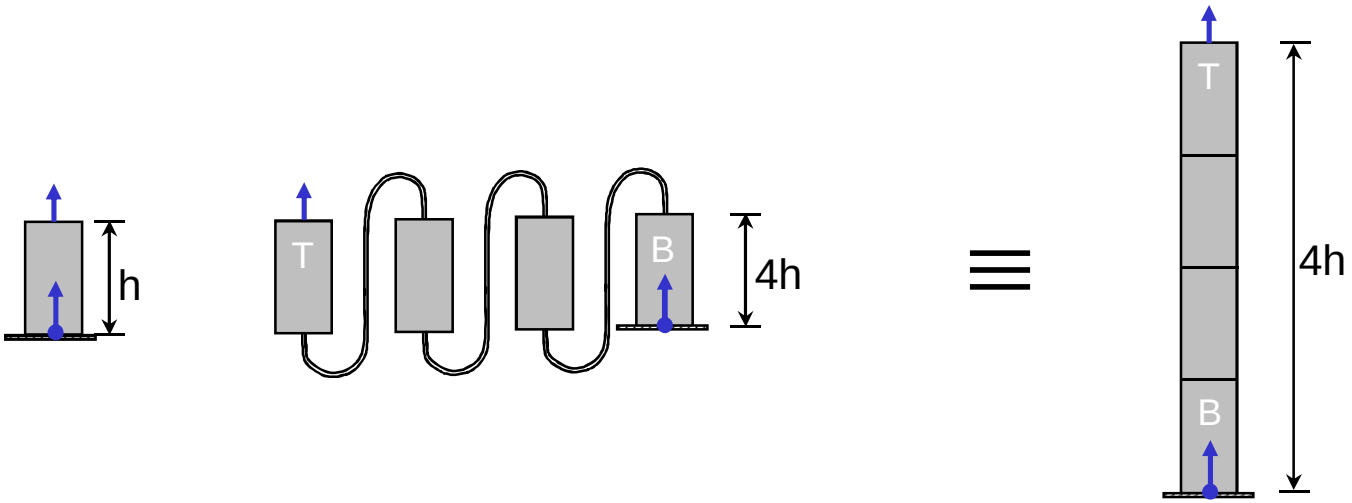

Fig.: Interconnected tests

Creep hypotheses for soil element compressibility

EOP strain-effective stress relationships: the creep hypotheses

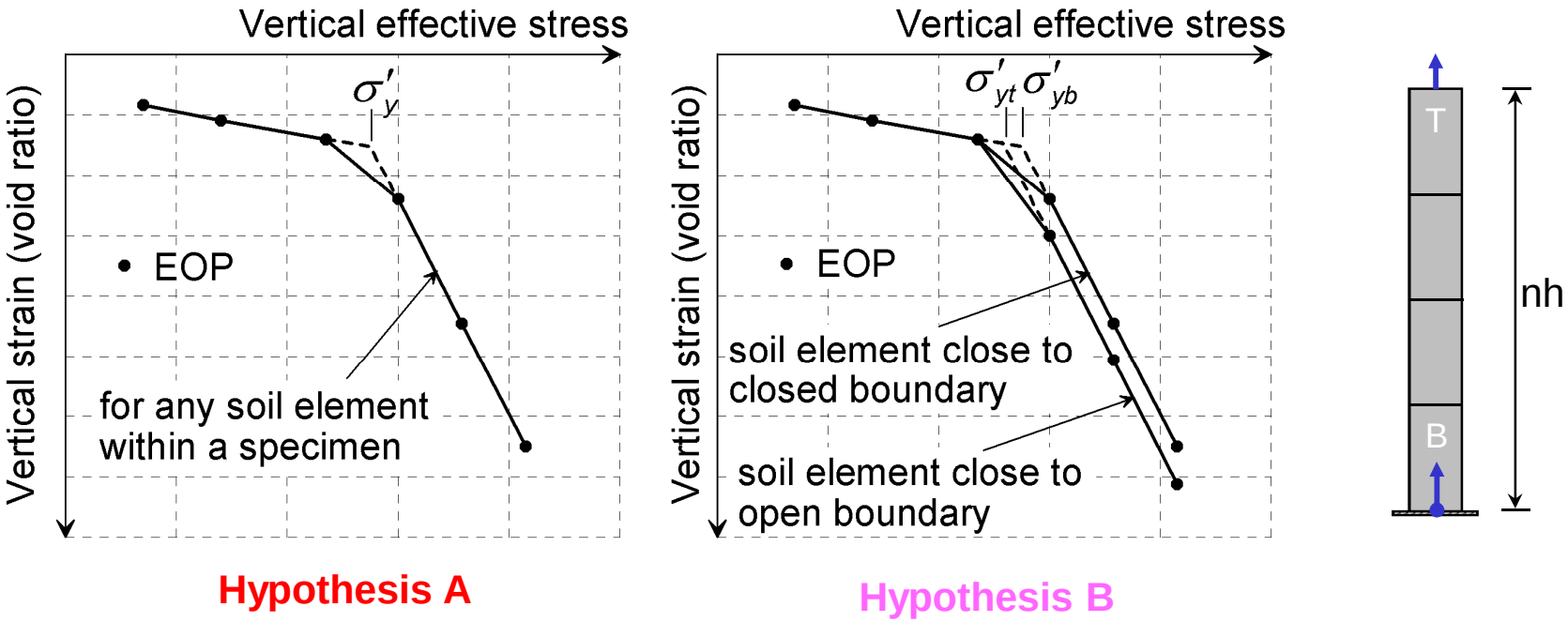

Fig.: Principle sketch of the two creep hypotheses for compressibility of soil elements within a specimen

EOP strain-effective stress relationships: laboratory test results

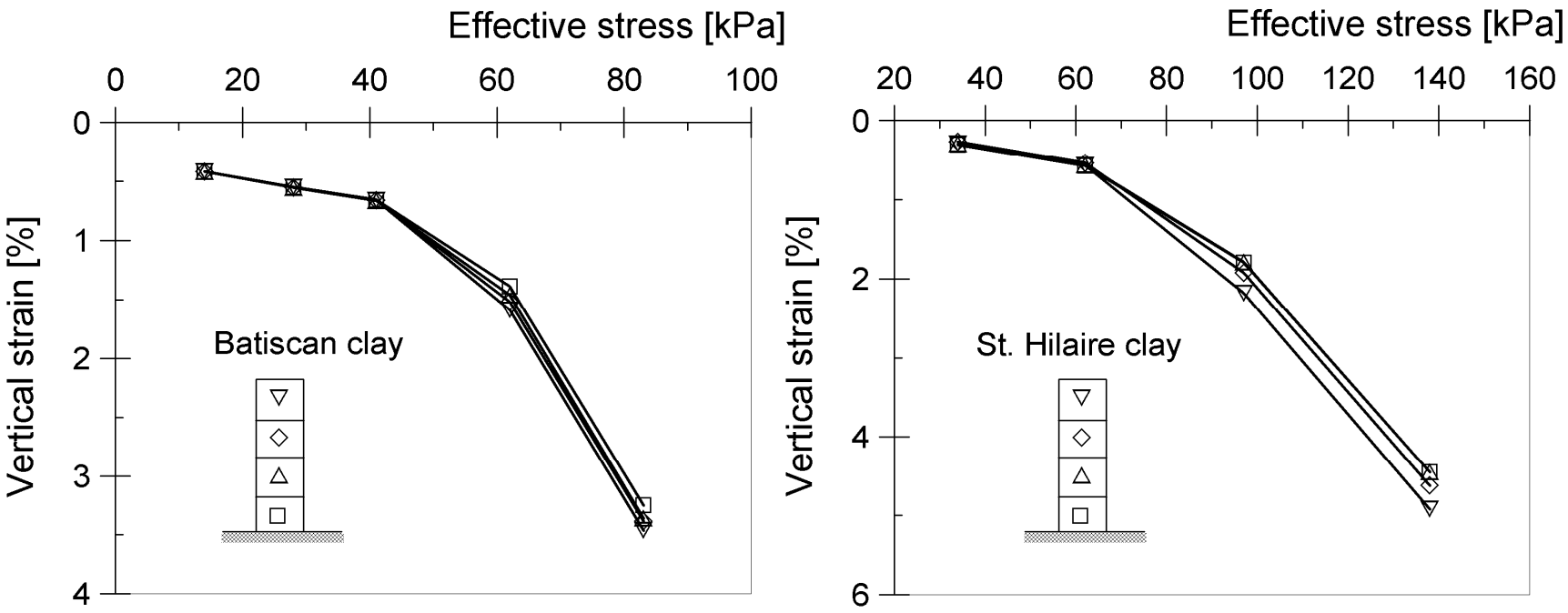

Fig.: EOP vertical strain–effective stress of sub-specimens (interpreted from Feng, 1991)

- Hypothesis B

Strain-time relationships: the creep hypotheses

Hypothesis A

- At EOP, the strain-time relationships of all sub-specimens converge to the same point

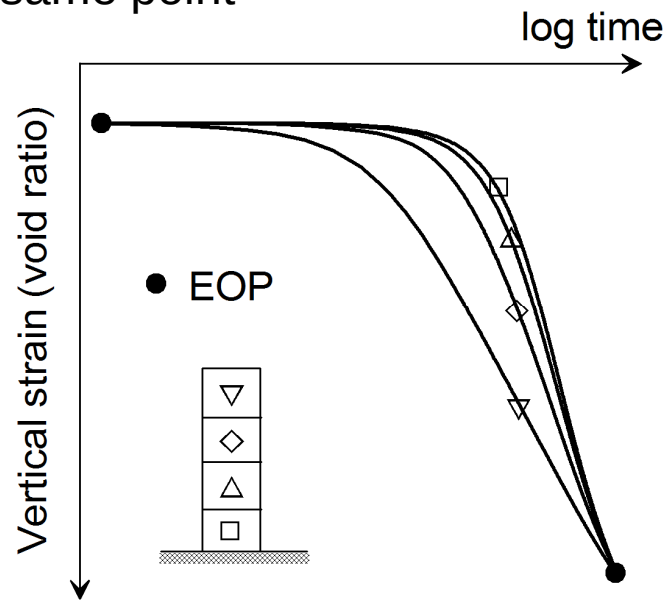

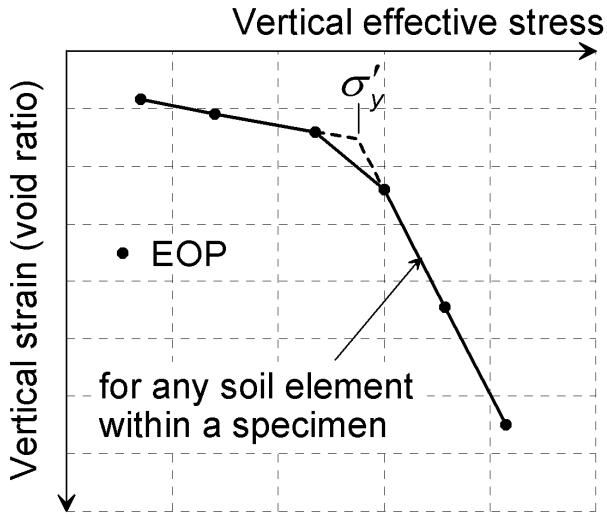

Fig.: Principle sketches of Strain-Time and Effective stress–Strain relationships according to hypothesis A

Hypothesis B

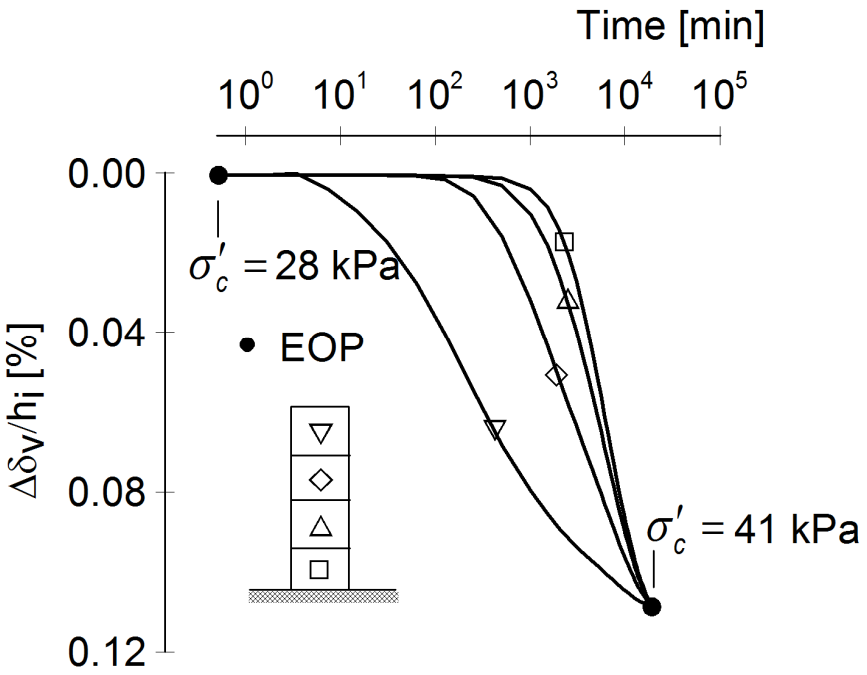

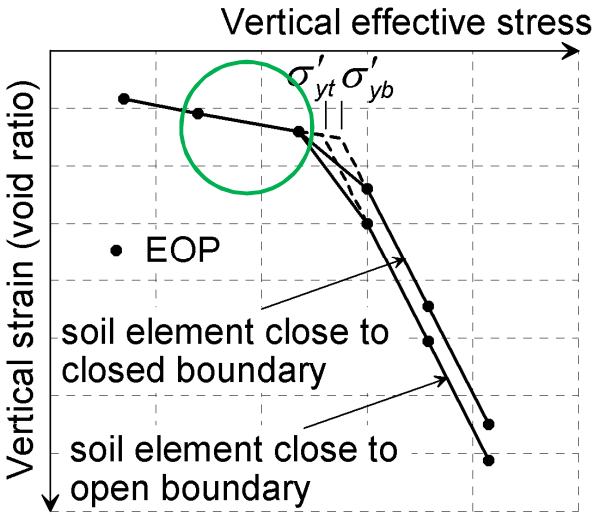

Fig.: Strain-Time and Effective stress–Strain relationships according to hypothesis B

Hypothesis B

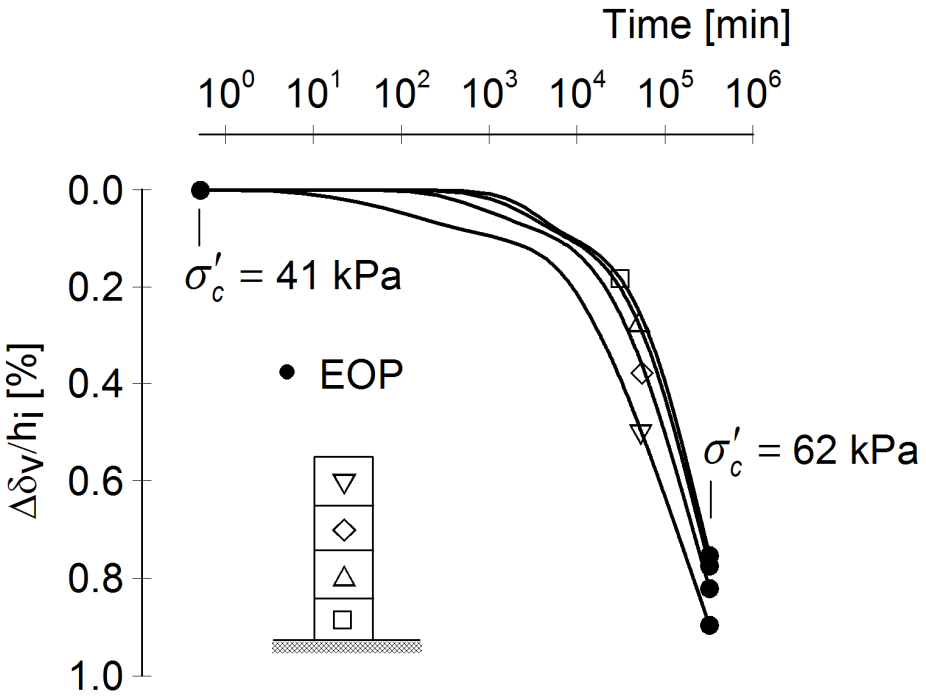

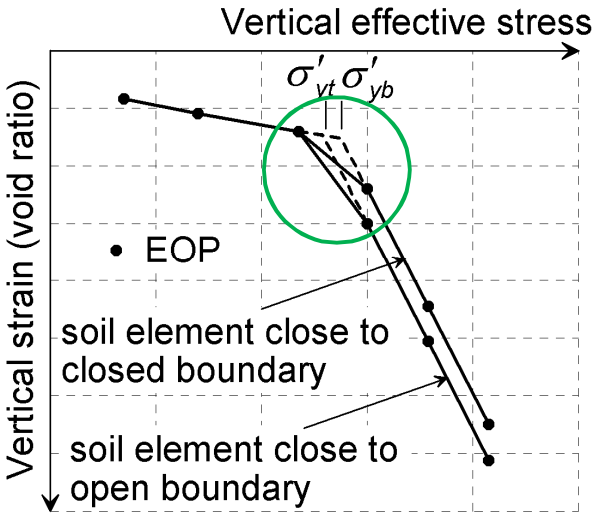

Fig.: Strain-Time and Effective stress–Strain relationships according to hypothesis B

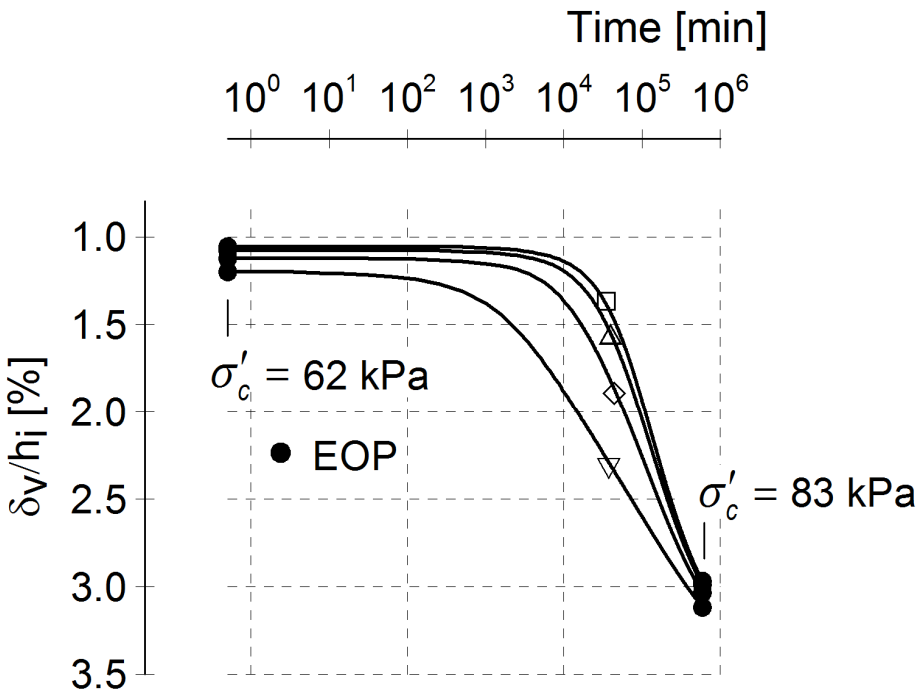

Hypothesis B

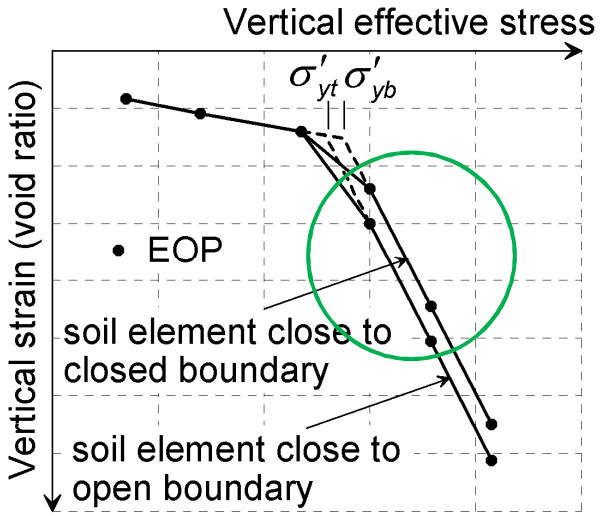

Figure : Strain-Time and Effective stress–Strain relationships according to hypothesis B

Strain-time relationships: laboratory test results

- Hypothesis B

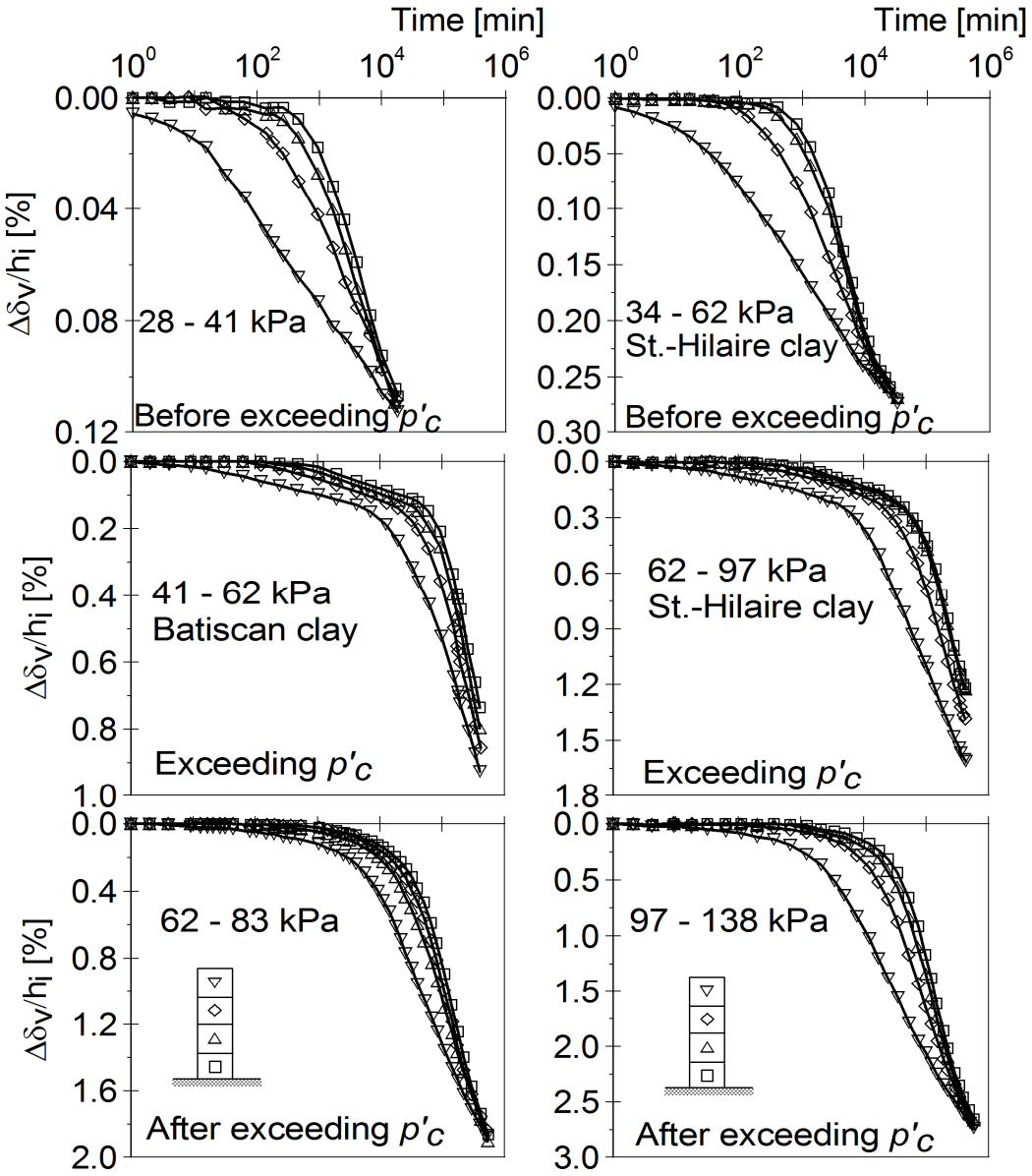

Fig: Experimental results on Batiscan and St. Hilaire clay (Feng, 1991)

- Strain-time relationships: numerical study
- Simulation using hypothesis B (SSC) model
- FE-code PLAXIS

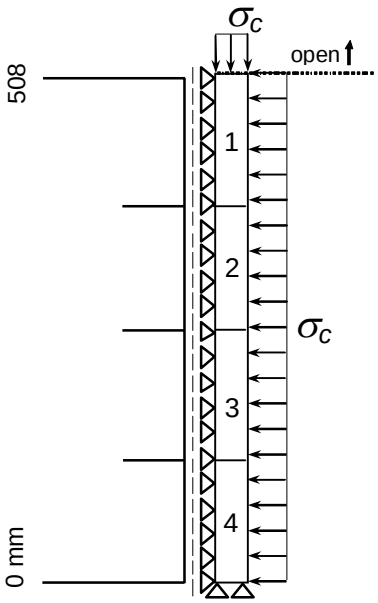

Fig.: Geometry adopted in FE simulation

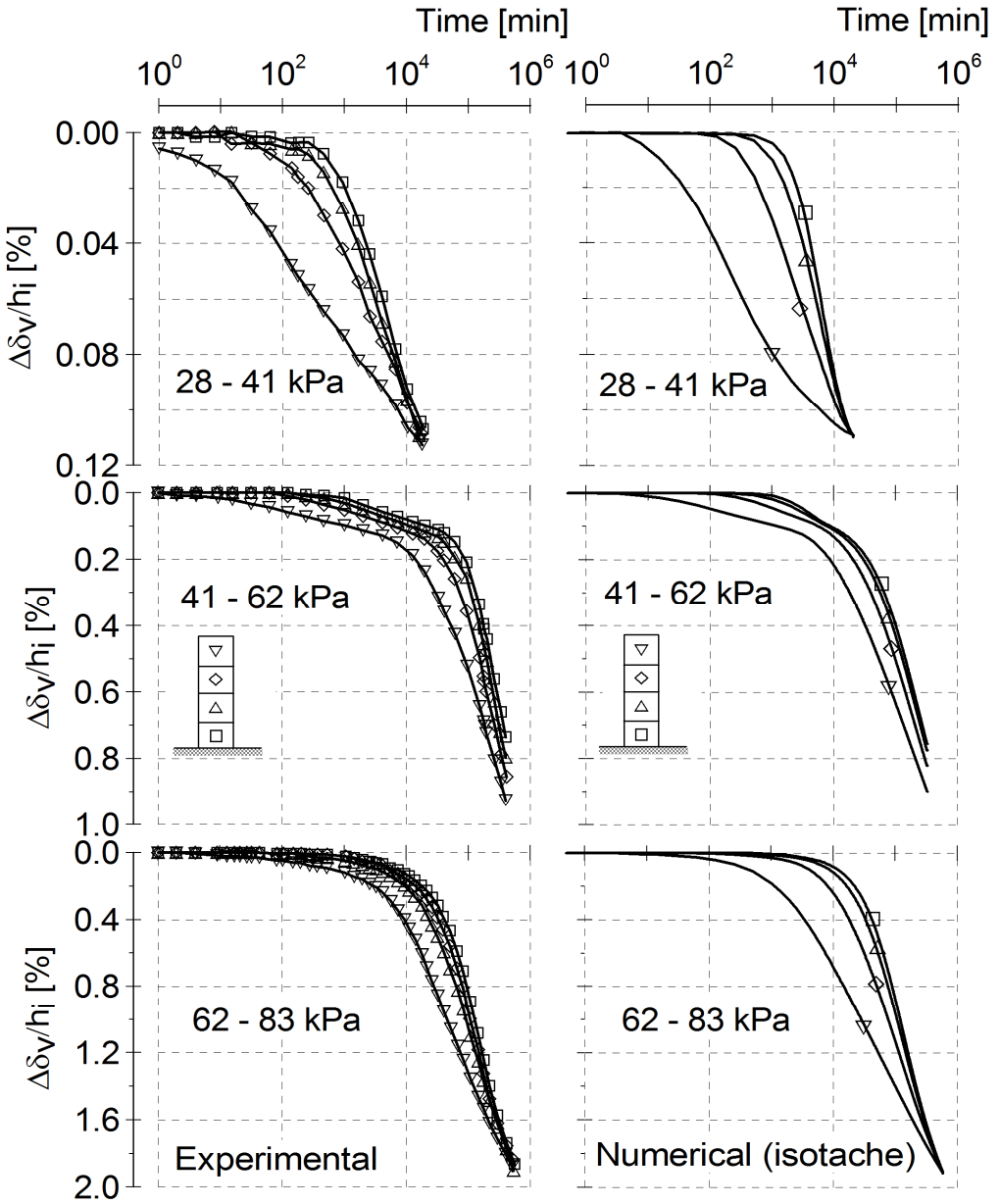

Fig.: Experimental measurements (Feng, 1991) Vs Simulation results of Batiscan clay

Tests conducted during this study

(@Chalmers University of Technology)

Hypothesis A :-

- The sub-layer at the drainage face does not experience any secondary consolidation until EOP state of the bottom sub-layer (Mesri & Vardhanabhuti, 2006).

Motivation

- Will a soil element at the drainage face really 'wait' for the EOP state of the bottom sub-layer to start its secondary consolidation? (Jostad, 2006 @CREBS I)

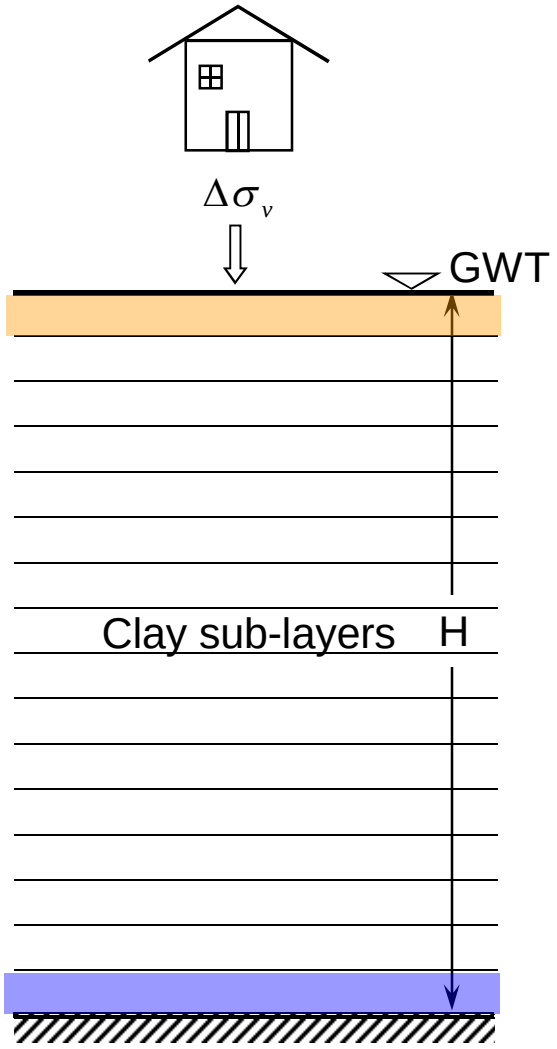

Fig.: A soil layer consisting of several soil sub-layers

An idealized case

- A clay layer placed on top of similar clay as compared to a clay layer placed on top of a soil material with different coefficient of consolidation.

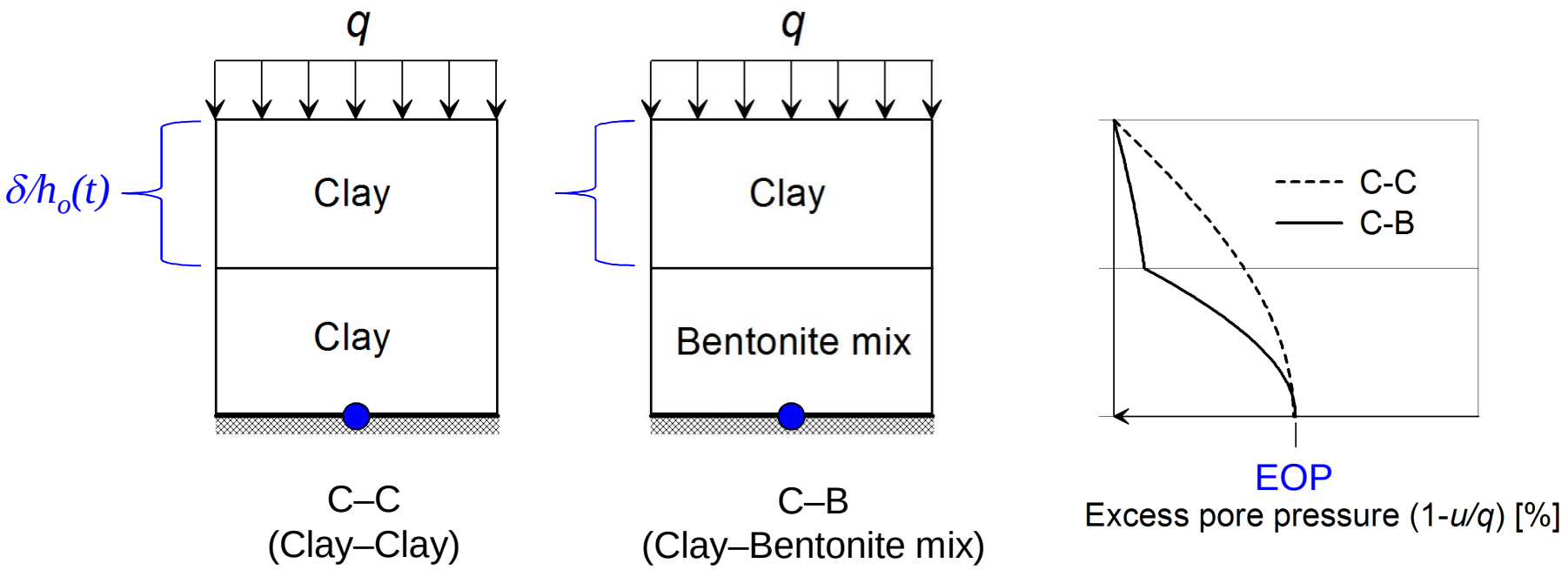

Fig.: Idealized cases

Expected strain-time relationship of the top clay: the creep hypotheses

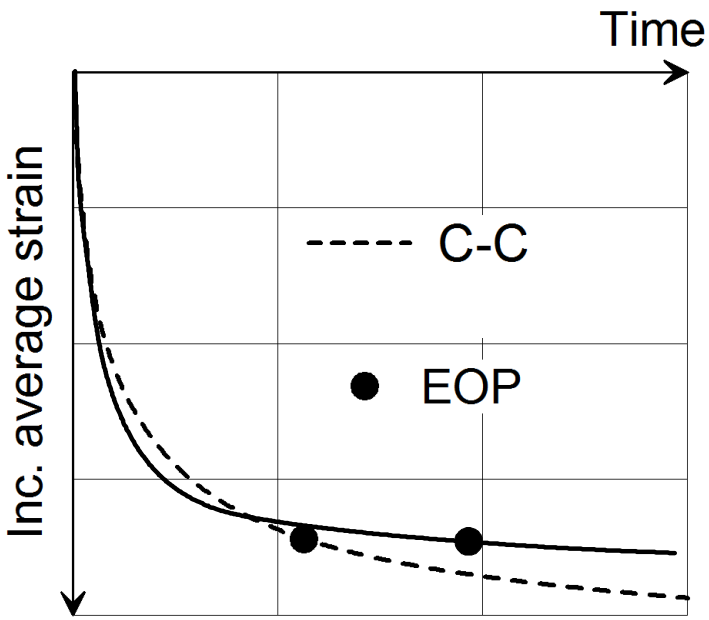

Hypothesis A

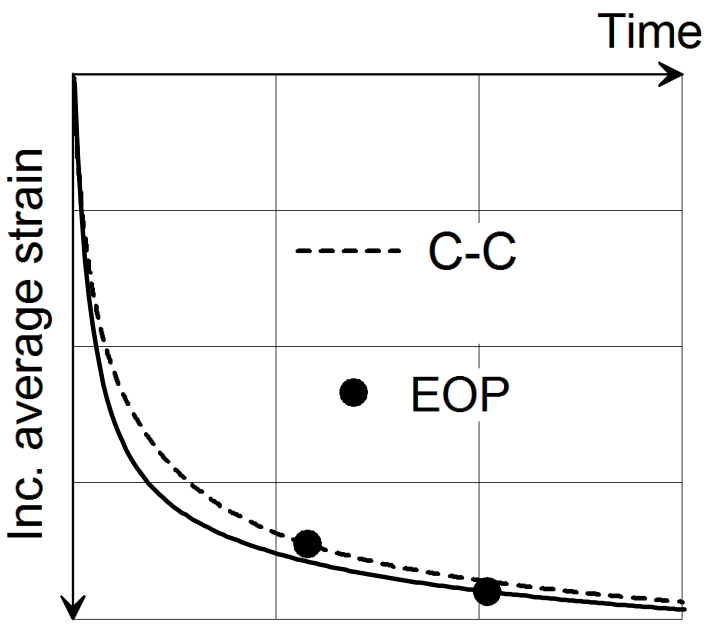

Hypothesis B

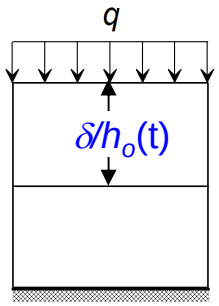

Fig.: Predicted incremental nominal strain-time relationship of the top clay

Test set up and measurements

- Conducted at Chalmers University of Technology
- Incremental load sequence of 10, 20, 30 and 80 kPa (EOP = 95 % EPP dissp.)
- Two sets of tests

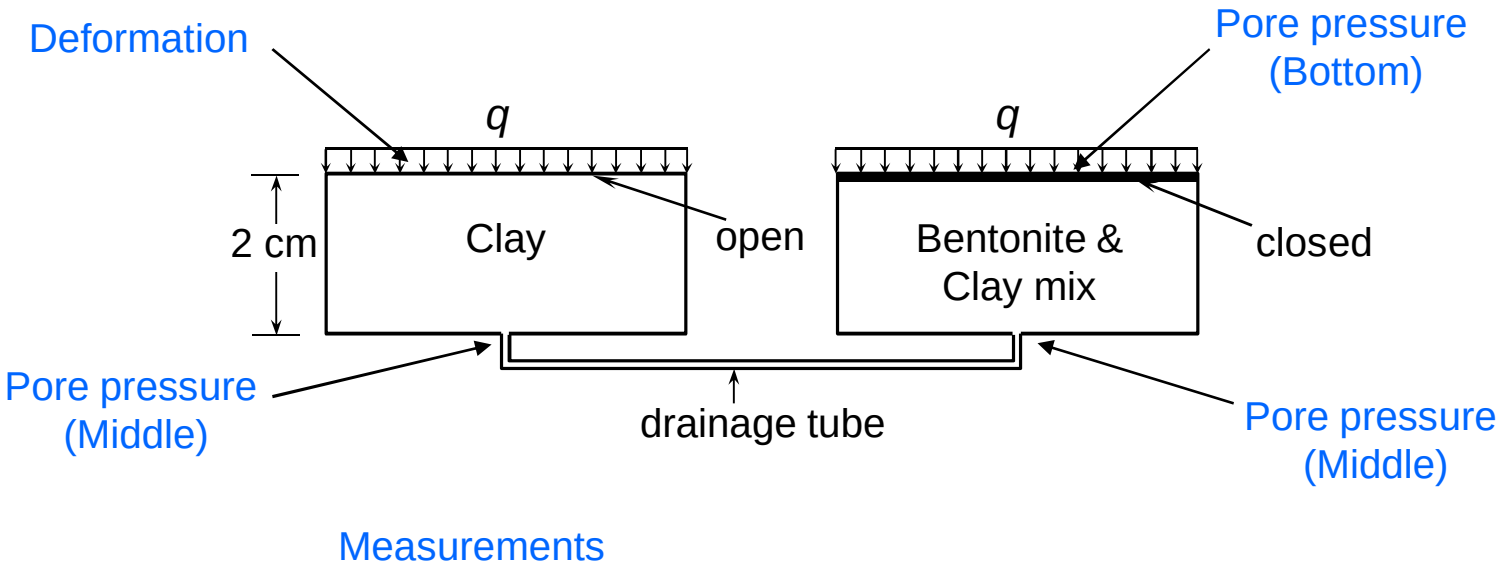

Fig.: Test set up and measurements

Fig.: Running the interconnected tests at Chalmers GeoEngineering laboratory

- Experimental results

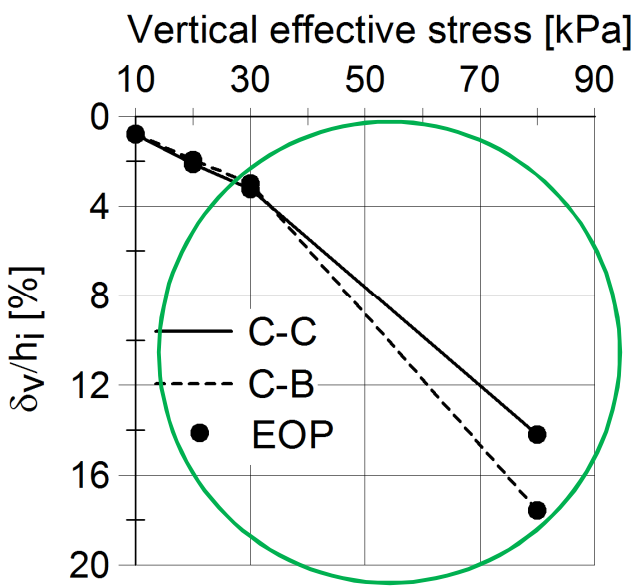

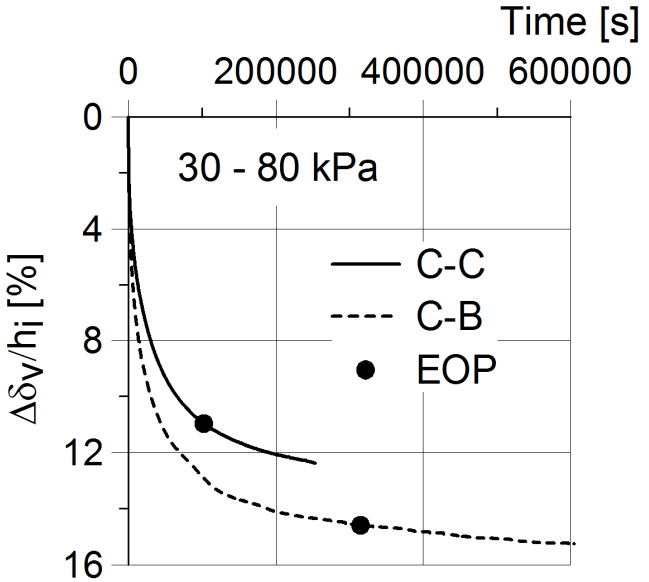

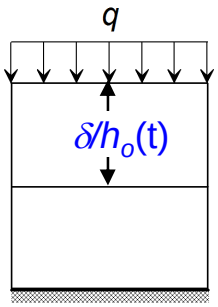

Fig.: Test measurements

- EOP is slightly more than expected for hypothesis B
- EOP strain not unique !

Numerical study

- Simulation using hypothesis B (SSC) model
- FE-code PLAXIS

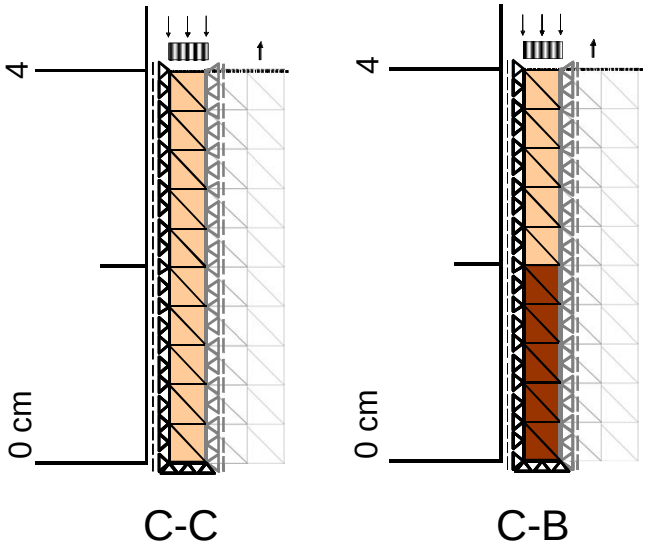

Fig.: Geometry adopted in FE simulation

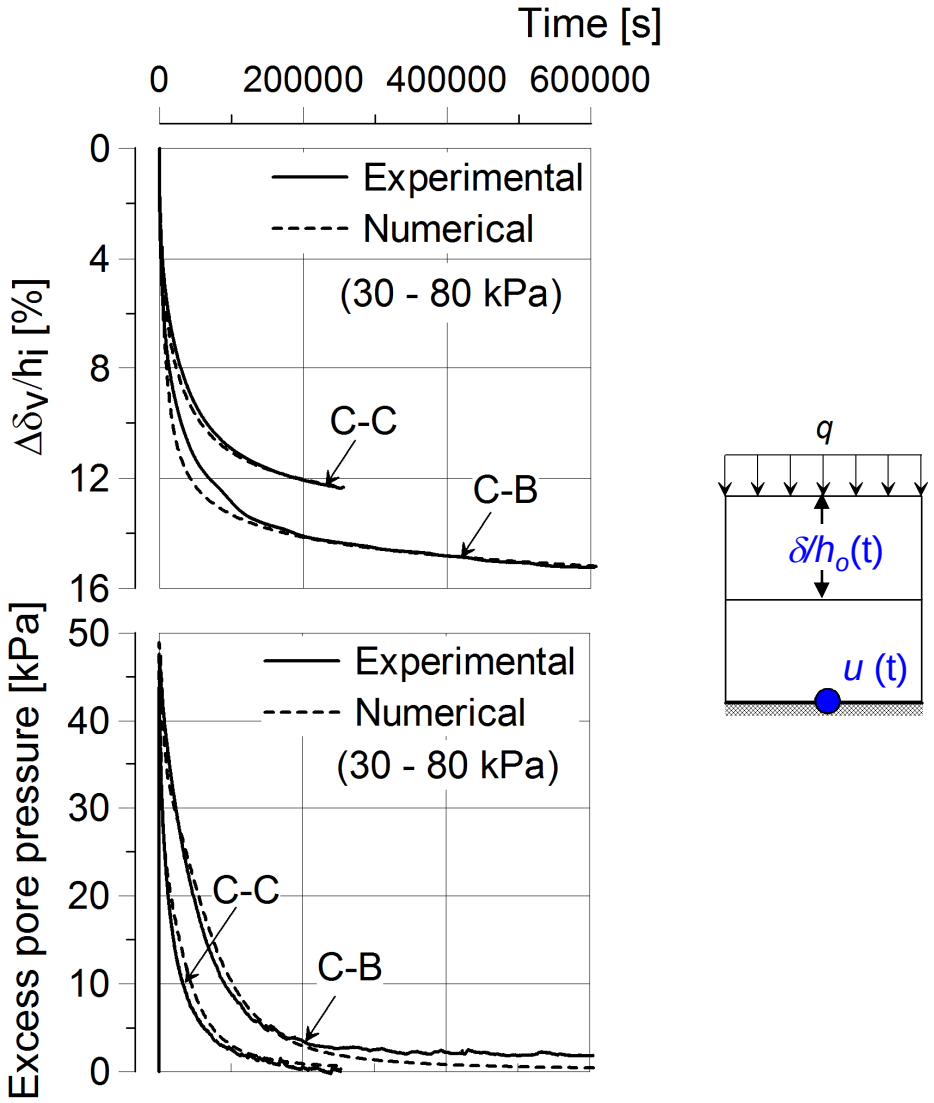

Fig.: Measurements vs. simulation (30-80 kPa)

Laboratory studies II: Creep hypotheses for soil element compressibility

Final remarks

- ✓ Laboratory studies on soil element compressibility imply hypothesis B.
  - Local compressibility of a soil element is governed by its prevailing effective stress-strain-strain rate on that particular soil element rather than what is happening elsewhere in the soil layer.
  - This means that a soil element creeps during primary consolidation and starts its secondary consolidation phase right after its primary consolidation phase rather than ‘wait’ until the completion of the primary consolidation of all the other soil elements
- ✓ Numerical simulation results using hypothesis B model can explain experimental measurements.

Field studies

- The two hypotheses could give significant practical differences when predicting settlements of in-situ soil layers
- However, on several occasions, the advocates of the two hypotheses have *independently* presented acceptable predictions of in-situ settlements to support the hypotheses.
- In this study, the *constitutive models* for the two hypotheses are evaluated based on the performance of a *common* and well-documented test fill.
- This is mainly motivated by the analogy to the hypothetical case exercises given to CREBS II participants in 2007 (Pisa) by Hans Petter Jostad.
- Constitutive models for hypothesis A (ILLICON), hypothesis B (SSC) and elasto-plastic model (SS) are considered.

Model comparisons – Strain formulations

- ILLICON strain decomposition

$$\Delta e_p = C_c^* \Delta \log \sigma_v' + \beta C_\alpha^* \Delta \log t$$

where C_α^* merely decomposes the input and out put Δe_p into two 'arbitrary' parts.

- SS is a rate-independent elasto-plastic model
- SSC is a rate-dependent elasto-viscoplastic model

- ILLICON is equivalent to SS model.

- The SSC would give larger EOP strain than both ILLICON and SS models.

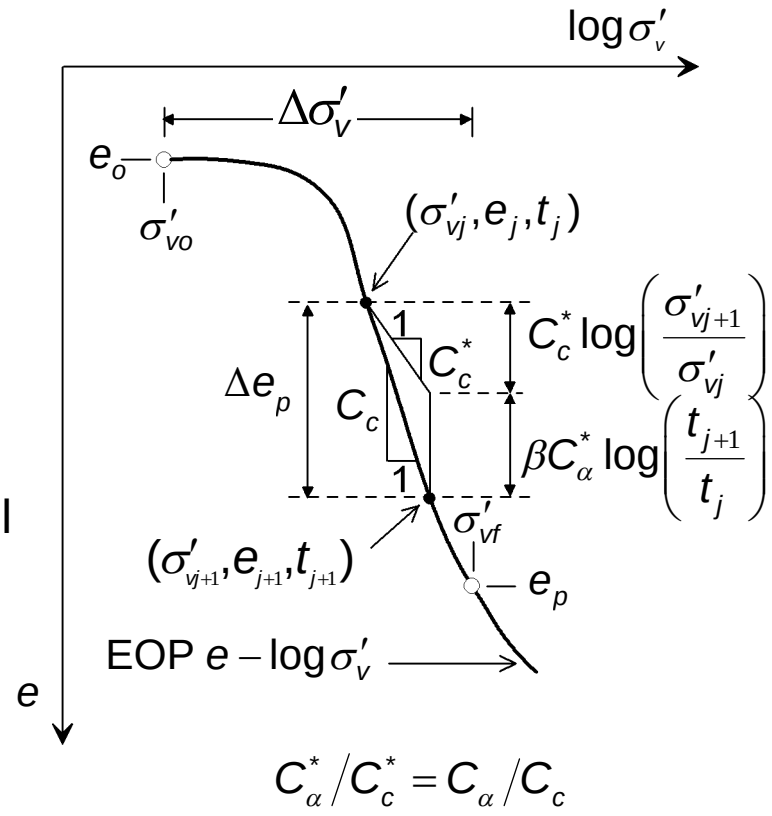

$$C_\alpha^* / C_c^* = C_\alpha / C_c$$

Fig.: ILLICON strain formulations (after Choi, 1982)

Model comparisons – Excess pore pressure formulations

- Continuity equation as used in ILLICON assumes that the excess pore pressure dissipation is only affected by the so-called stress-compressibility.

$$\frac{(1+e_o)^2}{\gamma_w}\frac{\partial}{\partial z}\left(\frac{k_v}{1+e}\frac{\partial u}{\partial z}\right)=\frac{de_\sigma}{dt}\neq\frac{de}{dt}\left(=\frac{de_\sigma}{dt}+\frac{de_t}{dt}\right)$$

- In SSC and SS model the continuity equation is controlled by total strain rate.
- ILLICON would give faster EPP dissipation than SS model.
- SSC would give significantly slower EPP dissipation than both ILLICON and SS model.

Comparison of the models based on analysis of Väsby test fill

- ILLICON vs. SS
- SSC vs. SS

- ILLICON, SSC and SS models are indirectly compared based on analysis of the test fills.
- For a given set of soil data, the SS model is used in order to provide reference predictions with respect to disregarding the effect of creep.

Analyses results ILLICON & SS – Väsby test fill

- "ILLICON-Equivalent" parameters were adopted for SS model.

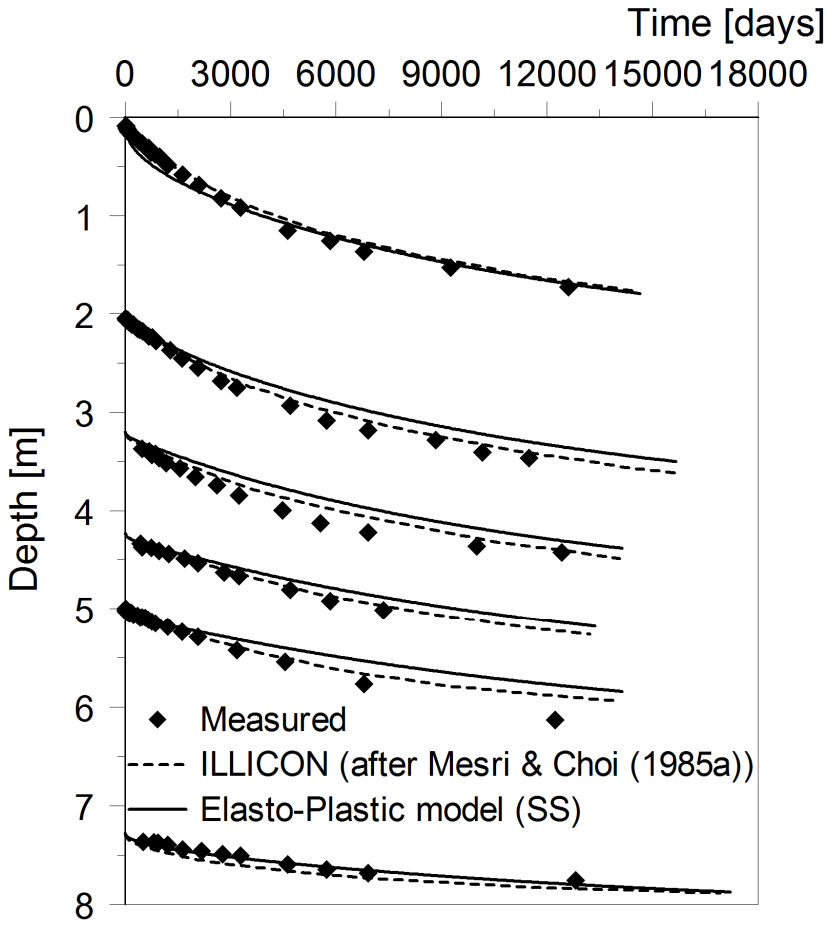

Fig.: Settlement history predictions (ILLICON vs. SS)

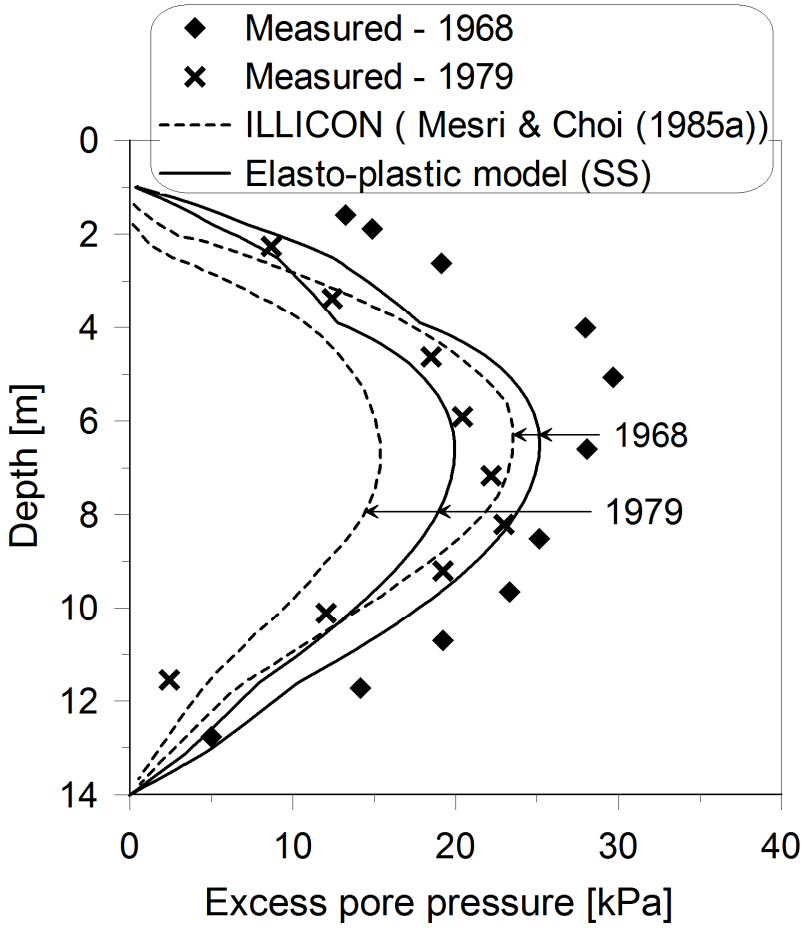

Fig.: Excess pore pressure profile predictions (ILLICON vs. SS)

ILLICON and SS model predictions vs. Measurements

- While disregarding creep, both ILLICON and SS model gave an overall acceptable predictions.
- This should not imply that the soft clays considered do not undergo creep deformation.
- The acceptable predictions were mainly due to two factors, i.e. use of soil data from disturbed samples and disregarding effect of large deformations.

(1) Sample disturbance

- Generally the OCR values used in ILLICON and SS analysis were low and are believed to be affected by sample disturbance.

- For instance,
  - Väsby test fill, EOP OCR = 1.31 or 1.82 ? (Leroueil and Kabbaj (1987))
  - In Skå-Edeby test fill, OCR = 1.0 ? (field tests by SGI)

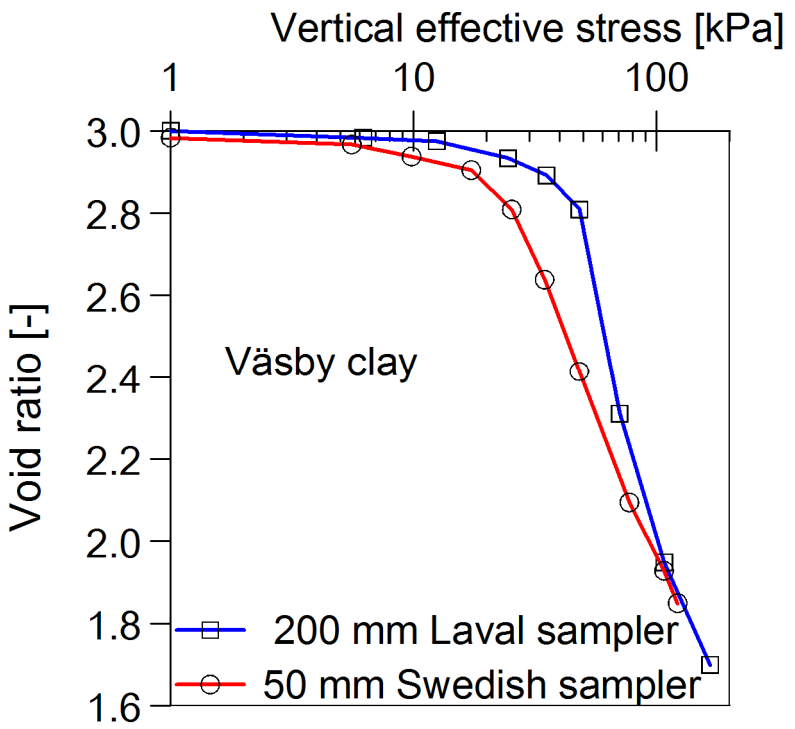

Fig. : Sample disturbance at Väsby test fill (after Leroueil & Kabbaj, 1987)

(2) Effect of large deformations (buoyancy)

- ILLICON and SS model analyses disregarded load reduction due to buoyancy forces.

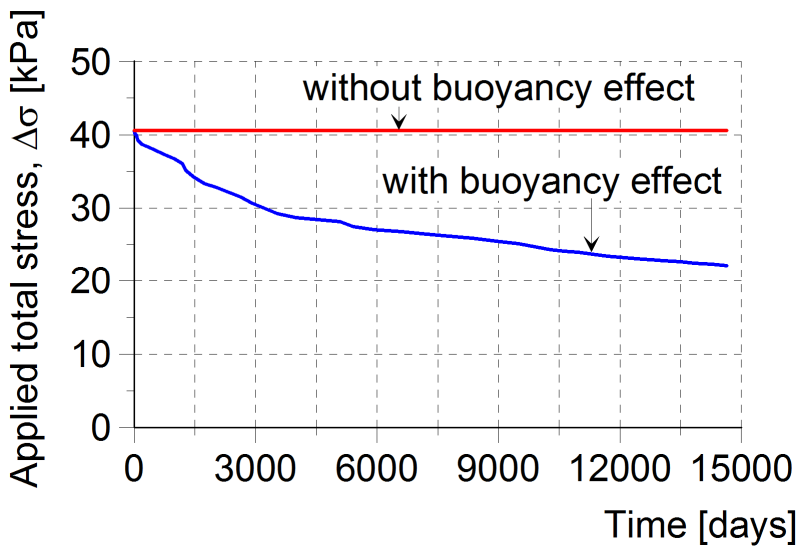

Fig. : Applied load with and without consideration of buoyancy effect (Väsby)

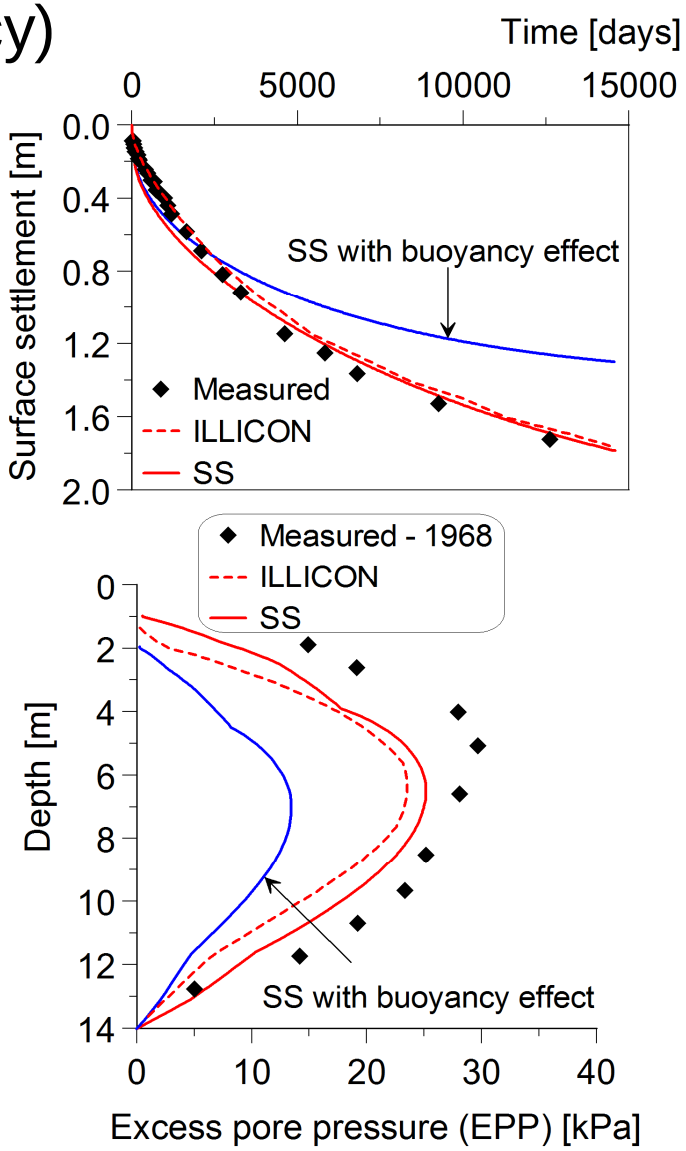

Fig.: Effect of buoyancy on predictions

Comparison of SSC vs. SS model

- ✓ Use of OCR values from high quality sample data or clay age considerations
- ✓ Effect of large deformation (buoyancy) taken into account

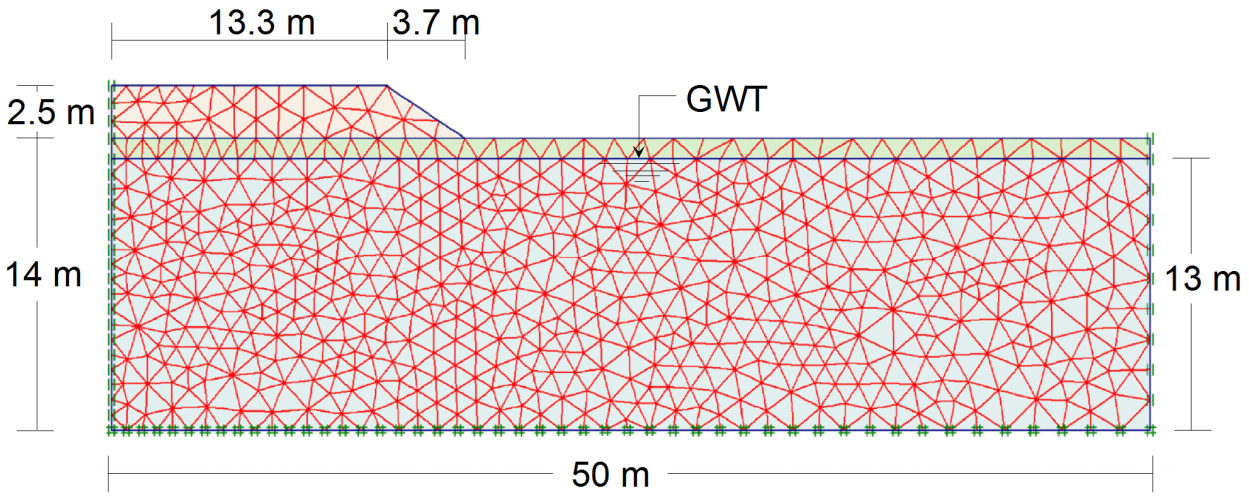

Fig.: Axisymmetric FE geometry adopted for Väsby test fill analysis

Analyses results SSC & SS – Väsby test fill

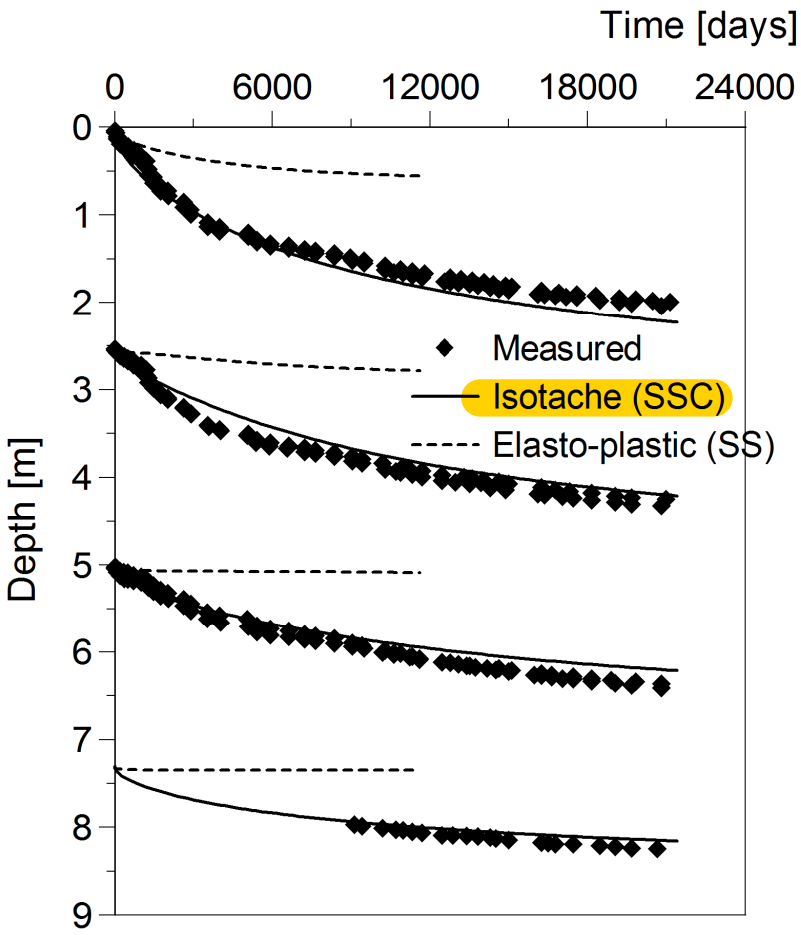

Fig.: Settlement history predictions (SSC vs. SS)

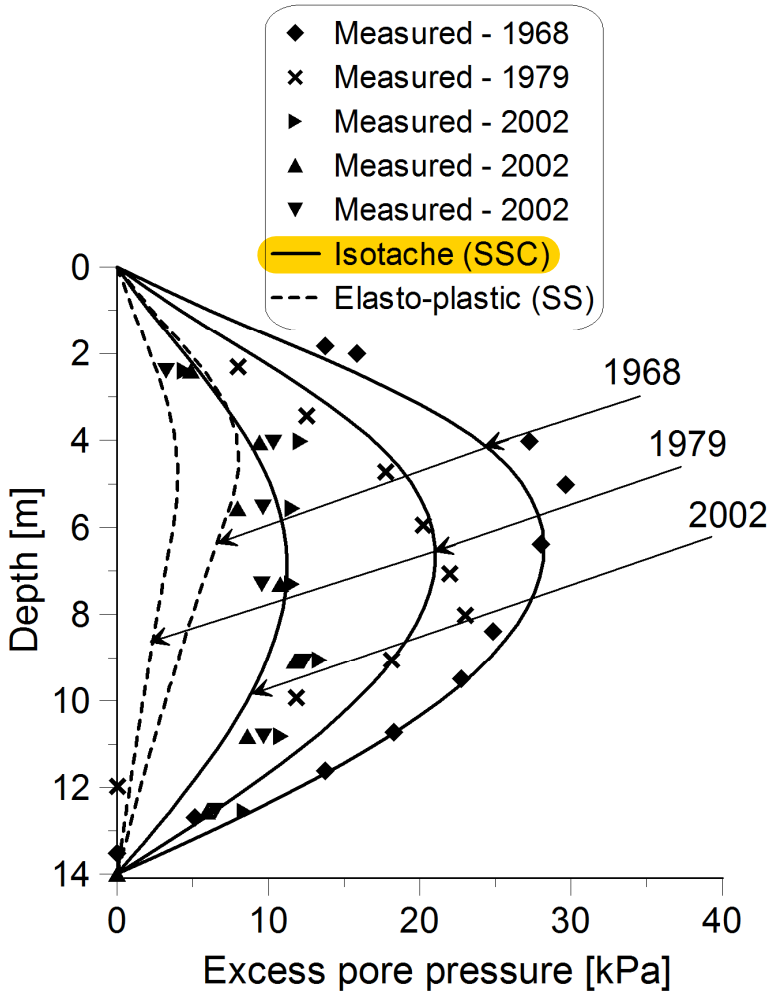

Fig.: Excess pore pressure profile predictions (SSC vs. SS)

Field studies

Final remarks (based on Väsby, Skå-Edeby & Ellingsrud test fills)

- ✓ When soil data are interpreted from tests on disturbed samples are used for settlement analysis then some effect of creep is already 'incorporated'.
  - A rate-independent elasto-plastic model, along with some simplifying assumption, could give acceptable settlement and reasonable but somehow low excess pore pressure responses.
  - An isotache model would significantly overestimate settlement and could give unrealistically large excess pore pressure responses.
- ✓ When soil data are interpreted from tests on high quality samples and used for settlement analysis,
  - A rate-independent elasto-plastic model significantly underestimates settlement and excess pore pressure responses
  - An isotache model would yield excellent prediction of settlements and excess pore pressure.

Conclusions

本研究已表明已有足夠確定數據驗明假說B與粘性土的測得的行為一致。

- In response to the important question raised by Ladd *et al*. in 1977, this study has shown that there exist definitive data to demonstrate that hypothesis B agrees very well with the measured behaviour of cohesive soils.

- Several EOP laboratory tests considered in this study demonstrated the validity of hypothesis B. In fact, this study disclosed that all the empirical data that were previously used to support substantiate hypothesis A actually imply hypothesis B.

在本研究中，幾組EOP(主固結完成時應力-應變關係)試驗室試驗數據證明假說B是對的。事實上，本研究發現之前所有支持假說A是對的試驗數據實質上是支持假說B是對。

- The experienced p'_c as well as EOP strain are rate dependent even for EOP loading conditions and this fact has been experimentally supported by several EOP tests and field observations.

- The isotache theory (hypothesis B (SSC)) can explain and convincingly capture important feature of various types of laboratory tests considered in this study.

等速理論(假說B, 即SSC)（SSC 是Soft Soil Creep model in Plaxis）可以解釋和令人信服的模擬到（再現到）本研究中討論到的各種試驗的重要特徵。

Conclusions

- Great care needs to be exercised during interpretation and use of preconsolidation stress (p'_c) in settlement analyses. With this aspect, sample quality deserves extra attention.

- Awareness regarding the significance of p'_c (OCR due to creep) on settlement analysis needs to be stressed by the profession.

- The isotache models are well suited to predict settlements of water saturated soft clay deposits when the input data are deduced from laboratory tests of good quality soil samples.

- Future developments related to the compressibility of natural clays such as anisotropy and destructuration should be focused on enhancing models that are based on the isotache framework or similar.

Thank you for your attention !

Statens vegvesen

Norwegian Public Roads Administration

Nash, D. F. T. & Ryde S. J. (2001). *Géotechnique* **51**, No. 3, 257–273

Modelling consolidation accelerated by vertical drains in soils subject to creep

D. F. T. NASH* and S. J. RYDE†

The settlement of embankments and reclamations over soft soils is frequently accelerated by the use of vertical drains. The magnitude of long-term settlement is sometimes reduced by the use of surcharge, although there is often uncertainty about how long the surcharge should be maintained to minimise creep movement. The design of vertical drains is generally based on closed-form solutions of Terzaghi's consolidation equation, and rarely takes into account non-linear stiffness and creep of the soil. In this paper a one-dimensional finite difference consolidation analysis is outlined showing how vertical and radial drainage of a multi-layer soil profile in the zone of influence of a vertical drain may be modelled. The analysis allows inclusion of a zone of peripheral smear around the drain and drain resistance, permeabilities may be varied with void ratio, and creep is modelled both during and after primary consolidation. The application of the model is illustrated with back-analysis of field data from construction of an embankment with temporary surcharge over estuarine alluvium.

KEYWORDS: clays; consolidation; creep; embankments; ground improvement; numerical modelling and analysis.

Le tassement des berges et la reconquête de sols tendre se trouvent fréquemment accélérées par l'utilisation de drains verticaux. L'ampleur du tassement à long terme est parfois réduite par l'utilisation d'une surcharge, bien qu'il existe souvent une incertitude quant à la durée de maintien de la surcharge pour minimiser le mouvement de glissement. L'étude de la forme des drains verticaux est généralement basée sur des solutions en forme fermée de l'équation de consolidation de Terzaghi et prend rarement en compte la rigidité non linéaire et le glissement du sol. Dans cette étude, nous décrivons une analyse unidimensionnelle de consolidation à différence finie, montrant comment le drainage vertical et radial d'un profil de sol à plusieurs couches dans la zone d'influence d'un drain vertical peut être mis en maquette. L'analyse tient compte de la zone de salissure périphérique autour du drain et des effets de la résistance de drain, les perméabilités pouvant être variées en fonction du taux de vide ; le glissement est mis en maquette pendant et après la consolidation primaire. L'application du modèle est illustrée par des rétro-analyses des données de terrain relevées pendant la construction d'une berge avec une surcharge temporaire sur des alluvions d'estuaire.

INTRODUCTION

Vertical drains are widely used in the construction of embankments and reclamations over compressible soils to accelerate their consolidation. Traditionally, vertical drains consisted of sand columns constructed by jetting, boring or displacement techniques, but nowadays the use of prefabricated band drains is widespread. When post-construction settlements are likely to be significant owing to lack of full pore pressure dissipation or creep it is common to attempt to reduce these by application of a temporary surcharge over critical areas. Such techniques have gained wide acceptance, and their design and application have been reviewed by several authors (for example (Johnson, 1970; Bjerrum, 1972; Jamiolkowski *et al.*, 1983; Holtz *et al.*, 1991). However, these authors acknowledged the difficulty of predicting settlement rates in soils exhibiting creep, and especially when the surcharge is removed.

The design of vertical drains is generally based on closed-form solutions of Terzaghi's consolidation equation (Terzaghi, 1943), in which the three-dimensional process of consolidation is simplified to that of one-dimensional movement arising from a combination of vertical flow and radial flow to the drain. Barron (1948) and Hansbo (1981) obtained solutions for equal strain (in which the surface displacements are constant but the applied stress is non-uniform), and Barron also considered free strain (in which the applied vertical stress at the surface remains constant and settlements are non-uniform). They also considered the important practical problems of smear around the drain and drain resistance effects.

Such solutions necessitate many simplifying assumptions, including that strains are only one-dimensional, that the vertical and radial coefficients of consolidation, c_v and c_r, remain constant during consolidation, and that the relationship between effective stress and void ratio is linear and independent of time. Terzaghi & Peck (1948) recognised that the stiffness of lightly over-consolidated clay deposits varies with stress level, and that secondary compression effects increase the settlements in the long term. They stated that, 'despite the radical simplifications involved, the theory of consolidation serves a useful purpose, since it permits at least a rough estimate of the rate of settlement due to consolidation, on the basis of laboratory tests'. Since then engineers have generally estimated settlement rates during primary consolidation on the basis of Terzaghi's theory (and later developments), adding on an allowance for subsequent secondary settlements. The advent of computers has enabled development of numerical methods for the analysis of consolidation. Such methods provide greater flexiblity than closed-form solutions, and permit the inclusion of a multi-layer profile including soils whose behaviour differs from that assumed by Terzaghi.

The authors recently undertook the back-analysis of field data from construction of the approach motorways to the new Second Severn Crossing in the UK, a project involving numerous embankments constructed in stages over estuarine alluvium. Previous motorway embankments in the area had exhibited large and ongoing secondary settlements. One of the objectives of this research was to examine the application of a state-of-the-art constitutive model in the back-analysis of real engineering data. In reviewing possible methods of settlement analysis, several numerical procedures were identified, but none was readily available that could model creep effects during primary consolidation. Accordingly a finite difference analysis was developed by Ryde (1997), to model one-dimensional consolidation arising from vertical and radial flow, incorporating an elastic visco-plastic constitutive model developed recently by Yin & Graham (1989, 1996). This finite strain analysis includes the effects of non-linear stiffness, creep, and permeability varying with void ratio as well as drain resistance and smear around the vertical drain. In this paper the finite difference algorithm is outlined,

Manuscript received 14 June 2000; revised manuscript accepted 11 December 2000.
Discussion on this paper closes 2 October 2001, for further details see inside back cover.
* Department of Civil Engineering, University of Bristol, UK.
†Scott Wilson Kirkpatrick and Co. Ltd, UK. Formerly Department of Civil Engineering, University of Bristol, UK.

and the way in which creep is incorporated is described. Its application in back-analysis of data from one of the new embankments is presented by way of illustration.

CREEP MODEL

Background

The first theory of secondary compression was formulated by Taylor & Merchant (1940), and since then straining under constant effective stresses has been an area of continual study. They showed that secondary compression movements decrease logarithmically with time, and Taylor (1948) stated that creep occurs during primary consolidation as well as subsequently. Following Taylor's ideas, Suklje (1957) and Bjerrum (1967, 1972) presented diagrams showing a system of approximately parallel curves of e against $\log \sigma'$ (Fig. 1) that describe secondary compression behaviour. In this widely used diagram, the lines indicate void ratio after constant time for delayed compression, or sometimes indicate constant strain rate (isotaches). Bjerrum introduced the terms *instant* and *delayed* compression to describe the behaviour of the soil skeleton in the absence of pore pressure effects, and argued that delayed compression (or creep) occurs during the whole consolidation process. Bjerrum (1972) drew attention to the significance of secondary compression for the design of vertical drain installations. He showed that although improved drainage accelerates primary consolidation, it does not affect the magnitude of total long-term settlement. He also discussed the use of temporary surcharge to reduce long-term movements.

Creep at constant effective stress is usually described using the secondary compression index $C_\alpha = \Delta e / \Delta \log t$ but there has always been a difficulty in deciding the time origin. The main area of debate (Ladd *et al.*, 1976; Jamiolkowski *et al.*, 1983; Mesri & Choi, 1985a; Leroueil, 1988) has been whether creep is significant during primary consolidation. If creep commences only after primary consolidation is complete (hypothesis A), the end of primary (EOP) e against $\log \sigma'$ curve is practically independent of the thickness of the compressible stratum and the duration of primary consolidation. If creep is significant both during and after primary compression (hypothesis B), field and laboratory stress–strain behaviour will be different.

Mesri & Choi (1985b) developed the finite difference proce-

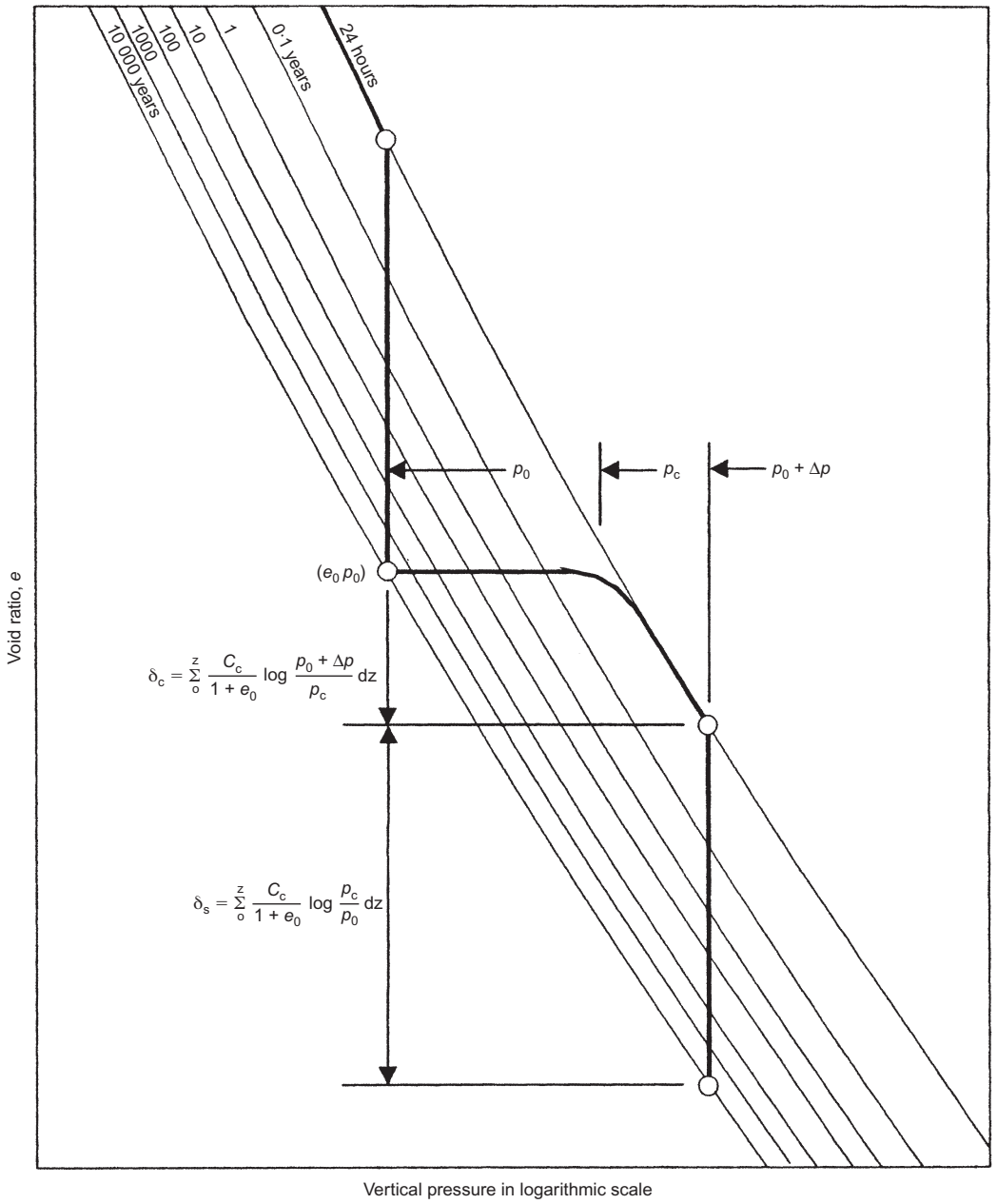

Fig. 1. Principle for evaluating secondary settlements in soft clay (Bjerrum, 1972)

dure ILLICON, which utilises hypothesis A, and the assumption is made that the secondary compression index, C_α, is linearly related to the compression index, C_c (Mesri & Godlewski, 1977). Subsequently ILLICON was extended to include flow into a vertical drain, and experience of its use was summarised by Mesri *et al.* (1994).

Bjerrum's ideas (hypothesis B) were expressed mathematically by Garlanger (1972), and Magnan *et al.* (1979) used a stress–strain–strain rate model in the one-dimensional consolidation analysis CONMULT. Kabbaj *et al.* (1986) proposed separating elastic and plastic components of strain, and subsequently Yin & Graham (1989) and Den Haan (1996) developed similar elastic visco-plastic (EVP) models that overcome previous limitations. While these EVP models have been used successfully in modelling laboratory data, there is little published on their application to full-scale problems. In selecting a model for use in back-analysis involving vertical drains, the authors concluded that it was logical to include creep during primary consolidation (hypothesis B), and desirable to be able to model creep after unloading. The EVP model of Yin & Graham was therefore adopted for this work.

Simple isotache model for one-dimensional compression

The elastic visco-plastic (EVP) model is summarised here, and the reader is referred to Yin & Graham (1989, 1994, 1996) for a fuller description. Yin & Graham used the λ–κ model from critical state soil mechanics to define the elastic–plastic behaviour of the soil skeleton, with the normal consolidation line (NCL) replaced by a reference time line (RTL), as illustrated in Fig. 2. On this diagram the parallel lines or isotaches connect soil states at which the creep strain rate is constant. One isotache on which the creep strain rate is known is chosen as the RTL, which is used to define the complete set of isotaches; equally spaced isotaches indicate a logarithmic change in strain rate. Although a lower limit to creep is observed in practice, particularly on unloading, it is not included in this simple isotache model.

The solid line ABD in Fig. 2 indicates a path that might be followed by an element of soil loaded by an instantaneous increment of total stress $\Delta\sigma$ as it consolidates. As the effective stress increases from the initial state at point A, the creep strain rate increases as the soil state moves towards the RTL, but the effective stress and strain rate are limited by the ability of the pore water to escape. After further consolidation the strain rate decreases until excess pore pressures have dissipated at point B, after which creep continues at decreasing rates towards point D. It is important to realise that the stress–strain behaviour of each element in the ground during primary consolidation will be different depending on its proximity to a drainage boundary. A soil element remote from a drainage boundary may follow the path AB indicated by the solid line, while another element closer to the drainage boundary may consolidate faster, with the path from A to B lying closer to the RTL as shown by the dashed line. For this element the end of primary consolidation occurs at point C. Indeed a small sample of the soil subjected to the same loading in an oedometer might follow a path that crossed the RTL.

The RTL is fixed by the stress[1] $\sigma_0'^{ep}$ and strain ε_0^{ep} at reference point O (see Fig. 2). The equation of the RTL is given by

$$\varepsilon^{ep} = \varepsilon_0^{ep} + \frac{\lambda}{\nu_0} \ln\left(\frac{\sigma'}{\sigma_0'^{ep}}\right) \tag{1}$$

where λ/ν_0 is its slope, and ν_0 is the specific volume at zero strain. Alternatively the equivalent expression in terms of void ratio may be used.

The incremental total strain $d\varepsilon$ resulting from a change of

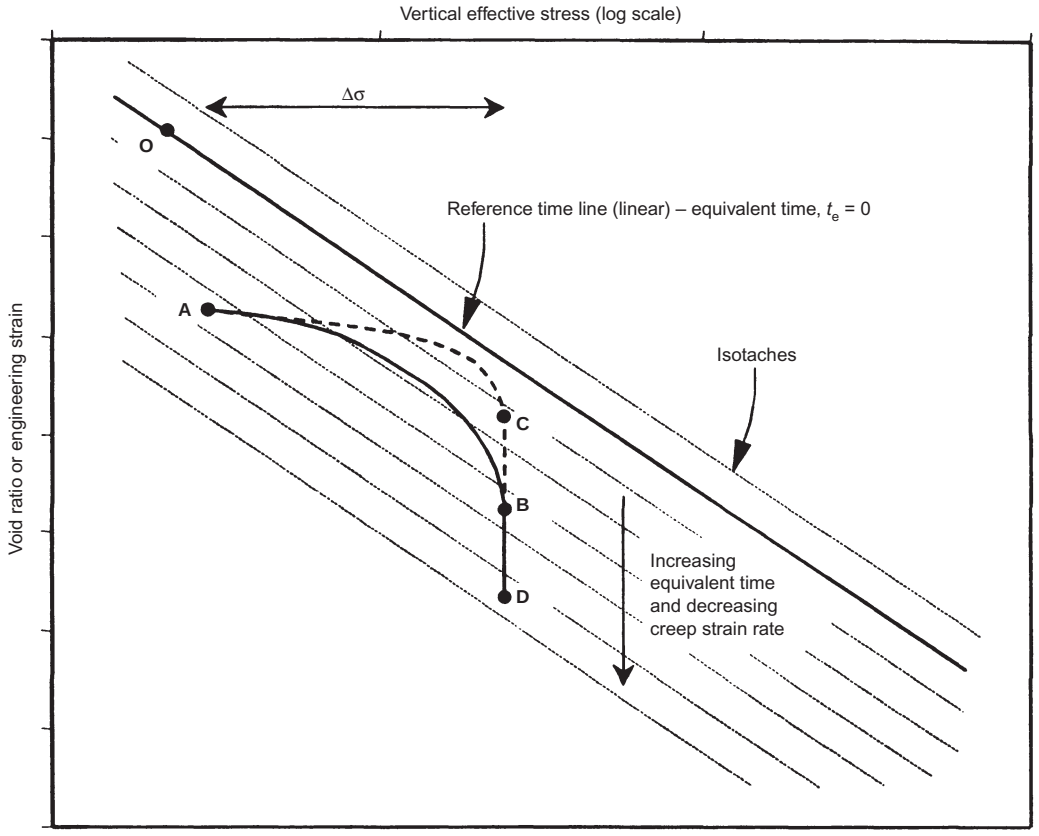

Fig. 2. Elastic visco-plastic constitutive model showing isotaches and stress–strain path during compression

[1] The superscripts *e*, *ep* and *tp* denote instantaneous (elastic), stress-dependent plastic and time-dependent plastic, respectively.

vertical effective stress $d\sigma'$ is the sum of the incremental elastic strain $d\varepsilon^{e}$ and the incremental creep strain $d\varepsilon^{tp}$ given by

$$d\varepsilon = d\varepsilon^{e} + d\varepsilon^{tp} = \frac{\kappa}{\nu_0 \sigma'} d\sigma' + d\varepsilon^{tp} \tag{2}$$

where σ' is the current vertical effective stress, and κ is the slope of the elastic unload–reload line (void ratio e against $\ln \sigma'$). The creep strain rate is defined by the relation of the current soil state to the RTL. Yin & Graham (1989) introduced the concept of equivalent time t_e, which is equal to the real time that would be taken to creep under constant effective stress from the RTL to the present state. On the RTL the equivalent time t_e is zero, and the creep strain rate is defined *a priori* using a constant t_0. The creep strain rate at other states is calculated from the expression

$$\dot{\varepsilon}^{tp} = \frac{\partial \varepsilon^{tp}}{\partial t} = \frac{\psi}{\nu_0 (t_0 + t_e)} \tag{3}$$

in which ψ/ν_0 is the slope of a plot of creep strain ε^{tp} against $\ln(t_e)$ (similar to the conventional coefficient of secondary consolidation, C_α). Thus the parallel isotaches in Fig. 2 are also t_e isochrones. It is easier to understand the model if the chosen RTL is located above the NCL, but this is not a requirement as t_e may assume negative values provided that $t_e > -t_0$.

It follows by integration of equation (3) that the difference in strain between the current state and that on the RTL at the same stress is given by

$$\Delta \varepsilon^{tp} = \frac{\psi}{\nu_0} \ln\left(1 + \frac{t_e}{t_0}\right) \tag{4}$$

and when this expression is combined with equation (1) for the RTL, the total strain is given by

$$\varepsilon = \varepsilon_0^{ep} + \frac{\lambda}{\nu_0} \ln\left(\frac{\sigma'}{\sigma_0'^{ep}}\right) + \frac{\psi}{\nu_0} \ln\left(1 + \frac{t_e}{t_0}\right) \tag{5}$$

This expression can be rearranged so that the equivalent time may be calculated from

$$t_e = -t_0 + t_0 \exp\left[(\varepsilon - \varepsilon_0^{ep}) \frac{\nu_0}{\psi}\right] \times \left(\frac{\sigma'}{\sigma_0'^{ep}}\right)^{-\lambda/\psi} \tag{6}$$

The model parameters may be obtained from high-quality incremental load oedometer tests. The RTL is first located on a plot of void ratio or engineering strain against $\log \sigma'$, passing through points of constant creep strain rate, approximately parallel to the normal consolidation line. Yin & Graham (1994) suggest an iterative procedure to locate the RTL above the NCL, particularly when load increments are applied after variable time intervals. However, the authors have found that in many oedometer tests with increments applied daily, the strain rate after 24 hours is approximately constant in the normally consolidated stress range. The 24 hour line may then be used directly as the RTL, and its position defined by projecting it back to the zero strain axis, taking the intercept to be the stress $\sigma_0'^{ep}$ and setting $\varepsilon_0^{ep} = 0$. Values of λ and κ are found from the slopes of the chosen RTL and the unloading/reloading curves, and the remaining parameters are found from the creep data. By combining equations (3) and (4) it follows that when the soil creeps at constant effective stress:

$$\varepsilon^{tp} = \psi/\nu_0 \left[\ln\left(\frac{\psi}{\nu_0 t_0}\right) - \ln(\dot{\varepsilon}^{tp})\right] \tag{7}$$

The parameter ψ or the combination ψ/ν_0 may readily be obtained from the slope of plots of logarithm of strain rate against strain for the later stages of each increment (Nash & Ryde, 2000). The value of t_0 is then calculated from the creep rate on the RTL.

The EVP model used here is formulated in terms of engineering strain and assumes a linear RTL on a plot of void ratio (or engineering strain) against $\log \sigma'$, but this is not a requirement. Many structured clays exhibit non-linear normal consolidation lines, and recently Nash & Ryde (2000) have extended this EVP model to include a curved RTL using natural strain (after Butterfield, 1979) or a power law (after Den Haan, 1992).

CONSOLIDATION EQUATION

The axisymmetric form of the one-dimensional consolidation equation (Terzaghi, 1943) is often written

$$c_v \frac{\partial^2 \bar{u}}{\partial z^2} + c_r \left(\frac{\partial^2 \bar{u}}{\partial r^2} + \frac{1}{r}\frac{\partial \bar{u}}{\partial r}\right) = \frac{\partial \bar{u}}{\partial t} \tag{8}$$

in which $\bar{u}$ is the excess pore pressure, and c_v and c_r are the vertical and radial coefficients of consolidation respectively. In derivation of this equation for a small element of soil, it is assumed that strain is one-dimensional in the vertical direction, but that flow may be vertical and radial. Furthermore it is assumed that the principal axes of permeability coincide with the vertical and radial directions, an assumption that is consistent with a horizontally layered soil.

Terzaghi (1943) discusses the application of solutions of equation (8) to a practical problem involving vertical drains. Each vertical drain is considered to be located at the centre of a cylinder of soil of external diameter approximately equal to the drain spacing, and with interior diameter equal to that of the drain. Drainage may occur at the permeable inner boundary and at the top and/or bottom surfaces. Terzaghi uses the work of Carrillo (1942) to show how the principle of superposition may be used to combine the theoretical solutions for separate radial and vertical flow problems. Similar procedures were adopted by Barron (1948) and Hansbo (1981). Such solutions to the consolidation equation necessitate a number of assumptions, including constant applied load during consolidation, constant coefficients of consolidation, deformations that are small compared with the original geometry and are one-dimensional, and constant boundary pore-pressure conditions. These assumptions are not valid for the consolidation of thick layers of soft clay in which a large proportion of the compression is due to creep, and closed-form solutions are not available.

The consolidation equation is generally expressed in terms of excess pore pressure, $\bar{u}$, on the assumption that the steady-state pore pressure, u_{ss}, remains constant. The terms involving $\bar{u}$ are derived from total head h and position head z, where

$$h = \frac{u}{\gamma_w} + z = \frac{\bar{u} + u_{ss}}{\gamma_w} + z \tag{9}$$

If the boundary conditions may change, it is convenient to use the full pore pressure u, with an additional term on the left-hand side of the consolidation equation to account for the variation of pressure with elevation. If there is spatial variation of permeabilities k_z and k_r in vertical and radial directions it is necessary to include them within each derivative in equation (8), which may then be written

$$\frac{\partial}{\partial z}\left[\frac{k_z}{\gamma_w}\left(\frac{\partial u}{\partial z} + \gamma_w\right)\right] + \frac{1}{r}\frac{\partial}{\partial r}\left[\frac{k_r}{\gamma_w} r \frac{\partial u}{\partial r}\right] = m_v \left(\frac{\partial u}{\partial t} - \frac{\partial \sigma}{\partial t}\right) + \frac{\partial \varepsilon^{tp}}{\partial t} \tag{10}$$

where m_v is the coefficient of volume compressibility. The variation of total vertical stress elastic σ with time, and creep are taken into account by inclusion of additional terms on the right-hand side, which expresses the elastic and plastic components of strain rate. If the boundary pore pressures do not change, the equation may be expressed in terms of excess pore pressure $\bar{u}$, and the extra term involving γ_w is omitted. The soil may be modelled as linear elastic (using a constant m_v) or non-linear (by varying m_v with stress level), with or without creep. The EVP model outlined above is expressed in terms of engineering strain, and was implemented by Yin & Graham

(1996) in a small-strain formulation of the consolidation equation. When applied to large-strain problems it is necessary to allow for the change of geometry, and the strains on the right-hand side of equation (10) must be expressed as natural strains. This is achieved by multiplying the expressions in equation (2) by the ratio v_0/v, where v is the current specific volume.

Finite difference formulation

In order to model the consolidation of layered soil profiles due to vertical and radial flow, equation (10) has been expressed in finite difference form (Ryde 1997).[2] The use of finite difference methods for the analysis of consolidation problems is well established in the geotechnical literature (e.g. Richart, 1959; Murray, 1971; Olsen *et al.*, 1974; Lee *et al.*, 1983; Onoue, 1988). However, Ryde (1997) adopted a numerical formulation technique different from that previously used, similar to that developed by Reece (1986) in the analysis of heat flow through a non-uniform metal bar. The soil is divided into a series of layers and annuli, as shown in Fig. 3. The grid is graded in both directions so that there are small layer and annulus thicknesses close to permeable boundaries. The state of the soil in each cell is represented by the conditions at a central node, which is positioned so that the cell boundaries lie midway between adjacent nodes. Phantom nodes and layers are placed just outside the boundaries of the grid to enable the boundary conditions to be defined. This contrasts with previous consolidation analyses in which the nodes were generally positioned at the cell boundaries.

Figure 4 shows part of the grid in the vicinity of a cell with a central node at coordinates $r_{i,j}$ and $z_{i,j}$. For this cell the left-hand side of equation (10) may be expressed in finite difference form:

$$\frac{\dfrac{k_T}{\gamma_w}\left(\dfrac{u^*_{i,j+1}-u^*_{i,j}}{z_{i,j+1}-z_{i,j}}+\gamma_w\right)-\dfrac{k_B}{\gamma_w}\left(\dfrac{u^*_{i,j}-u^*_{i,j-1}}{z_{i,j}-z_{i,j-1}}+\gamma_w\right)}{z_T-z_B} + \frac{1}{r_{i,j}}\frac{\dfrac{k_o}{\gamma_w}r_o\left(\dfrac{u^*_{i+1,j}-u^*_{i,j}}{r_{i+1,j}-r_{i,j}}\right)-\dfrac{k_I}{\gamma_w}r_I\left(\dfrac{u^*_{i,j}-u^*_{i,j-1}}{r_{i,j}-r_{i,j-1}}\right)}{r_o-r_I} \tag{11}$$

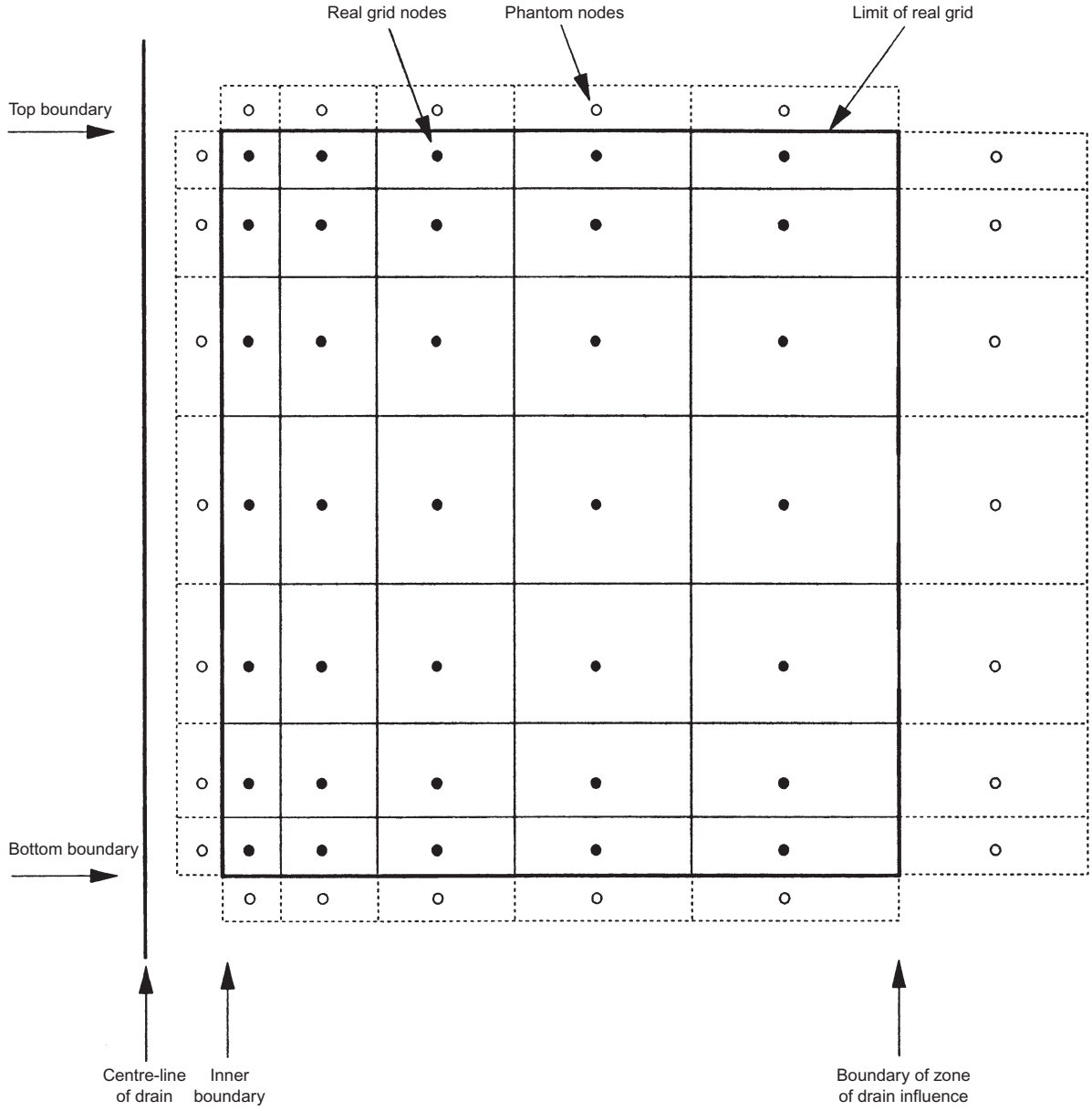

Fig. 3. Grid used in finite difference analysis

[2] Originally, Ryde (1997) formulated equation (10) in terms of excess pore pressure not full pore pressure.

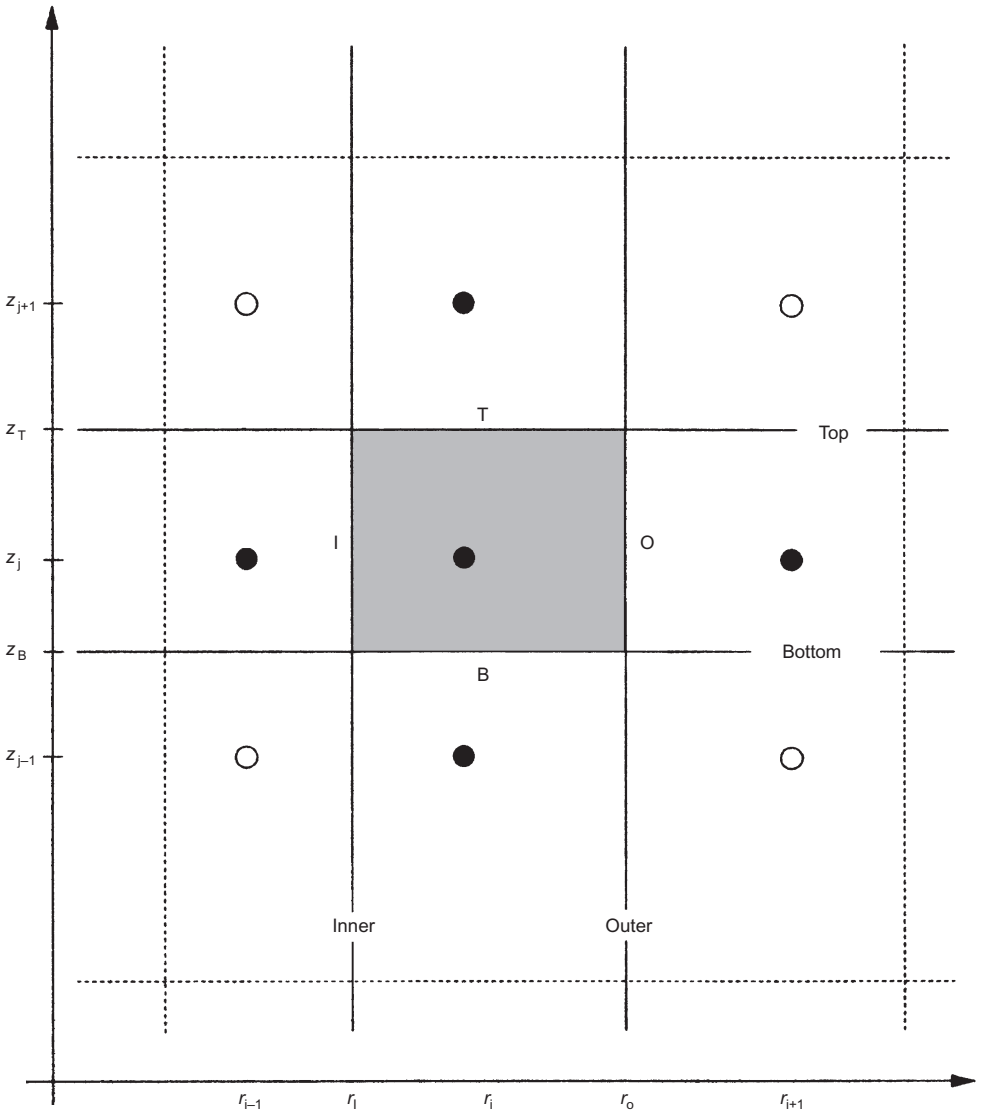

Fig. 4. Part of finite difference grid in vicinity of node *ij*

where u^* are values of the pore pressure at the central node and the nodes in the surrounding cells, and k_T etc. are the values of permeability at the boundaries between adjacent cells. Each boundary permeability is calculated from the permeabilities of the adjacent cells in the manner of:

$$k_T = \frac{2k_{i,j+1}k_{i,j}}{k_{i,j+1} + k_{i,j}} \tag{12}$$

and is applied at the cell interface to give a uniform hydraulic resistance between two adjacent nodes equivalent to the combined resistance of the two soils. This formulation has the advantage that discontinuities of permeability at layer and drainage boundaries can be handled without difficulty. It may be seen that if one soil has a very low permeability, the interface permeability is also very small, while if one soil has a very high permeability, the interface permeability is twice that of the other layer. This ensures the correct hydraulic gradient at the interface for use in equation (11). The detailed derivation of equation (12) is given in Appendix 1.

When an increment of total stress is applied, the pore pressure at depth is normally incremented by an equal amount. If appropriate, allowance may be made for the effects of reduction of applied stress with depth and partial saturation. If the total stress is only increased between small time steps, it remains constant during the time step, so the term $\partial\sigma/\partial t$ is zero. The finite difference form of the right-hand side of equation (10) may then be expressed as

$$m_v \frac{u_{i,j,t+\Delta t} - u_{i,j,t}}{\Delta t} + \dot{\varepsilon}^{tp*} \tag{13}$$

Here the first term is the elastic component of strain during the time step Δt and the second is the average creep strain rate. For each soil element, knowing the soil state (effective stress and void ratio) at any time, values of elastic compressibility and creep strain rate are determined using the constitutive model.

Boundary conditions

As noted above, phantom nodes are introduced outside the grid, as shown in Fig. 3. At a permeable boundary the pore pressure at each phantom node is set to the appropriate value, and the permeability of the phantom cell is set to a very high number. At an impermeable boundary, the permeability of each phantom cell is set to zero, resulting in zero interface permeability calculated with equation (12). This results in a zero term in equation (11), equivalent to setting the hydraulic gradient to zero.

While free drainage is normally assumed at the vertical drain, the effects of drain resistance may be modelled explicitly by incorporating the drain within the grid. The drain annulus is given equivalent discharge capacity and an impermeable core,

and the terms on the right-hand side of equation (10) for the relevant cells are set to equal zero.

Solution procedure

The terms in the finite difference equation marked with a * are used to predict the pore pressures at the end of the time step. In an explicit finite difference formulation, u^* are the values of pore pressure u_t at the *start* of the time step that are known, which enables a solution to be achieved without iteration. However, despite the simplicity of an explicit formulation, very small time steps have to be used to ensure numerical stability. In an implicit formulation the values u^* include the values $u_{t+\Delta t}$ at the *end* of the time step, which *a priori* are unknown, and for two-dimensional problems this necessitates integration. Ryde (1997) used a fully implicit formulation, and more recently the procedure has been extended to permit use of the form proposed by Crank & Nicolson (1947), where u^* is given by

$$u^* = (u_t + u_{t+\Delta t})/2 \tag{14}$$

In both forms, the creep strain is calculated from the average of the creep rates at the start and end of each time step.

By adopting a procedure of elimination and back-substitution using the Thomas algorithm or tri-diagonal matrix algorithm (TDMA), described for example by Morton & Mayers (1994), a solution is obtained efficiently. For one-dimensional problems without creep, no iteration is required, but for more complicated problems several iterations are needed at each time step. It is found that with the implicit formulation, which is inherently numerically stable, variable time steps may be used with small steps specified when strain rates are highest to achieve satisfactory accuracy. Using the Crank–Nicolson formulation similar results are obtained, but smaller steps are required when modelling creep to prevent numerical instability, while the explicit form requires very small steps. The solution has been implemented in a procedure termed BRISCON using Visual Basic for Excel, with data held on worksheets, permitting graphs to be plotted conveniently. The schematic solution algorithm is shown in Fig. 5.

At the start of the analysis the steady-state conditions are determined by iteration with the right-hand side of equation (10) set to zero. These pore pressures are used to determine the initial distribution of effective stress. As the analysis proceeds the coordinates may be updated, with the values of soil bulk density, permeability, stiffness and creep rate being those applicable to the current soil state. With increasing settlement the applied loading may change owing to partial submergence of the fill, and also the boundary conditions change as noted by Olsen & Ladd (1979). By updating the boundary pore pressures during the analysis this effect is taken into account, since the pore pressures obtained in the solution converge to the long-term steady-state values.

Free strain and equal strain solutions

The analysis described here is not a fully coupled axisymmetric analysis, since although the drainage is vertical and radial, the movements are vertical. The vertical strains in adjacent annuli at any time are not necessarily compatible, and the settlement adjacent to a vertical drain may be significantly larger than that midway between the drains. To simulate an equal strain condition the total stresses applied at ground level may be redistributed. Corrective loads are applied to the top of each annulus to maintain the surface horizontal within a specified tolerance as the analysis proceeds, and this requires additional iteration at each time step. The average settlement at any time is calculated from the settlement of each annulus using an area-weighting procedure. As expected, the difference of average settlement between the free and equal strain solutions is generally not of engineering significance, and for most analyses the extra solution time for the latter is generally not justified.

VALIDATION

During development, BRISCON was used to analyse some simple problems, and where possible comparison was made with closed-form solutions and also with solutions obtained using the finite element program CRISP (Ryde, 1997). Implementation of the creep model was checked by making comparison with problems analysed by Yin & Graham (1996). The analyses carried out are listed in Table 1, and some of these are presented here.

Comparisons with closed-form solutions

Analyses were undertaken for comparison with closed-form solutions for consolidation with vertical flow (Terzaghi 1943), and radial flow with and without a smear zone (Barron, 1948; Hansbo, 1981). In these analyses consolidation of a 6 m thick linear-elastic soil under an applied load increment of 100 kPa was modelled. In the analyses with radial flow, the radius of the drain was 0·02 m, and that of the equivalent soil cylinder was 2 m. The coefficients of permeability of the soil in the horizontal and vertical directions were 10^{-3} and 5×10^{-4} m/day respectively. In some of the analyses a smear zone was introduced out to a radius of 0·14 m, in which the permeability was reduced by a factor of 2 to equal the vertical permeability. The coefficient of volume compressibility, m_v, was 10^{-4} m^2/kN. The grid used contained eight layers of soil with twelve annuli (four of which were for the smear zone), with the grid size in each direction increasing with distance from the drainage boundaries. The results of several of these analyses are shown in Fig. 6, where average degree of consolidation is plotted against time factor for the three cases of vertical flow only, and radial flow only with and without smear. It may be seen that the finite difference procedure yields results that are very similar to the closed-form solutions. The figure also illustrates the similarity of the BRISCON results for the fixed and free strain solutions.

Comparisons with CRISP

Comparative analyses were performed for the case of radial flow with a smear zone using the finite element program CRISP with a mesh similar to the grid used in the finite difference analysis, and identical soil properties. CRISP uses a fully coupled consolidation formulation, and the stresses at any depth in the soil are redistributed within the ground to ensure strain compatibility. A uniform loading was applied to the ground surface, and since the ground surface was not maintained horizontal the solution was expected to be intermediate between a free and fixed strain analysis. The results for the case where smear was modelled are shown in Fig. 6 alongside those using BRISCON, and indicate good agreement between the progress of consolidation predicted by the two numerical analyses.

The surface settlement profile and radial pore pressure distribution were also compared at four stages during consolidation (after 5, 20, 50 and 100 days, corresponding to time factors of 0·03, 0·06, 0·32 and 0·64). Fig. 7(a) shows that for the equal strain analysis BRISCON maintained the surface level, whereas for the free strain analysis there were large settlements immediately adjacent to the vertical drainage boundary. The settlement profiles obtained using CRISP were intermediate between the two cases, as would be expected for a material with significant shear stiffness. The excess pore pressure distributions are shown in Fig. 7(b), and a distinct change of gradient at the boundary of the smear zone may be observed. The distributions were very similar for all three analyses. This is perhaps surprising since the distribution of stresses was different, but as the average settlement rates were similar, and settlement is related directly to the rate of expulsion of water, the hydraulic gradients at any time must also be similar.

Validation of creep model

To check implementation of the creep model, BRISCON was used to repeat analyses presented by Yin & Graham (1996) of

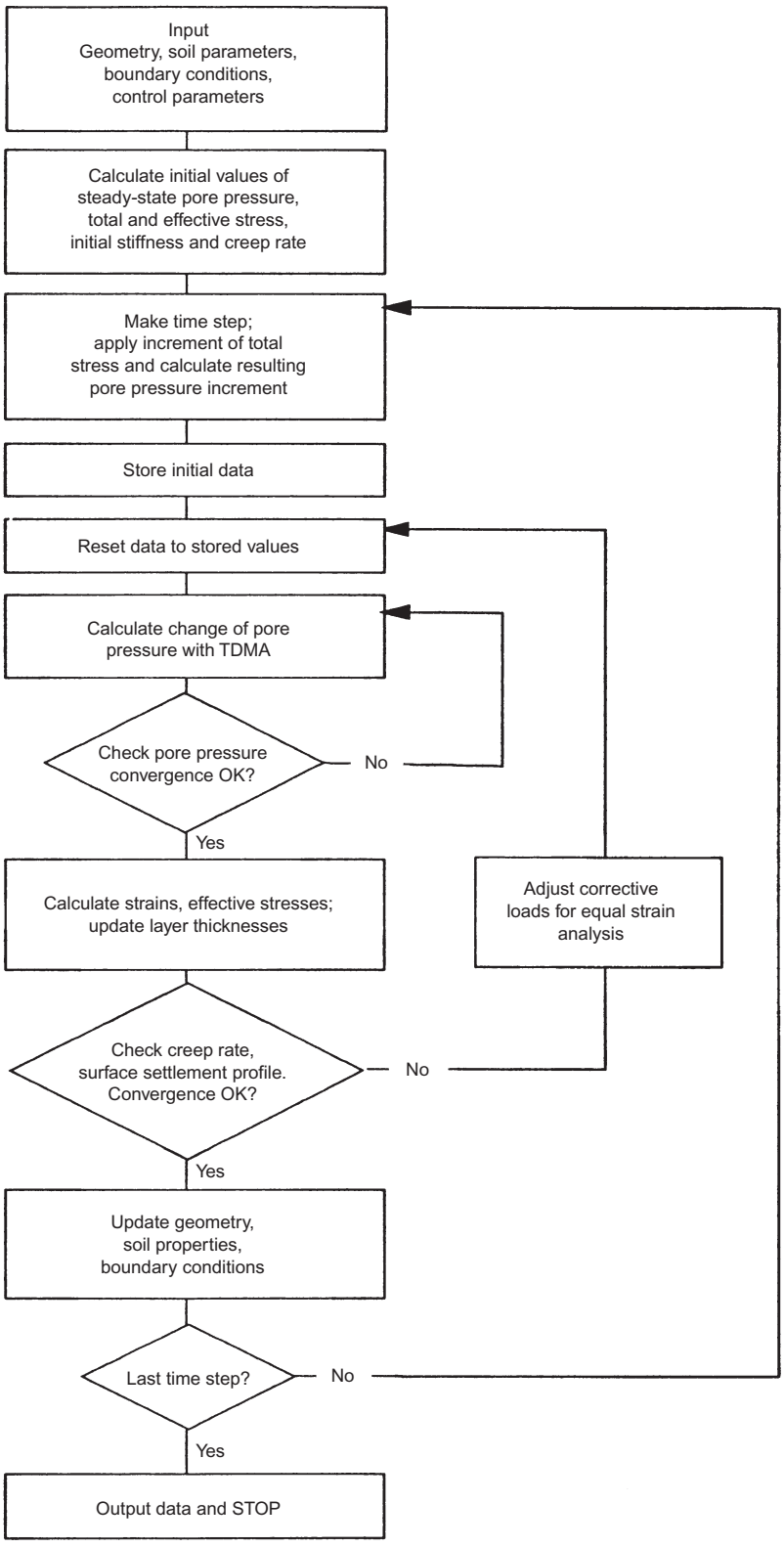

Fig. 5. Schematic algorithm for finite difference procedure BRISCON

Table 1. Analyses carried out during validation of BRISCON

Analysis	Flow direction	Soil type	Equal or free strain	Comparison with	
				CRISP	Closed form solution
1	Vertical	Linear elastic		✓	Terzaghi (1943)
2	Vertical	$\lambda\kappa$ without creep		✓	Mesri & Rokhsar (1974)
3	Vertical	$\lambda\kappa$ with creep			Yin & Graham (1996)
4	Radial	Linear elastic	Free	✓	Barron (1948)
5	Radial	Linear elastic	Equal		Barron (1948), Hansbo (1981)

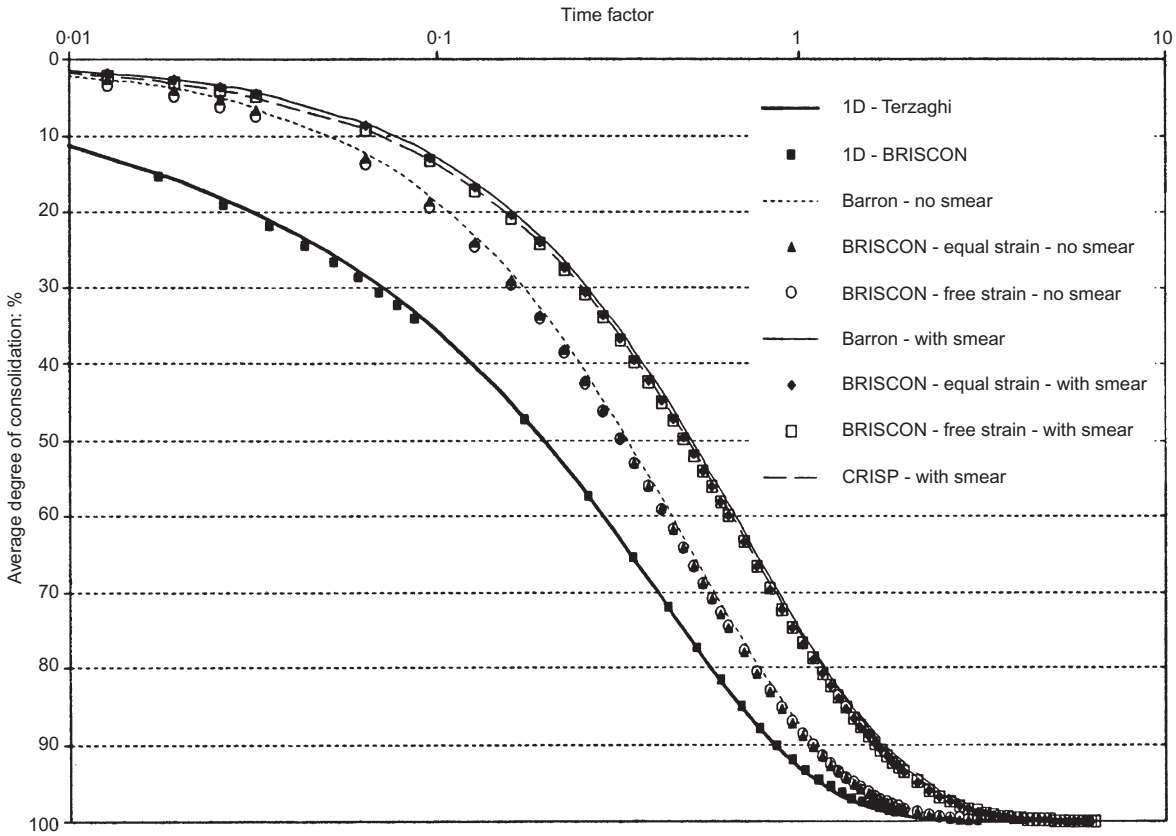

Fig. 6. Variation of average degree of consolidation with time factor in validation analyses

data from some oedometer tests on post-glacial marine clay from Drammen, Norway, published by Berre & Iversen (1972). Using identical soil/model parameters the results using BRISCON were very similar to those given by Yin & Graham (1996), which themselves provided a good fit to the laboratory data.

APPLICATION

The BRISCON procedure was developed for the back-analysis of settlement of embankments constructed as part of the new M4 and M49 approach motorways to the Second Severn Crossing, which connects England to South Wales. The 16 km length of motorways passes on low embankments across the Severnside Levels, an extensive area of estuarine alluvium bordering the estuary of the River Severn near Avonmouth, an industrial town near Bristol. Some 20 major roads, lanes and farm tracks cross the motorways on embankments typically 9 m high, which were constructed in stages and surcharged, with consolidation accelerated by vertical drains. Ideally, embankments would have been selected for particular study for which there were high-quality oedometer tests available, and class A predictions (Lambe, 1973) undertaken prior to construction followed by back-analysis of data from field monitoring. However, the variability of the estuarine alluvium coupled with insufficient good-quality laboratory data meant that only back-analysis of the field monitoring data was practicable. Accordingly the behaviour of one embankment (A403 overbridge on the M49 at Severn Beach) is described here, and the back-analysis is used to illustrate some of the features of BRISCON.

Ground conditions

The 10–20 m thick estuarine soils of the Severnside levels have a surface elevation of +6 to +7 m OD, and overlie the Mercia Mudstone bedrock. Above OD the soft silts and clays are extremely variable and often laminated with sands, and contain thin discontinuous peat bands. At depth, the strata consist of sandy sediments and terrace gravels. The silty clays are of medium to high plasticity, with undrained shear strengths of 10–30 kPa. The strata are generally lightly over-consolidated, with an OCR usually between 1·1 and 1·4. Reclamation and drainage has resulted in some groundwater lowering, with the result that the upper few metres of the soft clay are generally desiccated. Groundwater levels are controlled by lateral seepage through the granular deposits, generally varying from about +6 m OD inland to around OD at the estuary.

At the A403 overbridge the alluvium is approximately 11 m thick, as shown in the geotechnical profile in Fig. 8. The CPT profiles are shown here just for the soft clay, and indicate the heterogeneous nature of the estuarine alluvium. The alluvium is locally under-drained here, with the water table initially at 7 m depth at just below Ordnance Datum. The under-drainage arises from lateral seepage through the terrace gravel into a nearby cutting leading to a railway tunnel beneath the River Severn.

Construction

Before construction of the original M5 motorway across the Severnside levels in the 1970s, a trial embankment at Avonmouth (Murray, 1971) had shown that primary consolidation might take at least 2 years. Nevertheless the M5 was constructed without vertical drains, but in places lightweight fill was used to minimise imposed stresses. Subsequently large and ongoing settlements were reported on the M5 further south (Cook & Pereira, 1991). For the new motorways, consolidation beneath high embankments was accelerated by vertical drains, and surcharge was placed to minimise post-construction settlement.

The embankments for the A403 overbridge were constructed of Mercia Mudstone excavated from cuttings under construction elsewhere on the site. After placing a 0·6 m layer of granular fill, vertical Mebra drains were installed at 2–4 m spacing on a square grid through the compressible alluvium down into the silty sand, instrumentation was installed, and a further 0·9 m drainage layer was placed, with a geotextile separator on top.

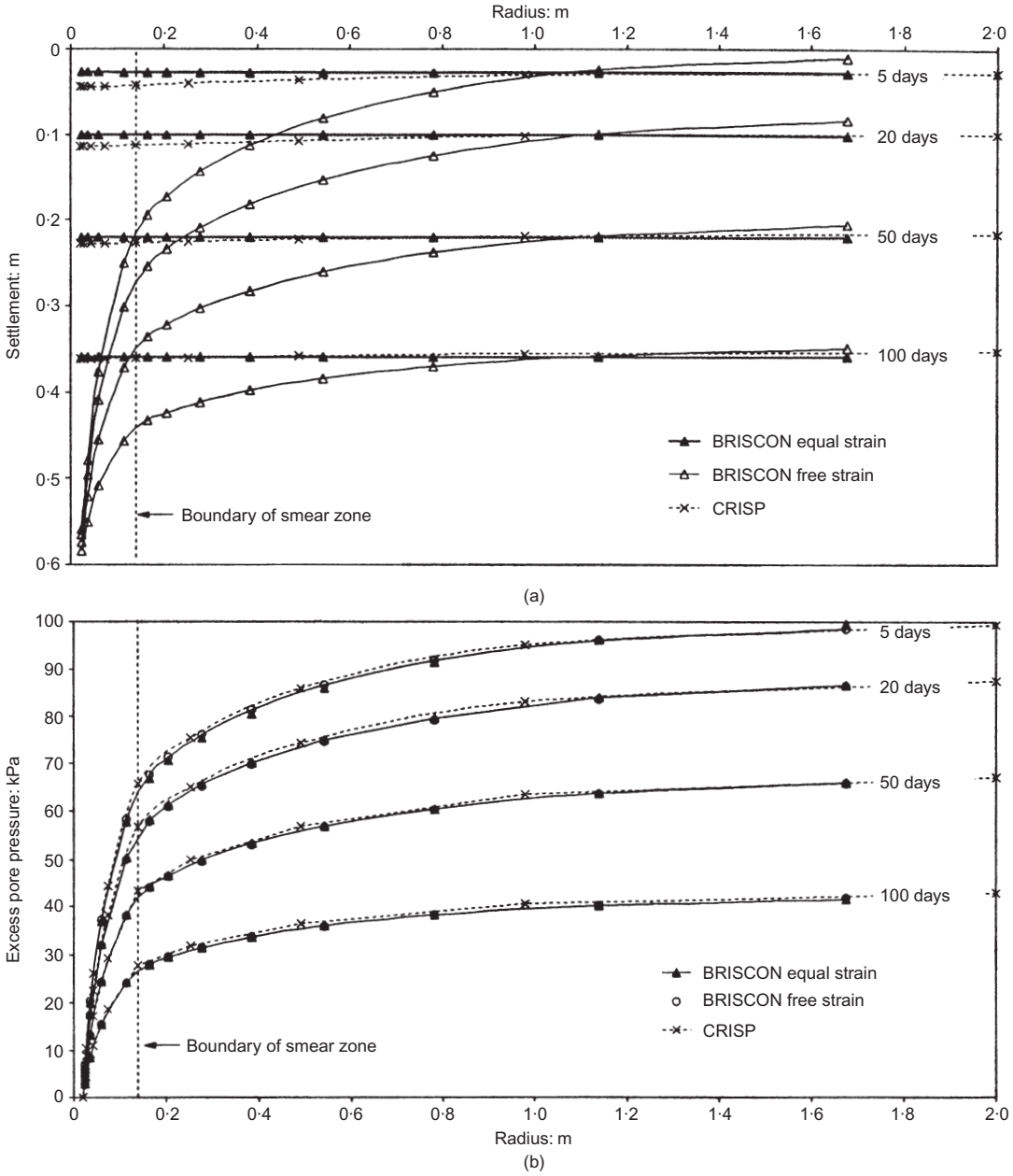

Fig. 7. Comparison of finite difference analyses (BRISCON) with finite element analysis (CRISP): (a) variation of surface settlement with radius; (b) variation of excess pore pressure with radius

After embankment construction in stages to a height of 9 m above original ground level, an extra 2 m surcharge was applied and left for 5 months. After removing the surcharge, bored piles for the bridge abutments were installed to bedrock. The finished crest width is 13 m and the side slopes are 1 in 2·5.

Observed performance of embankments

During construction of the high embankments, rod settlement gauges, magnet extensometers, inclinometers and pneumatic piezometers installed midway between vertical drains were monitored regularly to ensure embankment stability. In general, fill rates were slow and the vertical drains ensured that excess pore pressures were small, with the result that the response of the alluvium to loading was more *drained* than *undrained*.

Figure 9(a) shows the increase of maximum fill height at the A403 overbridge with time, together with the observed settlement of the original ground surface beneath the highest part of the embankment. The majority of the 700 mm settlement occurred as the fill was placed, and lateral movements (not shown here) beneath the embankment toe did not exceed 7% of the maximum settlement. It may be seen that there was a very small upward movement when the surcharge was removed, before creep settlements resumed.

Figure 9(b) shows the observations made with pneumatic piezometers beneath the centre of the embankment. Initially the pore pressures in the silty clays were small, and consistent with the under-drainage, and the piezometric levels indicated downward seepage. During the first stage of filling, when the embankment was raised to a height of 7 m over a period of 2 months, both the upper piezometers responded to the increase in vertical stress, but the response was small with maximum excess pore pressures of around 25 kPa ($\Delta u/\Delta\sigma \approx 0{\cdot}2$). The piezometric levels reduced almost immediately, and there was no further response 1 month later when the embankment was raised to its full height of just over 11 m (including surcharge). The pair of piezometers in the lower alluvium and underlying sand showed negligible response to filling, but there was a marked rise in pore pressures some time after the surcharge was placed. This appears to be unrelated to consolidation, since it affected the sand layer as well as the overlying clay, but it did occur after a period of heavy rain. By this time the original ground surface beneath the

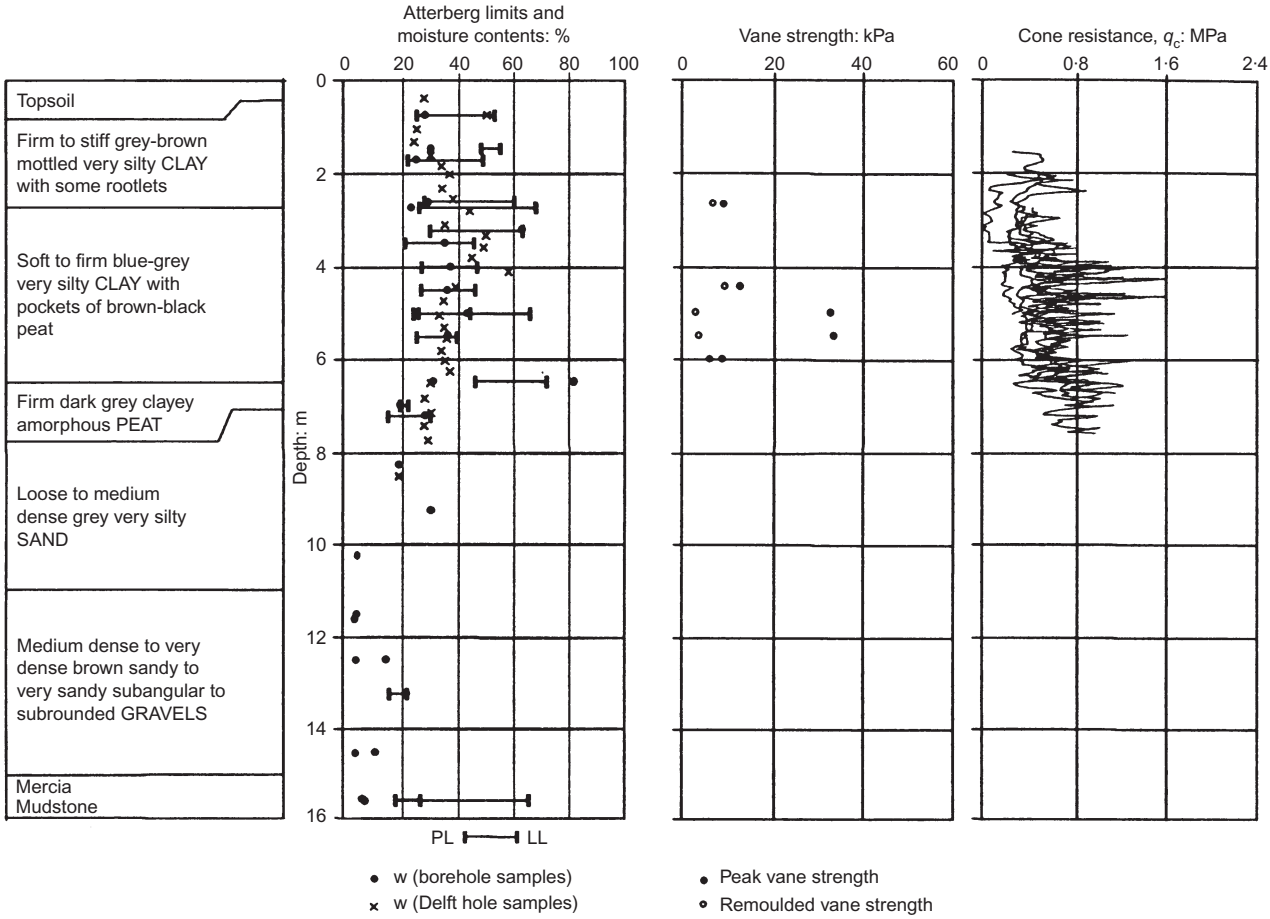

Fig. 8. Geotechnical profile at A403 overbridge on M49

embankment had settled by 600 mm, so that surface runoff (see Fig. 9(b)) may have ponded in the granular drainage layer beneath the fill. The water would then have entered the top of the vertical drains, draining into the alluvium at depth and temporarily raising the pore pressures.

Back-analysis

Back-analysis of the behaviour of this embankment was undertaken using BRISCON. Although the groundwater conditions were different from those elsewhere, this embankment was chosen because of the reliability of the instrumentation data. Since there were insufficient lab test data from this location to obtain reliable consolidation parameters, the modelling was based on the stress–strain behaviour in the field determined from piezometer and extensometer data. The profile was split into layers based on the extensometer magnet elevations: firm crust (0–3 m depth), soft silty clay and peat (3–7 m) and silty clay and sand (7–11 m); below 11 m the extensometers showed the strata to be incompressible.

Starting from the initial conditions, the average void ratio was determined for each clay layer for each stage of construction. The proportions of the embankment and underlying alluvium were such that the stress increment was reasonably uniform with depth, so that the vertical effective stress at the centre of each layer could be calculated using fill thickness and nearby piezometer data. The average void ratio could then be related to average vertical effective stress, as shown in Fig. 10.

The small strains under the first 60 kPa of the applied loading suggest that the strata were initially over-consolidated. Such behaviour was not generally observed elsewhere on this project, and was probably associated with the under-drainage. With the water table drawn down to 7 m depth comparatively recently, it might be expected that the OCR would be around 1·0. Although piezometers indicated small positive pore pressures in the clay at the start of construction, suctions developed during dry periods in the past would have left the clay over-consolidated. For the later stages of construction under high embankment loading these strata appear normally consolidated, and field normal consolidation lines (NCL) were drawn as indicated in Fig. 10, enabling average λ and κ parameters to be determined for each clay layer.

Reference time lines (RTL) for each layer were initially chosen parallel to each NCL. During construction there were two significant rest periods after fill lifts, and once excess pore pressures had dissipated there was creep at constant effective stress (see Fig. 10). Working with plots of average void ratio against $\log(t)$ for these rest periods, Ryde (1997) optimised the position of each RTL using an iterative procedure similar to Yin & Graham (1994), and determined the remaining creep parameters ψ and t_0. The full set of parameters together with m_v derived for the silty sand layer are given in Table 2. The ratio ψ/λ is around 0·1, somewhat higher than would normally be expected for the similar ratio C_α/C_c, and this is thought to be due to the presence of minor peat bands within the alluvium.

Recently the values of ψ have been confirmed by re-plotting the data in the form logarithm of strain rate against strain, as suggested by equation (7). Fig. 11 indicates reasonably linear and parallel data for each layer for the two rest periods. Two pairs of parallel lines with gradients ψ/ν_0 equal to 0·0065 and 0·0116 obtained from Table 2 for the crust and soft clay respectively have been superimposed on the data, and may be seen to fit the field data satisfactorily. This procedure appears to be more straightforward than the iterative method originally used.

Analyses with BRISCON

The analyses with BRISCON were carried out for a soil cylinder of radius 1 m with a central drain of radius of 0·033 m.

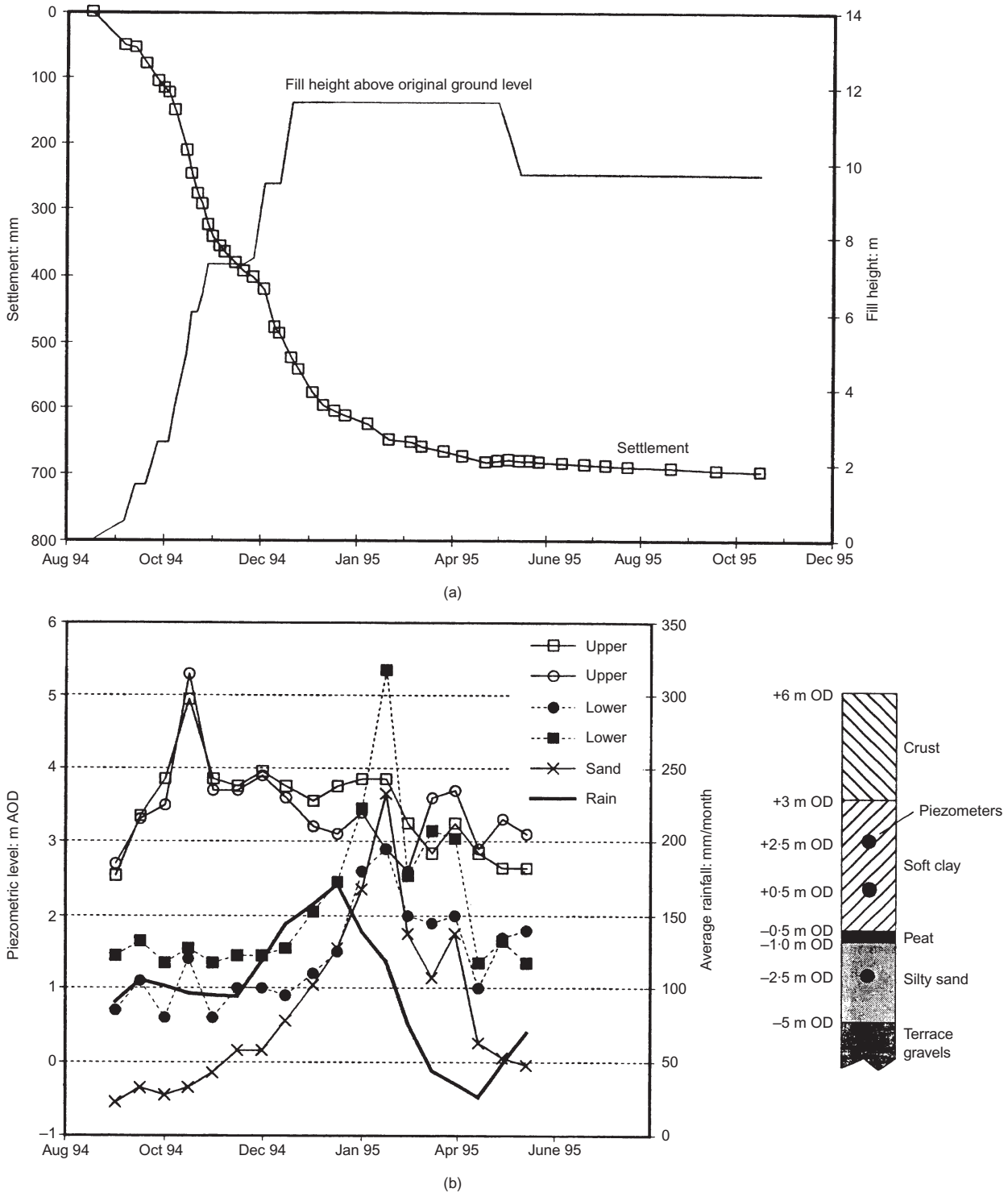

Fig. 9. Settlement and pore pressures observed during construction of A403 overbridge embankment

This configuration was approximately equivalent to Mebra drains of cross-section 100 mm by 3 mm spaced at 2 m on a square grid; the perimeter of the circular drain modelled was set equal to that of the rectangular vertical drain. The analysis used a finite difference grid of 14 layers and 6 annuli. There were few definitive data on the in-situ permeability at the A403 site, and reference was made to the report on the Avonmouth trial embankment (Murray, 1971), from which values of in-situ horizontal permeability of $1{\cdot}7 \times 10^{-4}$ and $1{\cdot}3 \times 10^{-3}$ m/day were obtained for the crust and soft clay respectively. Subsequently studies showed that satisfactory matching with the A403 field data could be obtained using a single value of initial horizontal permeability k_h of 10^{-3} m/day, and this has been used for the analysis reported here. A ratio of horizontal to vertical permeability $k_h/k_z = 1{\cdot}5$ was assumed, which probably underestimates the conditions in the field. The permeabilities of the smear zone were reduced by a factor of 2·5 within a radius equal to twice the drain radius, although there was uncertainty over whether to base the size of the smear zone on the drain size or that of the mandrel (Holtz *et al.*, 1991). In all analyses nodal coordinates and permeability were continuously updated as the analysis progressed.

The vertical drain, surface granular layer and underlying terrace gravel all provide free drainage, and with the piezometric level in the gravel set at 7 m below ground level, the boundary conditions are affected by the under-drainage. Although it might be expected that, with the installation of vertical drains, final piezometric levels in the soft clay would be

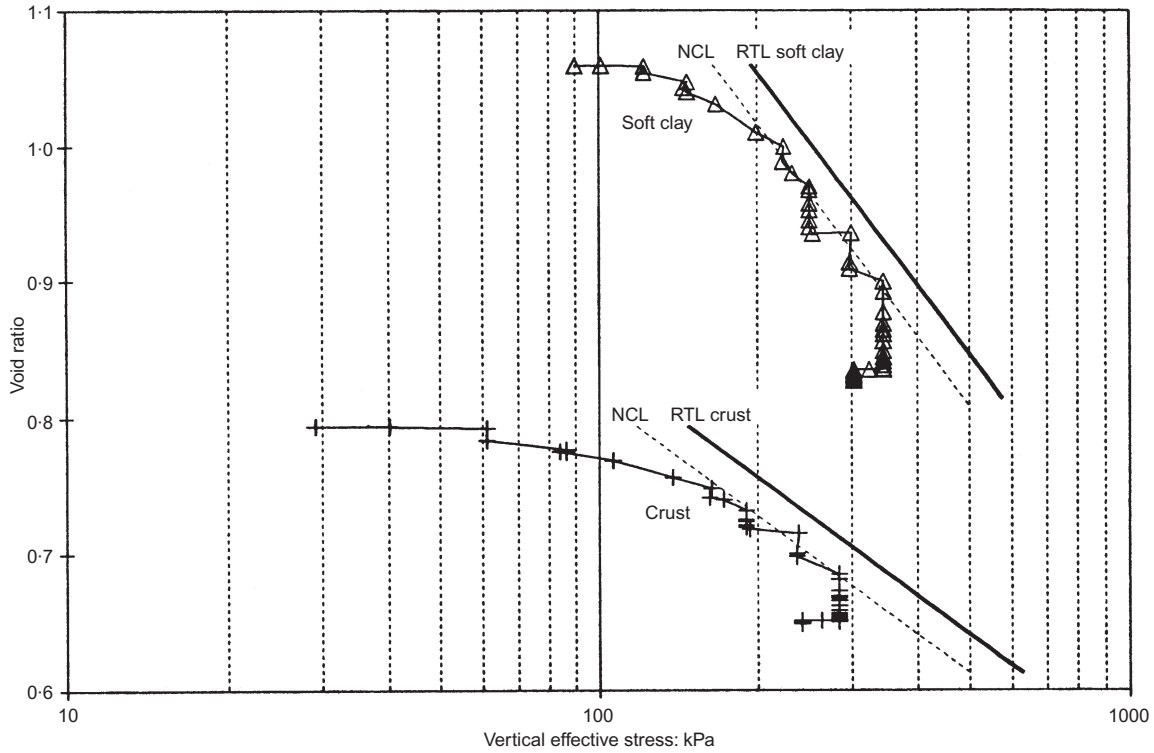

Fig. 10. Field observations of void ratio against effective stress for crust and soft clay layers, and reference time lines used in analysis

Table 2. Soil parameters for A403 embankment derived from back-analysis of extensometer data

Layer	Depth: m	m_v: m^2/kN	e_0	λ	κ	ψ	$\sigma_0'^{ep}$	ε_0^{ep}	t_0: days
Crust	0–3		0·794	0·125	0·018	0·0117	148	0	0·5
Soft silty clay	3–7		1·060	0·227	0·027	0·0239	195	0	2·0
Silty sand	7–11	$6{\cdot}8 \times 10^{-5}$							

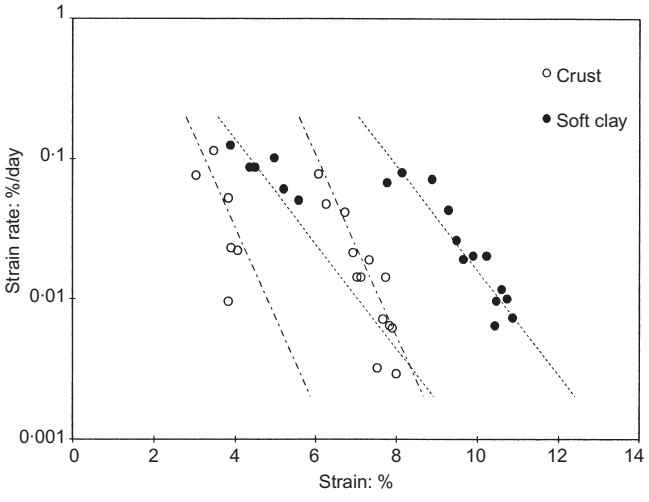

Fig. 11. Variation of strain rate with strain during two creep periods for crust and soft clay layers

lower than the initial ones, there was no field evidence for this. Accordingly it was decided to assume that initial and final pore pressure distributions would be similar, with zero pore pressure specified in the strata located initially above the piezometric level in the gravel. The analyses were therefore carried out using the original version of BRISCON, in which *excess* pore pressure is the dependent variable.

Before attempting to model the whole construction sequence, BRISCON was used to check that the creep behaviour of each layer could be predicted. Using the parameters in Table 2 the behaviour during the two rest periods was predicted, and Fig. 12 shows that a good matching of the magnitude and rates of compression was achieved.

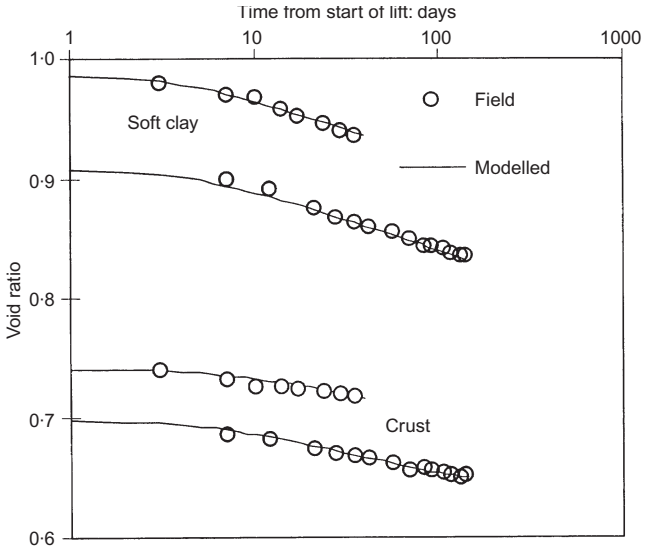

Fig. 12. Comparison of behaviour predicted with BRISCON with observed creep during two rest periods for soft clay layer and overlying crust

Finally the behaviour of the whole profile subjected to the field construction sequence was modelled using an initial horizontal permeability of 10^{-3} m/day As shown in Fig. 13(a), the whole time–settlement history could be predicted satisfactorily. The predicted excess pore pressures for a soil element near the top of the soft clay just below the crust are compared with the field data in Fig. 13(b), and it may be seen that they are underpredicted by a factor of 3. Although the difference may appear large it does not significantly affect the effective stress in the ground since the absolute pore pressures are small. The influence of permeability on the predicted excess pore pressures is discussed further in the next section. The predicted change of state of a soil element near the top of the soft clay layer has been compared with that deduced from the field instrumentation in Fig. 14. Here the void ratio and effective stress predicted by BRISCON may be seen to match well with data re-plotted from Fig. 10.

These analyses also show that the 2 m surcharge was not

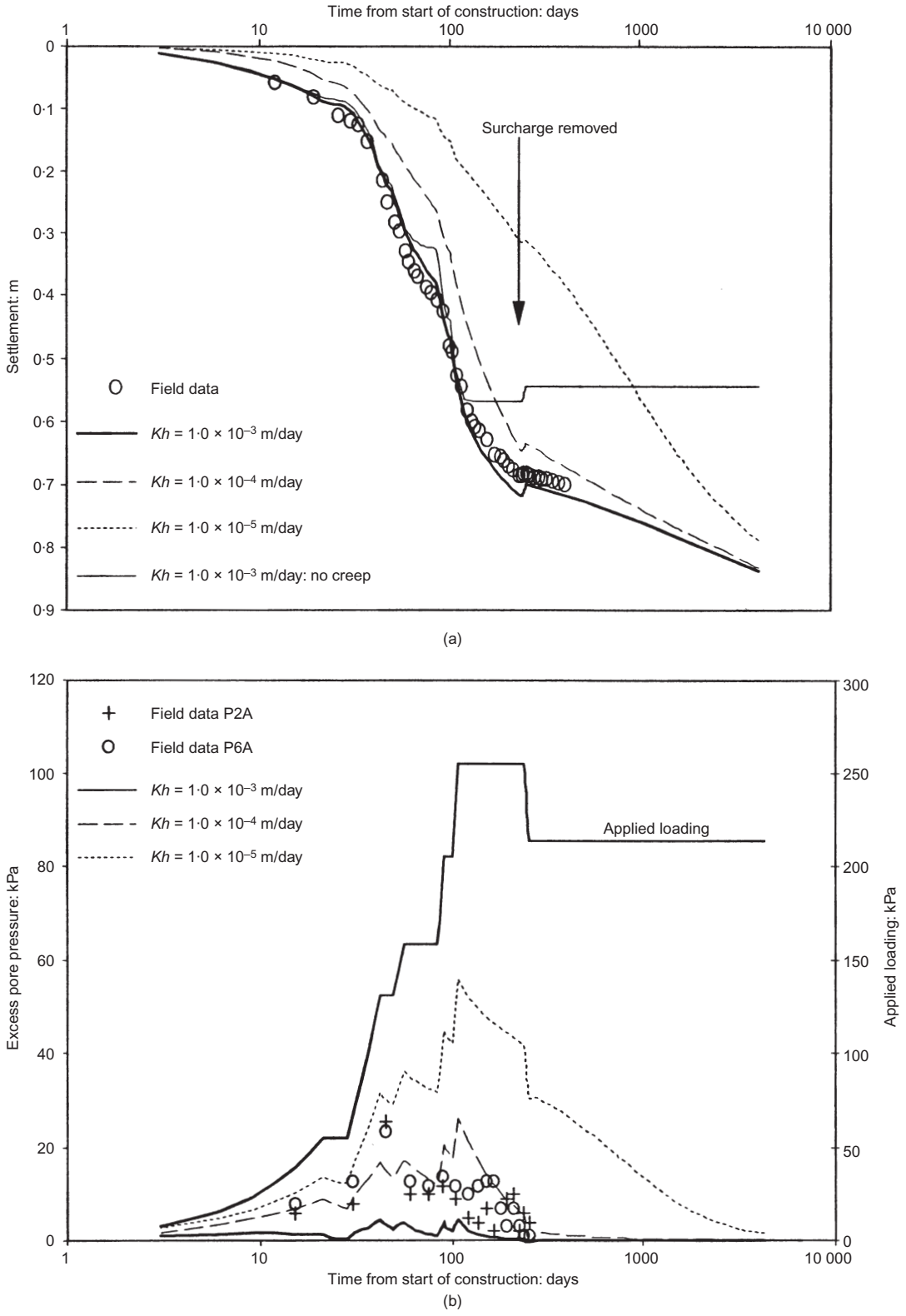

Fig. 13. Comparison between observed and predicted settlement and excess pore pressures at A403 overbridge embankment

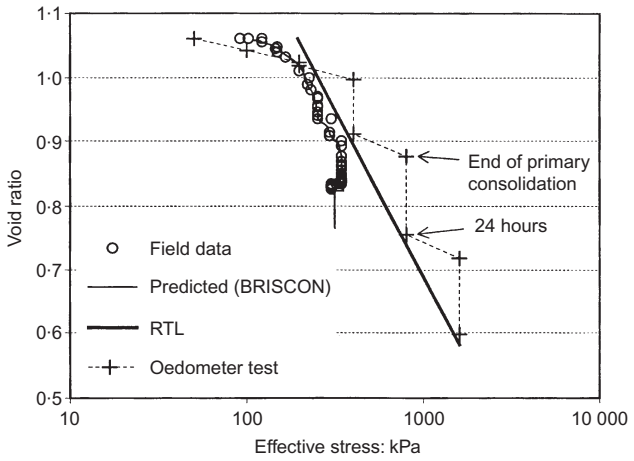

Fig. 14. Observed and predicted behaviour of soft clay in the field, and predicted behaviour in an oedometer test

sufficient to eliminate post-construction settlement. Indeed, it is predicted that in the long term the settlement will increase by a further 15 cm over 50 years. By extending the parametric study to examine the effectiveness of surcharge it was shown (Nash & Ryde, 1999) that at least 4 m surcharge would have been needed for the 5-month surcharge period to reduce the post-construction settlement by 50%.

Further analyses

On account of the uncertainty over the values of permeability, a parametric study was carried out in which the initial permeabilities (k_h of 10^{-3}m/day, $k_h/k_z = 1{\cdot}5$) were reduced by factors of 10 and 100. The predicted settlement behaviour is presented in Fig. 13(a), which shows that while a tenfold reduction of permeability has little effect, a hundredfold reduction significantly slows the consolidation. Examination of the predicted excess pore pressures shown in Fig. 13(b) indicates that, as expected, larger excess pore pressures develop when the permeability is reduced. These analyses suggest that for the best matching of settlement and excess pore pressure data, an initial average horizontal permeability of these soft silty soils of about 3×10^{-4} m/day should be used. With such a heterogeneous estuarine deposit, in which flow may be concentrated in the more permeable laminations, a single value of permeability can only represent an equivalent average value. Indeed, the predicted excess pore pressures are also sensitive to the assumed effective drain size, and the permeability and extent of the smear zone.

Additional analyses were carried out to explore aspects of the creep behaviour. First the behaviour in a conventional oedometer test on the soft clay was predicted, using the parameters given in Table 2, with loading increased every 24 hours with a load increment ratio of 2. The void ratio against effective stress behaviour is shown alongside the full-scale behaviour and RTL in Fig. 14. As might be expected for very short drainage paths, the laboratory strain rates are much higher than those in the field, and at higher stresses the void ratio lies above the RTL. Using this constitutive model, the soil state at end of primary consolidation (EOP) in the laboratory is quite different from that in the field, as was shown by Fig. 2 and discussed earlier in the paper.

Second, an analysis was carried out to explore the significance of not modelling creep. This was carried out using the field normal consolidation lines (NCL shown dashed in Fig. 10) to define the stress–strain behaviour. The results are presented in Fig. 13(a) alongside those using the creep model, and indicate very similar behaviour up to maximum load, but thereafter there is of course no further movement. The behaviour up to the end of primary consolidation is similar to that predicted with the EVP model since the chosen NCL coincides with the field NCL, which was well matched by the analysis with the creep model. To predict the long-term behaviour it would be necessary to add secondary consolidation in a conventional way with the usual difficulties of defining the time origin. If the modelled permeability had been lower, or if the location of the NCL had been higher (e.g. end-of-primary or 24-hour lines from oedometer tests indicated in Fig. 14), the analysis without creep would have underestimated the settlement at all stages.

DISCUSSION AND CONCLUSION

The consolidation of soft soils accelerated by vertical drains frequently presents difficulties to designers of embankments and reclamation schemes over soft clays if there is significant creep. The elastic visco-plastic constitutive model developed originally by Yin & Graham (1989, 1996) reproduces many features of soft clay behaviour commonly observed in the field and laboratory, and provides a helpful framework for the interpretation of data from high-quality oedometer tests and field instrumentation. It is axiomatic that the field and laboratory stress–strain paths predicted by the model are different on account of the longer drainage paths and slower strain rates in the field. The incorpation of this EVP model in the finite difference procedure BRISCON enables predictions to be made for full-scale problems. Parametric studies may be undertaken where there is uncertainty over soil properties such as permeability and creep parameters, and to examine the effects of varying the size and permeability of the smear zone and the effects of drain resistance.

The case study presented here has illustrated the application of the model to the analysis of a full-scale problem involving significant creep; its use in back-analysis of field consolidation behaviour is believed to be novel. The derivation of the creep parameters from the field instrumentation data was facilitated by the rapid dissipation of excess pore pressures so that there were significant periods of drained creep during construction. If pore pressures had not dissipated so rapidly a more complicated procedure would have been required on account of the continuous variation of effective stress. While BRISCON could predict the field settlement behaviour and rapid pore pressure dissipation at the A403 overbridge satisfactorily, its application to a future project where there are high-quality laboratory data is necessary to test its validity during primary consolidation.

A significant aspect of the EVP model is that the creep strain rate depends only on the current state of the soil. This enables predictions to be made of behaviour after removal of a surcharge without resorting to empirical methods. While simple hand calculations may be made to assess surcharge effectiveness where primary consolidation occurs quickly (Nash & Ryde, 1999), the BRISCON procedure facilitates design to reduce long-term secondary settlements even if primary consolidation is not complete before a surcharge is removed.

The satisfactory comparison of analyses of simple axisymmetric problems using BRISCON with analyses using CRISP suggests that the assumption of one-dimensional strains in the former may not result in significant inaccuracy. This supports the use of a one-dimensional procedure when analysing conditions near the centre-line of embankments, and of course for one-dimensional problems such as reclamations. Where significant shear strains may occur, a more comprehensive analysis is required using procedures such as those developed by Hird *et al.* (1992), in which the vertical drains are incorporated into a full two-dimensional finite element model. However, such analyses have not hitherto used a constitutive model incorporating creep, and would necessitate using a more comprehensive model such as that developed recently by Yin & Graham (1999).

ACKNOWLEDGEMENTS

The authors are grateful to the Second Severn Crossing Group for access to the field data, to them and the Engineering and Physical Sciences Research Council for sponsoring the research, and to Prof David Muir Wood for his helpful comments on the manuscript.

APPENDIX 1. DERIVATION OF THE BOUNDARY PERMEABILITY VALUES k_X

An equivalent value of permeability, k_X, is needed for use in the finite difference equation (9) when determining the hydraulic gradient at a cell boundary between two soils of different permeability. Fig. 15 shows point X on a boundary between adjacent nodes M and N in layers of permeability k_m and k_n. The total head differences between the various points are given by Δh_{mx} and Δh_{nx}. Considering the continuity of flow across the boundary, the discharge velocity V perpendicular to the boundary at all three points must be equal, and is given by

$$V = \frac{k_m \Delta h_{mx}}{L_m} = \frac{k_n \Delta h_{nx}}{L_n} = k_X \frac{\Delta h_{mx} + \Delta h_{nx}}{L_m + L_n} \tag{15}$$

Since the boundary is midway between the nodes $L_m = L_n$, and equation (15) may be rearranged to show that;

$$k_X = \frac{2k_m k_n}{k_m + k_n} \tag{16}$$

This equation may be used without modification at the grid boundaries to ensure that the correct boundary conditions are implemented. At an impermeable boundary between cells M and N, use of $k_m = 0$ leads to $k_X = 0$, ensuring that the discharge velocity is zero. At a permeable boundary the pore pressure or total head is specified at the phantom node outside the grid, and the use of $k_m = \infty$ leads to the equivalent boundary permeability $k_X = 2k_n$ for use in equation (11).

NOTATION

c_v, c_r	vertical and radial coefficients of consolidation $k_z/\gamma_w m_v$, $k_r/\gamma_w m_v$
C_α	logarithmic creep function with respect to void ratio
C_c	compression index
e	void ratio
k_z, k_h, k_r	vertical, horizontal and radial coefficients of (here $k_h = k$) permeability
k_T, k_B, k_I, k	coefficients of permeability at cell boundaries
m_v	coefficient of elastic volume compressibility
t, t_e	time and equivalent time
t_0	parameter used to determine strain rate on reference time line
u, $\bar{u}$, u_{ss}	pore pressure, excess pore pressure, steady-state pore pressure
u^*	pore pressure used for prediction of pore pressure at end of time step
v, v_0	specific volume, specific volume at zero strain
γ_w	unit weight of water
ε	strain
σ, σ'	vertical total and effective stresses
σ'_0, ε_0	values of effective stress and strain for fixing reference time line
κ, λ	logarithmic material parameters for elastic and stress-dependent plastic strains
ψ	logarithmic material parameter for creep

Superscripts and subscripts

e, ep, tp	instantaneous (elastic), stress-dependent plastic and time-dependent plastic
i, j	counters for radial and vertical position on grid

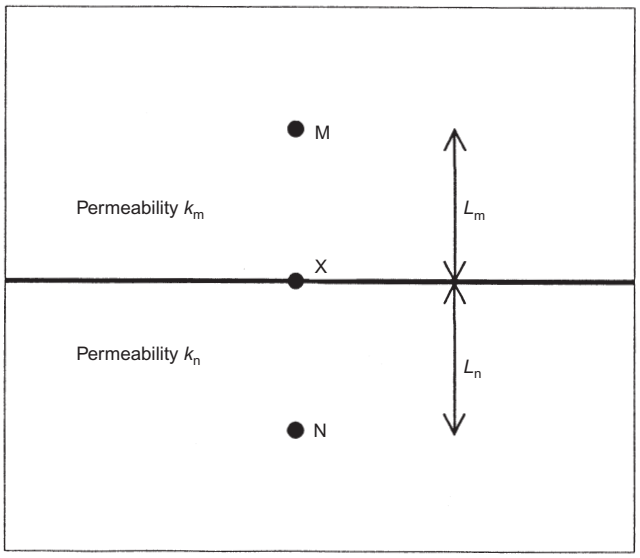

Fig. 15. Part of finite difference grid showing boundary between soils of different permeability

REFERENCES

Barron, R. A. (1948). Consolidation of fine-grained soils by drain wells. *Trans. ASCE* **113**, 718–754.

Berre, T. & Iversen, K. (1972). Oedometer tests with different specimen heights on a clay exhibiting large secondary compression. *Géotechnique* **22**, No. 1, 53–70.

Bjerrum, L. (1967). Engineering geology of Norwegian normally consolidated clays. Seventh Rankine Lecture. *Géotechnique* **17**, No. 2, 81–118.

Bjerrum, L. (1972). Embankments on soft ground. State of the art report. *Proceedings of the special conference on performance of earth and earth-supported structures*, Purdue University, Vol. 1, pp. 1–54. ASCE.

Butterfield, R. (1979). A natural compression law for soils (an advance on e–log p'). *Géotechnique* **29**, No. 4, 469–480.

Carrillo, N. (1942). Simple two- and three-dimensional cases in the theory of consolidation of soils. *J. Maths. Physics* **21**, No. 1, 1–15.

Cook, D. A. & Pereira, G. (1991). Records of settlement of the M5 motorway over the Somerset levels. In *Quarternary engineering geology*, Engineering Geology Spec. Pub. No. 7, pp. 627–635. London: Geological Society.

Crank, J. & Nicolson, P. (1947). A practical method for numerical evaluation of solutions of partial differential equations. *Proc. Camb. Phil. Soc.* **43**, 50–67.

Den Haan, E. J. (1992). The formulation of virgin compression in soils. *Géotechnique* **42**, No. 3, 465–484.

Den Haan, E. J. (1996). A compression model for non-brittle soft clays and peat. *Géotechnique* **46**, No. 1, 1–16.

Garlanger, J. E. (1972). Consolidation of soils exhibiting creep under constant effective stress. *Géotechnique* **22**, No. 1, 71–78.

Hansbo, S. (1981). Consolidation of fine-grained soils by prefabricated drains. *Proc. 10th Conf. on SMFE, Stockholm* **3**, 677–682.

Hird, C. C., Pyrah, I. C. & Russell, D. (1992). Finite element modelling of vertical drains beneath embankments on soft ground. *Géotechnique* **42**, No. 3, 499–511.

Holtz, R. D., Jamiolkowski, M., Lancellotta, R. & Pedroni, R. (1991). *Prefabricated vertical drains: design and performance*, CIRIA Ground Engineering Report: Ground Improvement. Oxford: Butterworth-Heinemann.

Jamiolkowski, M., Lancellotta, R. & Wolski, W. (1983). Precompression and speeding up consolidation, General Report to Spec. Session 6. *Proc. 8th Eur. conf. on SMFE, Helsinki* **3**, 1201–1226.

Johnson, S. J. (1970). Precompression for improving foundation soils. *J. Soil Mech. and Found. Div., ASCE* **96**, No. SM1, 111–144.

Kabbaj, M., Oka, F., Leroueil, S. & Tavenas, F. (1986). Consolidation of natural clays and laboratory testing. In *Consolidation of soils: testing and evaluation* (eds R. N. Yong and F. C. Townsend), ASTM STP 892, 71–103.

Ladd, C. C., Foott, R., Ishihara, K., Schlosser, F. & Poulos, H. G. (1976). Stress-deformation and strength characteristics: state-of-the-art report. *Proc. 9th Int. Conf. on SMFE, Tokyo* **2**, 421–494.

Lambe, T. W. (1973). Predictions in soil engineering. *Géotechnique* **23**, No. 2, 149–202.

Lee, I. K., White, W. & Ingles, O. G. (1983). *Geotechnical engineering*. Boston, Mass Pitman.

Leroueil, S. (1988). Recent developments in consolidation of natural clays. 10th Canadian Geotechnical Colloquium. *Can. Geotech. J.* **25**, No. 1, 85–107.

Magnan, J.-P., Baghery, S., Brucy, M. & Tavenas, F. (1979). Etude numérique de la consolidation unidimensionnelle en tenant compte des variations de la perméabilité et de la compressibilité du sol, du fluage et de la non-saturation. *Bull. Liaison Lab. Ponts et Chaussées* **103**, 83–94.

Mesri, G. & Choi, Y. K. (1985a). The uniqueness of the end-of-primary (EOP) void ratio-effective stress relationship. *Proc. 11th Int. Conf. on SMFE, San Francisco* **2**, 587–590.

Mesri, G. & Choi, Y. K. (1985b). Settlement analysis of embankments on soft calys. *J. Geotech. Engng Div., ASCE* **111**, No. GT4, 441–464.

Mesri, G. & Godlewski, P. M. (1977). Time- and stress-compressibility interrelationship. *J. Geotech. Engng Div., ASCE* **103**, No. GT5, 417–429.

Mesri, G. & Rokhsar, A. (1974). Theory of consolidation for clays. *J. Geotech. Engng Div., ASCE* **100**, No. GT8, 889–904.

Mesri, G., Lo, D. O. K. & Feng, T. W. (1994). Settlement of embankments on soft clays. In *Vertical and horizontal deformations of foundations and embankments*, ASCE. Geot. Spec. Pub. No. 40, pp. 8–55.

Morton, K. W. & Mayers, D. F. (1994). *Numerical solution of partial differential equations*. Cambridge: Cambridge University Press.

Murray, R. T. (1971). *Embankments constructed on soft foundations: settlement study at Avonmouth*, Report LR 419. Crowthorne: Road Research Laboratory.

Nash, D. F. T. & Ryde, S. J. (1999). Modelling the effects of surcharge to reduce long term settlement of an embankment on soft alluvium. In *Geotechnical Engineering for Transporation Infrastructre: Proc. 12th Eur. Conf. on SMGE, Amsterdam* **3**, 1555–1561. Rotterdam: Balkema.

Nash, D. F. T & Ryde, S. J. (2000). Modelling the effects of surcharge to reduce long term settlement of reclamations over soft clays. *Proceedings of the international symposium on coastal geotechnical engineering in practice*, **I**, 483–480 Yokahama. Rotterdam: Balkema.

Olsen, R. E. & Ladd, C. C. (1979). One-dimensional consolidation problems. *J. Geotech. Eng Div., ASCE* **105**, No. GT1, 11–30.

Olsen, R. E., Daniel, D. E. & Liu, T. K. (1974). Finite difference analysis for sand drain problems. *Proceedings of the conference on analysis and design in geotechnical engineering*, Vol. 1, pp. 85–110. ASCE.

Onoue, A. (1988). Consolidation of multi-layered anisotropic soils by vertical drains with well resistance. *Soils Found.* **28**, No. 3, 75–90.

Reece, G. (1986). *Microcomputer modelling by finite differences*. London: Macmillan.

Richart, F. E. (1959). Review of the theories for sand drains. *Trans. ASCE* **124**, 709–739.

Ryde, S. J. (1997). *The performance and back-analysis of embankments on soft estuarine clay.* PhD thesis, University of Bristol.

Suklje, L. (1957). The analysis of the consolidation process by the isotache method. *Proc. 4th Int. Conf. on SMFE* **1**, 200–206.

Taylor, D. W. (1948). *Fundamentals of soil mechanics*. London: Chapman & Hall; New York: Wiley.

Taylor, D. W. & Merchant, W. (1940). A theory of clay consolidation accounting for secondary compression. *J. Math. Phys.* **19**, No. 3, 167–185.

Terzaghi, K. (1943). *Theoretical soil mechanics*. London : Chapman & Hall; New York: Wiley.

Terzaghi, K. & Peck, R. B. (1948). *Soil mechanics in engineering practice*. London: Chapman & Hall; New York: Wiley.

Yin, J.-H. & Graham, J. (1989). Viscous-elastic-plastic modelling of one-dimensional time-dependent behaviour. *Can. Geotech. J.* **26**, No. 2, 199–209.

Yin, J.-H. & Graham, J. (1994). Equivalent times and one-dimensional elastic visco-plastic modelling of time-dependent stress–strain behaviour of clays. *Can. Geotech. J.* **31**, No. 1, 42–52.

Yin, J.-H. & Graham, J. (1996). Elastic visco-plastic modelling of one-dimensional consolidation. *Géotechnique* **46**, No. 3, 515–527.

Yin, J.-H. & Graham, J. (1999). Elastic viscoplastic modelling of the time-dependent stress–strain behaviour of soils. *Can. Geotech. J.* **36**, No. 4, 736–745.